HAL
open science

Youla-Kucera based multi-objective controllers : Application to autonomous vehicles

Imane Mahtout

To cite this version:

Imane Mahtout. Youla-Kucera based multi-objective controllers : Application to autonomous vehicles. Automatic Control Engineering. Université Paris sciences et lettres, 2020. English. NNT : 2020UPSLM044 . tel-03126748

HAL Id: tel-03126748

https://pastel.hal.science/tel-03126748v1

Submitted on 1 Feb 2021

HAL is a multi-disciplinary open access archive for the deposit and dissemination of scientific research documents, whether they are published or not. The documents may come from teaching and research institutions in France or abroad, or from public or private research centers.

L'archive ouverte pluridisciplinaire **HAL**, est destinée au dépôt et à la diffusion de documents scientifiques de niveau recherche, publiés ou non, émanant des établissements d'enseignement et de recherche français ou étrangers, des laboratoires publics ou privés.

PSL UNIVERSITÉ PARIS

THÈSE DE DOCTORAT
DE L'UNIVERSITÉ PSL

Préparée à MINES ParisTech

Youla-Kucera based multi-objective controllers: Application to autonomous vehicles
Contrôleurs multi-objectifs basés sur Youla-Kucera: Application aux véhicules autonomes

Soutenue par

Imane MAHTOUT

Le 21 décembre 2020

École doctorale n°621

Ingénierie des Systèmes, Matériaux, Mécanique, Energétique

Spécialité

INFORMATIQUE TEMPS REEL, ROBOTIQUE ET AUTOMATIQUE

Composition du jury :

Philippe MARTINET INRIA Sophia Antipolis	*Président/Rapporteur*
Concepción MONJE Universidad Carlos III	*Rapporteur*
Lydie NOUVELIERE Univ d'Evry	*Examinateur*
Joshué PÉREZ RASTELLI Tecnalia	*Examinateur*
Vicente MILANES Renault	*Examinateur*
Fawzi NASHASHIBI INRIA Paris	*Directeur de thèse*

MINES ParisTech | PSL

To Lila, this accomplishment is also yours. Thank you for all the courage and strength you gave me.
To Abderrezak, I hope that will make you proud. Thank you for the perseverance that you taught me.

II

Acknowledgments

This thesis is the result of three years of hard and challenging work, but also passion and completion. Many people accompanied me to accomplish this work. I hope these few lines would express my gratitude and acknowledgment to to those how made it possible.

First of all, I thank Almighty God for giving me the courage, strength and patience to complete this modest work.

Great gratitude to my parents for their encouragement, aid and education. Thanks to Nawel for all the coffees, Nesrine for the awakenings, and Adam for the good evening atmosphere.

I would like to thank my supervisors Vicente and Fawzi for giving me the chance to integrate their teams and benefit from their research expertise, I learned a lot from their knowledge, within the multiple technical discussions. Without their supervision, patience and kindness this work could not be achieved .

For all my friends and colleagues, the people who shared this work, a big and sincere acknowledgment for all. Especially Riadh, Madjda, Asma, Lucille, Nievsabel, Hussam, Kathia, Raoul, Luis, Jean Marc for their help and all rewarding discussions.

A special and great gratitude to my colleagues and friends David and Francisco, for having welcomed me into the "dream team" and having shared their knowledge and experience, without their efforts and their help my work would not have been successful. I have learned a lot from them during these three years.

Contents

1 Introduction **3**
1.1 Motivation . . . 3
1.2 Objectives . . . 4
1.3 Manuscript organization . . . 5
1.4 Contribution . . . 6
1.5 Publication . . . 7
1.5.1 Journals . . . 7
1.5.2 Conferences . . . 8
1.5.3 Patents . . . 8

2 Youla-Kucera state-of-the-art review and applications **11**
2.1 Origins of YK parametrization . . . 12
2.1.1 Coprime factorization . . . 13
2.1.2 Q-parametrization . . . 14
2.1.3 S-parametrization . . . 14
2.1.4 (Q,S)-parametrization . . . 14
2.2 Q-based controller reconfiguration . . . 15
2.2.1 Control implementation . . . 16
2.2.2 Applications . . . 18
2.3 Q-based noise rejection and vibration control . . . 19
2.3.1 Control implementation . . . 19
2.3.2 Applications . . . 22
2.4 S-based closed-loop identification . . . 23
2.4.1 Identification scheme . . . 24
2.4.2 Applications . . . 25
2.5 (Q,S)-based adaptive control . . . 26
2.5.1 Control implementation . . . 26
2.5.2 Applications . . . 28
2.6 (Q,S)-based fault tolerant control . . . 28
2.6.1 Control implementation . . . 29
2.6.2 Applications . . . 30
2.7 (Q,S)-P&P and Multi Model Adaptive Control . . . 31
2.8 YK and Dual-YK Time Evolution . . . 32

2.9 Discussion 34

3 Youla-Kucera parametrization: Theory and principles 39
3.1 Introduction 39
3.2 Single controller limitations 40
3.2.1 Single multi-criteria controller 42
3.2.2 Linear controller switching 43
3.3 YK: definition and stability 46
3.3.1 Doubly Coprime Factorization 47
3.3.2 The class of all stabilizing controllers 49
3.3.3 Controller transition 51
3.3.4 Youla-Kucera controller stability analysis 53
3.4 Numerical example 61
3.5 Conclusion 65

4 Transient behavior analysis for YK control structures 67
4.1 YK control structure implementations 68
4.2 Transient behavior 70
4.2.1 γ placement 70
4.2.2 Initial and final controllers dynamics 72
4.2.3 Switching frequency 74
4.3 Conclusion 76

5 Lateral Control 79
5.1 Experimental platform description 80
5.2 Problem description 82
5.3 Lateral control review 84
5.4 Motivation on using Youla Kucera 87
5.5 Control design 89
5.5.1 Vehicle model 90
5.5.2 Steering actuator 93
5.5.3 Lateral controller 97
5.5.4 Stability Analysis 101
5.6 Simulation results 103
5.7 Experimental results 105
5.8 Conclusion 106

6 Longitudinal Control 109
6.1 Problem description 110
6.2 Longitudinal control review 113
6.3 Motivation on using Youla Kucera 116
6.4 Control design 117
6.4.1 Performant controller criteria 117
6.4.2 Robust controller criteria 118

6.4.3 Nominal controllers design 118
6.4.4 Parametrized controller $K(Q)$ 120
6.5 H_∞ controller 122
6.6 Comparison results 124
6.6.1 Frequency domain comparison 124
6.6.2 Temporal domain comparison 126
6.7 Experimental results 129
6.8 Conclusion 133

7 Discussion **135**
7.1 Conclusion 135
7.2 Future works 137

Chapitre 1

Introduction

Below is a French summary of chapter 1.
Le véhicule autonome peut percevoir et comprendre son environnement grâce à des systèmes de prise de décision basés sur l'intelligence artificielle (IA). Ces systèmes sont de plus en plus populaires en raison des avantages qu'ils peuvent apporter pour améliorer les performances des véhicules. Cependant, ces systèmes sont basés sur un apprentissage de l'environnement, exigeant une évolution continue également du point de vue du contrôle du véhicule. Ainsi, la reconfiguration automatique des contrôleurs peut être une solution pour garantir des hautes performances de conduite, l'objectif étant que le système de contrôle s'assure que la réponse du véhicule soit adaptée aux besoins de la partie décisionnelle dans chaque situation de manière sûre, fiable et robuste.

Le problème principal se pose lorsque la transition entre de tels algorithmes de contrôle se produit, conduisant à des instabilités indésirables. Cette thèse se concentre sur une étude plus approfondie des environnements dynamiques complexes qui conduira à des structures de contrôle avancées, permettant des transitions multi-contrôleurs tout en prenant en compte les dysfonctionnements de capteurs ou les circonstances de la circulation.

Cette thèse est développée dans le cadre du doctorat CIFRE. Les travaux de recherche ont été réalisés entre l'équipe Robotique et Systèmes de Transport Intelligents (RITS) de l'Institut National de Recherche en Informatique et en Automatique (INRIA) , en collaboration avec le constructeur automobile Renault (Technocentre). La motivation de la thèse, les objectifs, l'organisation du manuscrit et ses principales contributions sont présentés ce chapitre.

Chapter 1

Introduction

Autonomous vehicle can perceive and understand their environment thanks to Artificial-Intelligence (AI) based decision-making systems. Such systems are getting more and more popular because of the benefits they can bring to improve vehicle performance. However, these systems are based on a constant learning of the environment, demanding a continuous evolution also from the system control point of view. Thus automated controller reconfiguration can be a solution for guaranteeing the desired vehicle performance.

The aim is that the control system ensures that the vehicle response is suitable for the needs of the decision-making part in each traffic situation, being able to manage them in a safe, reliable and robust manner. The main problem arises when the transition between such control algorithms occurs, leading to undesirable instability responses. This PhD is focused on further investigate complex dynamic environment that will lead to advanced control structures, enabling multi-controller transitions while taking into account sensors failures or traffic circumstances.

This thesis is developed within the framework of the PhD CIFRE (from french: Convention Industrielle de Formation par la Recherche), research work has been accomplished between the Robotics and Intelligent Transportation Systems team (RITS) at the French national institute INRIA for research in computer science and automatics (from french: Institut National de Recherche en Informatique et en Automatique), in collaboration with Renault research centre (from french: Technocentre). The motivation of the thesis, the objectives, manuscript organization and its main contributions are presented below.

1.1 Motivation

Interest in intelligent vehicles research has been growing in the last two decades, with the aim of improving transportation security and comfort. Autonomous vehicle refers to technology that has the capability to drive

a vehicle without active physical control or monitoring by a human operator [1]. According to the Society of Automotive Engineers (SAE), five automation levels are defined: Levels 0–2 are those where the human driver needs to monitor the driving environment, and levels 3–5 are those where an automated driving system monitors the driving environment. The term "Autonomous driving" should refer only to the case where all the dynamic driving tasks, at all driving environment perception, can be performed by the vehicle's automated system [2]. This corresponds to SAE level 4 when it happens in a pre-defined Operational Design Domain (ODD) or SAE level 5 if the vehicle is able to deal with all circumstance no matter the ODD.

Driving requires a variety of functions, including localization, perception, planning and control [3]. Information acquisition is specific to localization and perception functions. Communications with other vehicles vehicle-to-vehicle (V2V), or with the infrastructure vehicle-to-infrastructure (V2I), can also be additional source of information to help the vehicle when negotiating intersection maneuvers [1]. However, the accuracy of these information may be degraded because of the on-board sensors' limitations, or the complexity of the algorithm processing the perceived data. Furthermore, the driving situations change depending on the road layout and potential interactions with other traffic agents. The aforementioned factors can lead to inappropriate vehicle motion. This work focuses on developing control structures and algorithms, ensuring the desired system performance regardless to the operating conditions, able to drastically change vehicle dynamics while keeping its stability.

The concept of controller reconfiguration by interpolating multiple controllers is tackled in the literature using different techniques. In this thesis, Youla-Kucera (YK) parametrization is explored as a controller reconfiguration framework, guaranteeing stable transition under arbitrary switching.

1.2 Objectives

The main objective of this PhD work is to further explore complex scenarios where autonomous vehicles can drive. Situations where different expectations can interact as keeping the vehicle in the lane but at the same time having a potential obstacle to avoid.

- Review of the state-of-the-art on YK and dual YK parametrizations field, and its use on different control applications.
- Understand different YK structures in the field of controller reconfiguration and switching, and analyze their respective responses according to the different benefits and drawbacks.
- Study the transient behavior when doing controller reconfiguration using YK parametrization.

- Application to lateral control of autonomous vehicles. Focusing on handling different driving situations involving lateral motion with a high performance level and keeping a comfortable feeling in the vehicle.
- Application to longitudinal control of autonomous vehicle. When dealing with the problem of inaccurate measurement caused by the limitations of the perception system. Longitudinal controller should be able to provide the best possible response in all circumstances, while maintaining longitudinal control stability, string stability and measurement noise rejection.
- Automatic control reconfiguration to achieve optimal performance in both lateral and longitudinal control is the principal challenge of this work. The final goal is to find the optimal control law to achieve the best performance possible when structural changes have been introduced.
- Focus is in obtaining control algorithms running in a real experimental research platform validating the efficiency of the proposed solutions in a real traffic conditions.

1.3 Manuscript organization

This PhD thesis has been organized in seven chapters. A brief overview of each of the remaining chapters is given below:
Chapter 2, Youla-Kucera state-of-the-art review and applications: This chapter presents a review of the YK and dual YK parametrizations related to different control fields. Especially, controller reconfiguration, identification, Plug&Play control, disturbance rejection, adaptive control, and fault tolerant control. Important groups worldwide are reviewed, classifying the recent work according to the use of YK or dual YK parametrizations or both, providing the latest advances with main successful applications developed in the last two decades in different control fields.
Chapter 3, Youla-Kucera parametrization: Theory and principles: The basis on building a multi-objective controller based on YK parametrization are presented in this chapter. It also introduces the mathematical framework of doubly coprime factors. A deep stability analysis of YK based controller is provided using stability notions of system with impulse effects. Numerical examples are given, showing the steps to build a YK based controller, and proving how it stabilizes a transition between two controllers where direct linear change results unstable, having a state dependent switching signal.
Chapter 4, Transient behavior analysis for YK control structures: This chapter studies the transient behavior of the different YK implementations according to different design parameter: switching signal placement,

closed-loop bandwidth capabilities of each controller; and switching signal frequency. The evaluation is carried out from the time-to-convergence point of view using a numerical example.
Chapter 5, Lateral Control: YK parametrization is explored to deal with lateral control problem of automated vehicles. The controller reconfiguration is based on a decision taking into account the lateral error corresponding to the driving situation, which allow the steering system to perform different maneuvers, while maintaining stability, control performance and passengers comfort.
Chapter 6, Longitudinal Control: This chapter presents a YK based ACC system for automated vehicles. The proposed control structure extends the classical ACC system capabilities by providing the best possible response when facing variable noise measurement, meaning that the controller is able to change in real time according to the noise level in the perception system, while maintaining longitudinal control stability, string stability and measurement noise rejection.
Chapter 7, Discussion: It includes conclusions and most important remarks, with respect to the problems addressed in the present thesis. As well as research perspective that could be derived from the results of this PhD work.

1.4 Contribution

The main contributions in the present dissertation are as follows:

1. YK parametrization allows stable controller reconfiguration within the set of the stabilizing controller for a given plant. Eight different implementations are derived in the literature with different benefits and drawbacks. A first comparative study concluded that one structure presents the best transient behavior without oscillations. However, the transient behavior could be enhanced from time to convergence point of view. In this thesis, the eight structures are compared with respect to three design parameters: 1) The position of the switching signal γ with respect to the YK parameter Q; 2) The nominal controller dynamic; 3) The frequency of the switching signal γ. This study results on implementation guidelines for each YK structure, in order to enhance the control performance during the transient behavior.

2. YK based lateral controller for autonomous vehicle is proposed to deal with the trade-off between precision in trajectory tracking and comfort when the driving situation changes in lateral motion. The proposed control strategy switches gradually between different controllers based on a look-ahead distance designed separately for each driving situation (i.e. lane change, lane tracking). It ensures smooth and stable

transitions between controllers and provides a smooth vehicle response regardless of the driving situation. The controller reconfiguration is based on a decision taking into account the lateral error corresponding to the driving situation.

3. A novel multi-objective YK based controller is designed to solve the trade-off between robustness and performance when noise measurement appears in Adaptive Cruise Control (ACC) systems. The YK based controller adapt the longitudinal vehicle motion to the perception system status. This solution extends the ACC system capabilities by providing the best possible response in all circumstances, meaning that the controller is able to change in real time according to the noise level in the perception system, while maintaining longitudinal control stability, string stability and measurement noise rejection.

4. YK based multi-objective controllers are proposed in this thesis, enhancing the performance of both longitudinal and lateral motion of autonomous vehicles. Proving the efficiency of the YK parameterization as a control framework when dealing with conflicting control objectives. For an initial validation the designed controllers was tested in simulation. Also experimental results demonstrate real implementation of stable controller reconfiguration using an electric automated Renault ZOE.

1.5 Publication

The scientific contributions derived as a result of the developed research work are listed below:

1.5.1 Journals

Title: Advances in Youla-Kucera parametrization: A Review
Authors: I. Mahtout, F. Navas, V. Milanés, F. Nashashibi
Journal: Annual Reviews in Control
Status: Published by Elsevier. **Volume:** 49, 2020. **Pages:** 81-94.

Title: On the Passenger Acceptance of Driverless Shuttles
Authors: V. Milanés, F. Navas, D. Gonzalez, I. Mahtout.
Journal IEEE Intelligent Transportation Systems Magazine
Status: Published by IEEE. **Date:** April 2020

Title: Youla-Kucera based Multi-objective Car Following Controller
Authors: I. Mahtout, F. Navas, D. Gonzalez, V. Milanés, F. Nashashibi
Journal Control Engineering Practice
Status: 1st revision.

1.5.2 Conferences

Title: Youla-Kucera based lateral controller for autonomous vehicle
Authors: I. Mahtout, F. Navas, D. Gonzalez, V. Milanés, F. Nashashibi
Conference: 2018 21st International IEEE Conference on Intelligent Transportation Systems (ITSC)
Place: Maui, Hawaii, USA **Date:** November 4-7

Title: Youla-Kucera control structures for switching
Authors: F. Navas, I. Mahtout, V. Milanés, F. Nashashibi
Conference: 2018 IEEE Conference on Control Technology and Applications (CCTA)
Place: Copenhagen, Denmark **Date:** August 21-24, 2018

Title: A first approach for a passenger-centered behavior on driverless vehicles
Authors: D. Gonzalez, F. Navas, I. Mahtout, V. Milanés
Conference: 2020 28th Mediterranean Conference on Control and Automation (MED)
Place: Saint-Raphael, FRANCE **Date:** September 16-18, 2020

1.5.3 Patents

Because of the CIFRE opportunity at Renault, I had the opportunity to collaborate on several projects, leading to different patents submissions. Below includes a list of my cooperation within my working time at Renault.

Title: Safety positioning device for autonomous vehicle with apparatus for taking the vehicle to a safe state
Authors: V. Milanés, I. Mahtout, D. Gonzalez, F. Navas
Status: Accepted in RENAULT SAS **Date: October 14, 2019**

Title: A vehicle dynamic model corrector with side slip estimation for adding safety capabilities in autonomous vehicle
Authors: I. Mahtout, V. Milanés, D. Gonzalez, F. Navas
Status: Accepted in RENAULT SAS **Date: September 23, 2019**

Title: Safety starting vehicle alignment apparatus for automated vehicle applications in autonomous mode engagement, docking/undocking and tele-operation maneuvers
Authors: V. Milanés, I. Mahtout, D. Gonzalez, F. Navas
Status: Accepted in RENAULT SAS **Date: August 28, 2019**

Title: Safety collision-free and string stable automated car following device
Authors: V. Milanés,I. Mahtout, D. Gonzalez, F. Navas
Status: Accepted in RENAULT SAS **Date: August 29, 2019**

Title: Apparatus and method for automatically model multi-brand multi-vehicle steering systems for auto-tuned autonomous lateral guidance device
Authors: V. Milanés, I. Mahtout, D. Gonzalez, F. Navas
Status: Accepted in RENAULT SAS **Date: April 04, 2020**

Title: Perception-adapted controller device for autonomous vehicles
Authors: I. Mahtout, V. Milanés, D. Gonzalez, F. Navas
Status: Under review in RENAULT SAS

Chapitre 2

Etat de l'art de la parametrisation de Youla-Kucera et ses applications.

Below is a French summary of chapter 2.

Ce chapitre correspond à un état de l'art réalisé du point de vue des applications utilisant la parametrisation de Youla-Kucera et son duel. Ces paramétrisations ont été utilisées dans différents systèmes de contrôle pratiques, couvrant la reconfiguration des contrôleurs, l'identification, le contrôle Plug&Play (P&P), le rejet des perturbations, le contrôle adaptatif et la commande tolérantes aux défauts.

L'origine de la paramétrisation de YK se situe dans les années 70, Youla [4, 5] et Kucera [6] ont développé la base scientifique. Ils ont proposé une paramétrisation qui fournit tous les régulateurs stabilisant un systeme linéaire dans une boucle de régulation à retour de sortie. Tous les régulateurs de stabilisant sont paramétrés en utilisant une fonction de transfert appelée paramètre de YK Q, conduisant à une forme de contrôlleurs $K(Q)$. Le paramètre $Q(s)$ garantit la stabilité de la structure de contrôle resultante. De même, sa théorie duelle (également connue sous le nom de paramétrisation duel de YK) fournit tous les systèmes linéaires stabilisées par un contrôleur donné. La classe de tous les systèmes stabilisés par un contrôleur dépend de la fonction de transfert appelée paramètre duel de YK S, donc $G(S)$. Ce paramètre peut représenter n'importe quelle variation du système. Ainsi, cette façon utile de paramétrer soit les systèmes, soit les contrôleurs, soit les deux, est utilisée pour résoudre de nombreux problèmes de contrôle.

Ce chapitre rassemble les travaux récents et les classifie selon l'utilisation de la paramétrisation YK ou de la duelle paramétrisation de YK ou des deux, en fournissant les dernières avancées avec les principales applications réussies développées au cours des deux dernières décennies dans différents domaines de contrôle. Une discussion finale donne un aperçu des tendances futures dans ce domaine.

Chapter 2

Youla-Kucera state-of-the-art review and applications

This chapter corresponds to a state-of-the-art review that was carried out from the applications of YK and dual YK parametrizations point of view. These parametrizations have been used in different practical control systems, covering controller reconfiguration, identification, Plug&Play (P&P) control, disturbance rejection, adaptive control, and fault tolerant control.

YK parametrization was formulated in the late 70s for obtaining the set of controllers stabilizing a linear plant. This fundamental result of control theory has been used to develop theoretical tools solving many practical control problems. This chapter collects the recent work and classifies them according to the use of YK parametrization or dual YK parametrization or both, providing the latest advances with main successful applications developed in the last two decades in different control fields. A final discussion gives some insights on the future trends in the field.

The rest of the chapter is organized as follows: Section 2.1 presents fundamentals and mathematical basis of YK and dual YK parametrizations. Section 2.2 presents the use of the YK parameter Q as a technique of controller reconfiguration for both Linear Time-Invariant (LTI) and Linear Parameter-Variant (LPV) systems. Disturbance and noise rejection control structure based on the YK parameter Q is explained in section 2.3. In section 2.4, the use of dual YK parameter in closed-loop identification is presented. The combination of both YK parameter and dual YK parameter in adaptive control field is detailed in section 2.5. The fault tolerant control scheme based on YK framework is detailed in section 2.6. In section 2.7, the use of YK parametrizations in Plug & Play control and Multi Model Adaptive Control is briefly reviewed. Finally, some challenging issues about the use of YK parametrization are discussed in the last section.

2.1 Origins of YK parametrization

The origin of the YK parameterization is in the 70s, Youla [4,5] and Kucera [6] developed the scientific basis. They proposed a parameterization that provides all linear stabilizing controllers for a given LTI plant in a feedback control loop (see Fig. 2.1). All stabilizing controllers are parametrized based on the transfer function called YK parameter Q, leading to a control form $K(Q)$. The parameter $Q(s)$ is the one guaranteeing the stability. Similarly, its dual theory (also known as the dual YK parametrization) provides all the linear plants stabilized by a given controller. The class of all the plants stabilized by a controller depends on the transfer function called dual YK parameter S, so $G(S)$. This parameter could represent any plant variations. Hence, this useful way of parametrizing either plants, controllers or both is employed to solve many control issues.

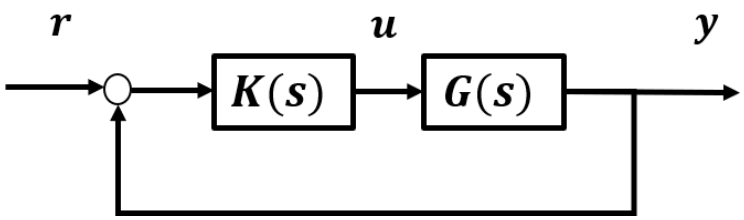

Figure 2.1: Feedback control loop block diagram.

According to the control objectives, three main configurations can be targeted:

- **Controller parametrization** allows stable controller reconfiguration when some change occurs. It is also widely used in disturbance and noise rejection control. A number of successful applications can be found in the last two decades, being the most used approach in different control fields [7].

- **Plant parametrization** is employed to solve the problem of closed-loop identification. Some successful implementation can be found in Plug & Play control where the dynamics of new sensors or actuators are identified on real-time without system disconnection [8].

- **Simultaneous control and plant parametrization** provides a new control structure that changes according to new identified dynamics on the plant. This principle is mainly used in fault tolerant control and adaptive control [9].

Let's consider a Single-Input-Single-Output (SISO) stable plant $G(s)$ connected to a given controller $K(s)$ in a stable feedback loop depicted in

fig. 2.1. Closed-loop transfer function $CL(s)$ from reference r to output y is in the following equation:

$$CL(s) = \frac{K(s)G(s)}{1 + K(s)G(s)} \tag{2.1}$$

The transfer function from the reference $r(s)$ to the controller output $u(s)$ yields:

$$Q(s) = \frac{K(s)}{1 + K(s)G(s)} \tag{2.2}$$

if $Q(s)$ and $G(s)$ are known, the controller $K(s)$ can be expressed as:

$$K(s) = \frac{Q(s)}{1 - G(s)Q(s)} \tag{2.3}$$

If $K(s)$ is stabilizing $G(s)$, $Q(s)$ is stable and proper. Reciprocally, if $Q(s)$ is stable and proper, it is easy to demonstrate that $K(s)$ stabilizes $G(s)$ using Eq. 2.3.

Thus, stabilizing controllers can be parametrized in terms of the set of all stable proper functions $Q(s)$ for a given plant $G(s)$.

Furthermore, the closed-loop transfer function $CL(s)$ in Eq. 2.1 becomes linear in terms of $Q(s)$ and $G(s)$ which is not the case with $K(s)$.

$$CL(s) = G(s)Q(s) \tag{2.4}$$

From those two results (2.3,2.4), the concept of controllers parametrization appeared in [10] applied to scalar only known and stable plants.

Youla et *al.* [4,5] and Kucera [6] explained simultaneously how the initial idea of controller parametrization can be extended to cover Multi-Inputs-Multi-Outputs (MIMO) plants and that are not necessarily stable. A set of all stabilizing controllers for a given plant is characterized using the so called YK parameter $Q(s)$.

Conversely, a dual concept is proposed by leading the same reasoning in equations (2.2) and (2.3) and use the fact that $K(s)$ and $G(s)$ are commutative. The set of all plants stabilized by a given stabilizing controller is characterized using the so called dual YK parameter $S(s)$ [8].

2.1.1 Coprime factorization

Both YK and dual YK parametrization are based on the doubly coprime factorization [11, 12] to reduce algebraic complexity in computing $Q(s)$ and $S(s)$.

The plant model and controller matrix transfer functions are factorized as a product of a stable transfer function matrix and a transfer function matrix with a stable inverse with no common unstable zeros as follows:

$$G = NM^{-1} = \tilde{M}^{-1}\tilde{N} \tag{2.5}$$

$$K = UV^{-1} = \tilde{V}^{-1}\tilde{U} \tag{2.6}$$

These coprime factors are calculated using pole placement technique (see section 3.3.1 for details) to satisfy the following double *Bezout identity* [13]:

$$\begin{bmatrix} \tilde{V} & -\tilde{U} \\ -\tilde{N} & \tilde{M} \end{bmatrix} \begin{bmatrix} M & U \\ N & V \end{bmatrix} = \begin{bmatrix} M & U \\ N & V \end{bmatrix} \begin{bmatrix} \tilde{V} & -\tilde{U} \\ -\tilde{N} & \tilde{M} \end{bmatrix} = \begin{bmatrix} I & 0 \\ 0 & I \end{bmatrix} \tag{2.7}$$

2.1.2 Q-parametrization

The YK parametrization Q describes how the set of all stabilizing controllers for a given plant $G(s)$ can be characterized from knowing a controller $K(s)$ stabilizing the given plant $G(s)$.

Lemma 1. Let a plant $G = MN^{-1}$, with N and M coprime and stable, be stabilised by a controller $K = UV^{-1}$, with U and V coprime and stable. Then the set of all stabilizing controllers for G is given as a function of a stable filter YK parameter Q with appropriate dimensions (see [7]):

$$\begin{aligned} K &= \left\{ K(Q) = (U + MQ)(V + NQ)^{-1} \right\} \\ &= \left\{ K(Q) = (\tilde{V} + Q\tilde{N})^{-1}(\tilde{U} + Q\tilde{M}) \right\} \end{aligned}$$

2.1.3 S-parametrization

The dual-YK parametrization S describes how the set of all the plants stabilized by a given controller $K(s)$ can be characterized from knowing a plant $G(s)$ stabilized by the given controller $K(s)$.

Lemma 2. Let a plant $G = NM^{-1}$, with N and M coprime and stable, be stabilized by a controller (in positive feedback loop) $K = UV^{-1}$, with U an V are coprime and stable. Then the set of all the plant stabilized by K is given as:

$$\begin{aligned} G &= \left\{ G(S) = (N + SV)(M + SU)^{-1} \right\} \\ &= \left\{ G(S) = (\tilde{M} + \tilde{U}S)^{-1}(\tilde{N} + \tilde{V}S) \right\} \end{aligned} \tag{2.8}$$

2.1.4 (Q,S)-parametrization

Finally, let's consider the connection between both parametrizations. The parametrized controller $K(Q)$ described in Eq. 2.3 is connected to the parametrized plant $G(S)$ described in Eq. 2.8. The resulting closed loop is in Fig. 2.2.

Lemma 3. The stability of $[G(S), K(Q)]$ is equivalent to the stability of the positive closed-loop $[Q, S]$ [9].

Hence, this useful linear way of parametrizing either controllers, plants or both is employed to solve many control issues. The rest of the chapter

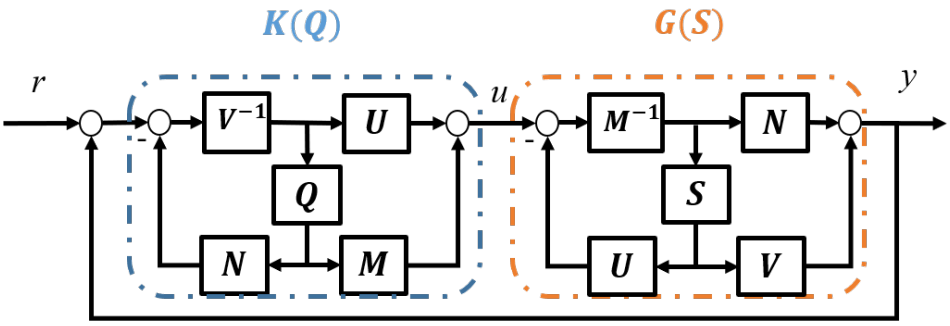

Figure 2.2: $K(Q)$ is the set of all controllers stabilizing the plant $G = MN^{-1}$. $G(S)$ is the set of all the plants stabilized by the controller $K = UV^{-1}$.

reviews the control applications developed in the last two decades by using Q, S or both in one system.

2.2 Q-based controller reconfiguration

The main motivation behind controller reconfiguration is performance enhancement while controlling complex systems with multiple control objectives in dynamical environments. Achieving different performance specifications (i.e desired bandwidth, time response, robustness against modeling errors) can be hard while using a single controller. The design process inevitably requires compromises or trade-offs between various conflicting performance objectives. A common solution is designing a controller for each objective, and appropriately switching/interpolating among them in order to accommodate the changing operating conditions, reaching a satisfactory performance level and guarantying overall system stability.

The concept of controller reconfiguration by switching/interpolation different controllers is tackled in the literature [14] using different techniques as self-scheduled approach [15], ad-hoc technique [16] or bumpless transfer [17].

Controller reconfiguration using YK parametrization is done by mapping a set of linear stabilizing controllers onto a Q-based controller. Main advantages of using YK parametrization in controllers switching/interpolation are: 1) It allows stable switching between open-loop unstable controllers [18]; 2) Switched/interpolated controllers can be designed and tuned separately using different techniques (H_∞, LQR, PID) [7]; 3) The closed-loop stability is guaranteed under arbitrary interpolation/switching between different stabilizing controllers [19].

The first application of YK parametrization in controller reconfiguration was in the 80s. Two controllers $K1$ and $K2$ were designed to ensure reference tracking and disturbance minimization respectively [20]. Both controllers

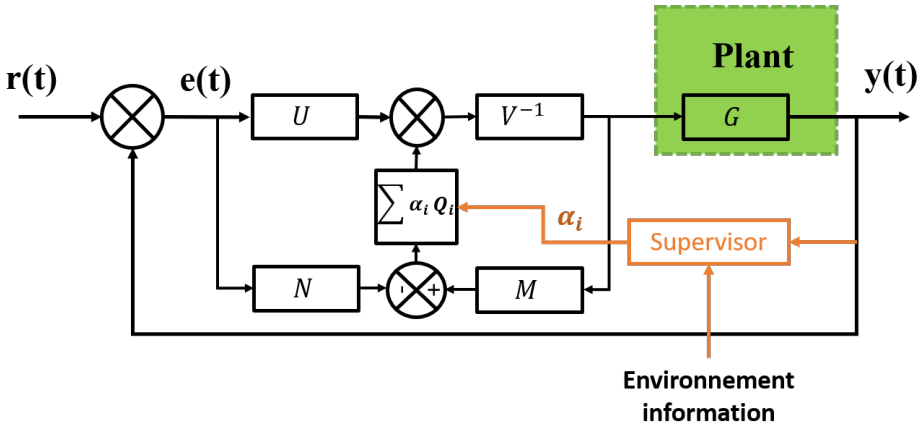

Figure 2.3: Q-based multi-controller scheme.

were mapped in a single controller structure using two YK parameters $Q1$ and $Q2$.

After that, the use of YK parameter Q in controller reconfiguration evolved from interpolating two controllers mapping many controllers and switching arbitrary between them. Covering both LTI and LPV frameworks.

In this section, YK Q-based controller reconfiguration in both LTI and LPV frameworks are reviewed. Different applications are highlighted showing the transfer from theory to practice in real time experimentation.

2.2.1 Control implementation

In LTI control framework, a fixed LTI plant is considered $G = NM^{-1}$. Several LTI controllers K_i are designed separately, all of them stabilizing the plant G and each controller fulfilling a specific control objective. The set of controllers K_i are mapped in a multi-controller architecture shown in Fig. 2.3 using YK parameter Q as follow :

$$K(\alpha_i Q_i) = (U + M\sum_{i=1}^{i=n} \alpha_i Q_i)(V + N\sum_{i=1}^{i=n} \alpha_i Q_i)^{-1} \tag{2.9}$$

Each parameter Q_i is computed to connect the controller K_i to the nominal controller $K = UV^{-1}$:

$$Q_i = (\tilde{U}_i V - \tilde{V}_i U) \tag{2.10}$$

The interpolation signal $\alpha_i \in [0, 1]$ represents the fraction of the controller K_i that is activated at each instant. α_i is computed online by a supervisor that orchestrates the switching between the pre-designed controllers with respect to a performance metric. It is computed using the system output and the current operating conditions described by the environment information.

The goal of the Q-based multi-controller is not only keeping closed-loop stability while switching/interpolation between controllers, but also satisfying a desired level of performance at each instance.

In LPV framework, a LPV plant is assumed $G(\theta)$, where θ is a scheduling parameter within a predefined range $\theta \in [\theta_{min}, \theta_{max}]$, with a set of critical design points $\theta_i, i = 1, .., n$.

In many cases, a LPV plant model is a result of a linearisation technique applied to a non linear system, and θ is tied to the system physics (i.e. speed-dependent on lateral vehicle dynamics using the bicycle model, where the parameter θ is the vehicle speed and its inverse). In each critical design point $\theta = \theta_i$, a controller K_i stabilizing $G(\theta_i)$ is designed to satisfy specific performance criteria, the controller K_i is thus named local controller.

Using YK Q parameter, local controllers can be interpolated in a control scheme that satisfies: 1) stability of the closed-loop including the nonlinear plant (linearized into LPV system) under fast changes of the system parameter θ; 2) recovering the local controllers K_i in the critical design points; 3) covering a broad class of local controllers as in LTI framework, including those with multiple inputs/outputs, open-loop unstable dynamics, and controllers with different orders and designed by different techniques (H_∞, PID, LQR).

Q-based multi-controller structure for LPV plant is designed following the steps: first, a nominal controller $K_0(\theta)$ is designed to stabilize the LPV plant over the range $[\theta_{min}, \theta_{max}]$ without any performance specification (not necessarily LPV controller). Then, local controllers $K_i(\theta_i)$ can be designed to achieve high performance in critical operating points. Once controllers are designed, they need to be decomposed to LPV coprime factors satisfying a LPV double Bezout identity as the one in [21]:

$$G(\theta) = N(\theta)M(\theta)^{-1} = \tilde{M}(\theta)^{-1}\tilde{N}(\theta) \tag{2.11}$$

$$K_0(\theta) = U_0(\theta)V_0(\theta)^{-1} = \tilde{V}_0(\theta)^{-1}\tilde{U}_0(\theta) \tag{2.12}$$

$$K_i = U_i V_i^{-1} = \tilde{V}_i^{-1}\tilde{U}_i \tag{2.13}$$

The set of all controllers K_i assumed stabilizing the LTI plants $G(\theta_i)$; are mapped in a Q-based controller $K(\theta) = F_l(J_K(\theta), Q(\theta))$, where F_l is a lower fractional transformation of the interconnection system $J_K(\theta)$ and $Q(\theta)$ (see [7] for details).

The interconnection system $J_K(\theta)$ includes the nominal controller $K_0(\theta)$ stabilizing the LPV plant over the range of θ:

$$J_K(\theta) = \begin{bmatrix} U_0(\theta)V_0(\theta)^{-1} & \tilde{V}_0(\theta) \\ V_0(\theta)^{-1} & V_0(\theta)^{-1}N(\theta) \end{bmatrix} \tag{2.14}$$

and the YK parameter Q is computed to recover the local controllers K_i in the design point $\theta = \theta_i$ using a polytopic system $Q(\theta)$ formed by Q_i and a selected weighting function $\alpha = f(\theta)$ such as:

$$Q_i = (\tilde{U}_i V_0(\theta_i) - \tilde{V}_i U_0(\theta_i)) \tag{2.15}$$

The stability of the Q-based LPV controller is proved using a common Lyaponov function all over the range of the parameter θ [22].

An important consequence of using the YK LPV framework is that LTI design techniques can be adopted for LPV plants too.

2.2.2 Applications

YK parametrization Q in LTI controllers switching/interpolations has been used in different applications requiring multiple control objectives.

Related to LTI, the intrinsic conflict between performance and robustness in standard feedback loop is tackeled in in [19], a Q-based YK controller is used to control the roll angle of an aircraft. Based on a supervisor [23], the YK controller switches between a high performance controller when the measured angle is not noisy, to a robust controller when there are model uncertainties and external disturbances.

In [24] Q-based controller is used to control two classes of complex systems: Irrigation systems and Hypersonic vehicles with flexible dynamics. Both classes are generally described by hyperbolic partial differential equations. The Q-based controller switches between different LTI controllers to accommodate time-domaine specifications (i.e. peak value of control signal, overshoot). In [25, 26] a method for introducing new components in the control loop in a stable way is presented using the Q-based controller. The controller reconfiguration is illustrated on a livestock stable climate system, where a new temperature measurement becomes available during system operation and a new controller is added to the existent control loop. In [27] a sequential stepwise commissioning controller for a steam boiler is developed, the Q-based controller switches gradually between two stabilizing controllers with different objectives, the primary one is to keep the water level within max and min bounds, and the second control objective is to keep the feed water flow steady. In [28, 29] the Q-parametrization is used in the field of Intelligent Transportation Systems (ITS), the proposed control structure ensure stable switching between Cooperative Adaptive Cruise Control system (CACC) and ACC when the communication between vehicles fails. Another application in ITS is provided in [30], a lateral control structure is proposed to deal with different initial lateral error by switching between two controllers with different objectives.

The use of YK parametrization Q in LPV plants is illustrated in different LPV systems. In [22] a parameter varying mass-spring-damper system with varying stifnessis is controlled using Q-based controller. In [21] a nonlinear MIMO plant modeling a quadruple tank system controlling the water height in four tanks using two valves; the plant changes from minimum phase to a non minimum-phase with respect to the operating points (valves values).

The Q-based LPV controller switches between a MIMO PID controller designed in the minimum phase operating point to an H_∞ controller in the non-minimum phase operating point. The Q-based controller shows optimal performance in both operating conditions. In [31] the LPV Q-based controller is used in fixed pole assignment application, the Q-based controller switches among different controllers to locate the closed-loop poles always at the same place independently of the varying parameter. Thus, the LPV closed-loop achieves the same performance in the range of the varying parameter without loosing stability. In [32] a Q-based LPV controller is designed to control a simulated missile autopilot, the system is modeled using a LPV plant with four design points. The LPV Q-based controller achieves higher performance compared to a classical gain scheduling LPV controller.

2.3 Q-based noise rejection and vibration control

The problem of noise rejection and vibration control is widely studied in control systems. Such imperfections in control structures are often due to hardware problems (i.e. signal acquisition in sensors, delays in actuators) or environmental disturbances (i.e. external vibrations).

Disturbance and noise rejection have been tackled using different techniques: Pole placement [33], output sensitivity shaping [34], H_∞ [35] and linear matrix inequality (LMI) approach [36].

YK parametrization is used in noise rejection and vibration control through Q-based controller adaptation. Since the plant is assumed known and constant with eventual small variations, disturbance and noise can be handled just by Q modification.

The first application of YK parametrization in disturbance rejection was in 1992 where a feedback controller that can achieve: closed-loop stability; a unit step response and a known sinusoidal disturbance rejection [37] was designed. Authors used the relation between the sensitivity function of the closed-loop and YK parameter Q to design the required parametrized controller. After that, the design of YK parameter Q evolved from offline to online and adaptive design, covering feedback and feedforward implementations.

This section presents the advantages of using YK parametrization both in adaptive feedback configuration as well as in adaptive feed-forward compensation schemes. Recent developments and applications are gathered in a non exhaustive list.

2.3.1 Control implementation

During the last two decades, the use of YK parameter Q in noise and disturbance rejection evolved from rejecting a known noise signal with a given

frequency to variable known and unknown spectral characteristics. Different implementations of the YK parameter Q are proposed according to the disturbance type [38].

When a non-correlated measurement with the disturbance signal is available, adaptive feedback controller (see Fig. 2.4) is used. If the disturbance structure is a priori known (i.e. single frequency signal) the adaptation is direct, otherwise it is indirect.

In direct feedback adaptation, the objective is to directly estimate YK parameter Q which minimizes the disturbance effect without affecting closed-loop stability. This is possible since the disturbance structure is known, thus allowing to define the order of Q. According to [39] two coefficients in the polynomial Q are enough to characterize the frequency of an unknown sinusoidal disturbance. Parameters of the Q filter are adjusted online by minimizing an adaptation error describing the mismatch between the response of the theoretical system model and the disturbed measured response. Error minimisation requires using Parametric Adaptation Algorithm (PAA) [40].

In indirect feedback adaptation, the objective of noise attenuation is reached in two steps: 1) identify the disturbance structure by building a disturbance observer (DO); and 2) design a feedback controller achieving different attenuation levels in the frequency domain (not necessarily total rejection as in direct adaptation), by shaping in real time the output sensitivity function to a desired one, assigning an amount of attenuation for each narrow-band disturbance. The updated controller is computed by solving the Bezout equation, the use of YK parametrization allows to reduce the computation load since it simplifies the optimized error equation [41].

Successful application on rejecting unknown and time varying multiple narrow band disturbances on active suspension test bench is published in [42]. The proposed benchmark validates comparatively seven various approaches to adaptive rejection of multiple narrow-band disturbances in active vibration control. Interestingly, all the approaches can be interpreted as YK parametrization of a special kind. The seven approaches has several differences from a methodological point of view: 1) Plant factorization method; 2) The disturbance observer based signal (i.e. input error, output error, equation error); 3) Type of Q filter (i.e. FIR, IIR, combination of both FIR and IIR and others); 4) Nominal controller design (i.e. H2, LQR, pole placement); 5) Disturbance rejection technique (i.e. Output sensitivity shaping, inverse model principal); 6) Type of adaptation (i.e. direct, indirect); 7) Error signal for adaptation. The seven approaches are tested in simulation and in practice using a test bed based in an inertial actuator and equipped with a shaker and a measurement of the residual force. Results are evaluated according to following criteria: 1) Control performance in both steady state and transient responses; 2) Robustness is evaluated with respect to plant uncertainties (low damped complex zeros non identified in the test-bed), this criteria is assessed by defining a normalized performance

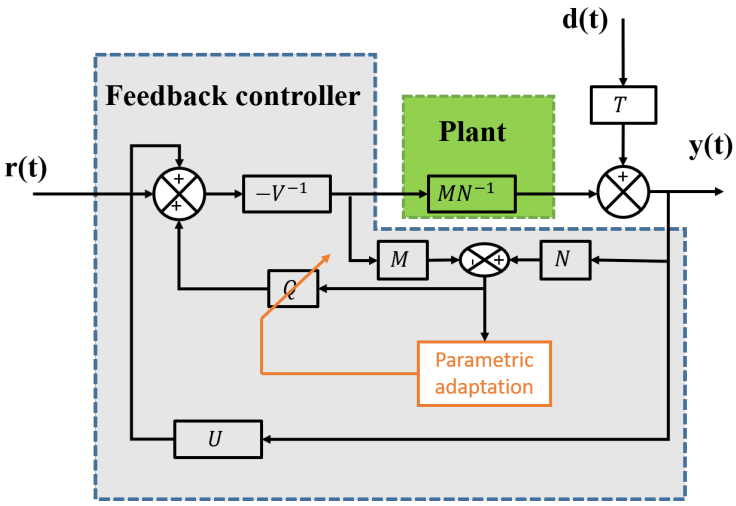

Figure 2.4: YK feedback controller scheme: the disturbance propagates through the plant T (so called primary path) and the compensation is done through the plant (MN^{-1}) driven by a feedback compensator. [39]

loss between simulation and practical results; 3) The complexity of each method is evaluated using the measurement of the Task Execution Time (TET) is used. This benchmark provides useful insights for choosing the best approach according to given constrains.

When a correlation exists between the disturbance signal and measurement, adaptive feedforward controller is used to compensate broad-band disturbances [44].

The main problem in adaptive feedforward control is the internal positive feedback between the compensation system and the reference source that can cause instabilities (see Fig. 2.5) while adapting the controller parameters. The use of the YK parametrization allows the separation between the stabilization of the internal positive feedback problem and the optimization of the feedforward controller parameters minimising the residual noise [45]. The feedforward controller can be designed either using direct adaptive configuration or indirect one; In indirect configuration, the controller is estimated over a certain time horizon. Then, the YK parameter Q is deduced to switch from the nominal controller to the updated one (see Section 2.2). In direct configuration, a tuning algorithm is developed to define design adaptive Finite Impulse Response (FIR) or Infinite Impulse Response (IIR) compensators as a YK parameter Q and update directly the controller that minimizes the residual noise [38].

The main difference between the use of feedback and feedforward implementations relies on the availability of a measurable signal correlated with the noise or the vibration. Also, adaptive feedback implementation is

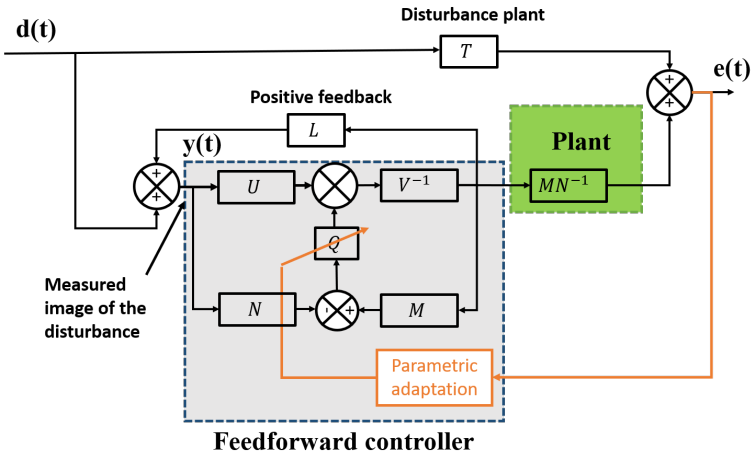

Figure 2.5: YK feedforward controller scheme: the disturbance d(t) propagates through T (so called primary path) and its effect is compensated through the plant (MN^{-1}) driven by a feedforward compensator. The input to the feedforward compensator is the sum of the image of the disturbance and of the internal positive feedback. [43]

more dedicated to single and multiple narrow-band disturbances and vibrations rejection. While adaptive feedforward implementation is particularly dedicated to the attenuation of broad-band noise with unknown and time-varying characteristics [43].

2.3.2 Applications

The use of YK parametrization Q in adaptive noise and vibration rejection context covered different applications requiring high control precision and low noise sensitivity as: wafer scanning in semiconductors [46], data storage systems (reading/writing) [39, 47, 48], mechatronics [49], active suspension systems [40, 50] and biochemistry [51] where the regulation problem is to maximize the biomass productivity in the fed-batch fermentation of a specie of yeasts and the cell growth is an undesirable consequence and considered as an unstable disturbance. The specificity of this application is that the YK parameter Q represents an extra degree of freedom in the controller considering the disturbance model, and allowing the rejection of this unstable.

A YK based feedback controller rejecting bounded disturbances is extended to cover LPV systems using LMI computation toolbox in [52].

Those encouraging experimental results showed how YK can be used to deal with different disturbance types rejection. Table 2.1 presents an overview with the different practical applications, including details on the disturbance type and YK controller design.

Table 2.1: Applications on the use of YK in disturbance rejection.

Noise	Controller	Applications
No information is available on real time	Feedback controller using a DO (Indirect adapation)	Data storage system [48]: - Multiple narrow band disturbance. - Controller is computed online to filter the observed disturbance. - Q is deduced as a weighted notch filter to switch to the final controller.
	Feedback controller with PAA (Direct adaptation) -YK parameter Q is computed by the PAA to mininize the noise effect.	Acoustic duct [53]: - Single varying sinusoidal disturbance. - Q parameter is a FIR with 2 parameters. Active suspension [50]: - Single varying narrow band disturbance . Blu Ray Disc [39]: - Repetitive narrow band disturbance . Road profiler [40]: - The road profile is modeled as a disturbance with time varying charachteristics acting on the vehicle dynamics . - The estimated Q polynome represents the road profile
Correlated measurement is available on real time	Feedforward controller using DO (Indirect adaptation)	Astronomical Telescope [54]: - Low frequency large-magnitude narrow-band disturbances. - Different Q designed offline are compared experimentally .
	Feedforward controller with PAA (Direct adaptation)	Duct active noise test-bench [43]: - Broad band disturbance. - Comparaison between IIR and FIR YK parameter Q is provided. - FIR Q filter is more robust.

2.4 S-based closed-loop identification

System dynamics identification is an essential step for any control design. Initially, identification techniques were developed to carry out open-loop identification. However, in practice many plants cannot be easily operated in open loop for carrying an identification protocol for different reasons (i.e. open loop unstable, integrator behavior). Additionally, some controllers may be already in place without the option to be disconnected to the plant, being the close loop identification the only way to obtain a better model for either designing a new controller or re-tuning the exiting one in an adaptive way. Several theoretical tools for closed loop identification are proposed in the literature [55]. Dual YK parameterization S has been used to cope with some of the problems related to closed-loop identification of system dynamics [56].

In order to clarify the differences between both, and to see in which case is useful to use the YK-based closed-loop identification, this section compares a general open-loop identification setup with a general closed-loop identification setup, highlighting the advantages of using the second one. Origin and evolution of this dual YK-based identification scheme are also explained. Finally, some practical applications are provided in subsection 2.4.2.

2.4.1 Identification scheme

The identification procedure is the first step to achieve the linear models of the unknown systems. First let's consider two kinds of identification setups:

- Open-loop identification: This method used when the control input u and measurement noise n are assumed to be non-correlated. Some control input u can be applied to the system G, obtaining the corresponding output y with noise n:

$$y = Gu + n \tag{2.16}$$

  If measurements u and y are available, many open-loop identification schemes (Auto Regressive model with eXternal inputs ARX [57], PBSIDopt [58] ...) can be used to find cross-correlation with u, and estimate G_i

$$\Phi_{yu} = G\Phi_{uu} + \Phi_{nu} \tag{2.17}$$

  where $\Phi_{nu} = 0$ as n and u are independent.

- Closed-identification: This method is used when the control loop is closed and the system is connected to a controller K, where reference signal r and output noise n are non-correlated. Equation 2.17 remains, but Φ_{nu} is not zero, as n is feedback through the controller K affecting the control signal u. Cross-correlation expression results:

$$\Phi_{yu} = G\Phi_{uu} - (1 + K^*G^*)^{-1}\Phi_{nn} \tag{2.18}$$

  where the superscript * denotes complex conjugation on the $j\omega$ axis.

  The identification process becomes complex. Even if Φ_{nn} is really small, Eq. 2.18 denotes that G should be stable, which could not be the case. As a solution, one could seek to estimate the closed-loop transfer function from the reference signal r to y: $P = KG(1+KG)^{-1}$. Once an estimation of the CL function is obtained $\hat{P}$, an estimation of the real system $\hat{G}$ would be:

$$\hat{G} = \frac{\hat{P}}{K(1-\hat{P})} \tag{2.19}$$

  but problems could occur if K has some unstables poles/zeros; the estimation could result again unstable.

It is then logical to disconnect the plant in order to carry out an open-loop identification. But there will be cases in which this is not possible: The plant is unstable, disconnecting the plant supposes a great economic cost, the feedback controller is embedded in the system, or an online estimation of the system is needed for controller improvement.

Between open-loop and closed-loop identification methods, it is well-known that for model-based control design, closed-loop identification gives better performance [59]. However, one needs to deal with its associated difficulties: Linear matrix inequality (LMI) feasibility [60], linear fractional dependence with respect to measured variables [61] or linear-deterministic subspace selection [62] are some examples picturing these difficulties.

The dual YK-parameterization S is used in closed-loop identification as a solution to suppress its difficulties [63,64] (called Hansen scheme). Specifically, given a LTI initial model and a controller, the key idea was to identify the dual YK S instead of the plant model G. Interestingly, the identification of S was a standard open-loop identification problem, so a closed-loop problem is transformed into an open-loop-like problem. Several analysis demonstrated how the obtained model with the Hansen scheme is superior than an open-loop identification solution for subsequent control design [65] [66].

The original LTI Hansen scheme has been modified and extended to deal with more complex systems:

- Related to LTI, [67] presented a modification able to tune the order of the resulting model given by the Hansen scheme. The idea is to have control over the possible order explosion when the model is employed in any adaptive control law; [7] extended the scheme when connected to a controller with the YK filter Q. Robust stabilization results connecting $K(Q)$ and $G(S)$ are here useful for unbiased identification of S when a YK parameter Q is applied; [68] modified the original identification scheme in order to avoid the use of indirect excitation signals in reference and feedforward inputs. It imposes any desired excitation signal for the identification of S without affecting those.

- The Hansen scheme has been also extended to LPV systems [69] [70]. Interesting results are obtained in terms of stability, and doubly coprime factors based on these scheduling parameters of the LPV system.

- Related to system with a changing number of inputs/outputs, [71] modified the Hansen scheme in order to deal with new measurements that become available during online operation. New dynamics related to new sensors are identified by the dual YK parameter S.

- A non-linear initial model G_0 connected to a stabilizing controller K_0 is considered in [72] [73].

2.4.2 Applications

Closed-loop identification of a piezoelectrically controlled gas bearing using the modified version of the original Hansen scheme in [68] was presented in [74]. It highlights the need of closed-loop identification since the system is unstable without feedback control.

Related to LPV, simulation results of coupled dynamics identification in heat distribution systems with different valve settings are in [70]. Corresponding experimental results are in [75]. Specifically, strong coupling dynamics in the network are identified after a consumption increment. On the other hand, experimental results related to low-speed longitudinal vehicle dynamics are presented in [76].

Concerning the identification of new sensors added to a system, simulation results with a livestock stable ventilation system were presented in [71]. A new temperature sensor is added in order to regulate better the temperature of the stable. The proper identification of the sensor allows the correct adaptation of the corresponding temperature control system.

2.5 (Q,S)-based adaptive control

As already stated, the linearity of Q within the closed-loop function facilitates optimization over the class of all stabilizing controllers. The YK parameter Q allows to achieve various control performance objectives. Every single controller could be augmented with Q and results in another controller having different control objectives. The assumption the implementation of YK-based multi controller as presented in section 2.2 is that the pant model is known and the controllers are predefined.

In this section, Q is seen as a stable filter that can be optimized/adapted offline or online in order to improve the system performance depending on the desired response. Also, this section reviews the methods that adapt the parameter Q using the parametrized plant $G(S)$, where the augmentation S contains the dynamics that are not modeled in the nominal plant G.

Notice that this differs from the solution in section 2.2, where controllers for different system responses are designed a-priori, switching between them depending on any intelligent algorithm that considers the system environment.

2.5.1 Control implementation

There are many different ways of designing the corresponding Q to adapt the controller to the specific system situation. This section summarizes some of them highlighting in which situations each solution should be employed. Q, S or both are employed depending if an identification process would be needed to correctly modify the corresponding controller.

- Q-offline optimization: The most basic approach used to compute YK parameter Q in designing Q-based adaptive controllers is offline optimization. The idea is to design a controller in the class of all stabilizing controllers. Different control performance objectives can be set in order to optimize Q. These performance requirements can be described

in time or frequency domain. System norms in the frequency domain is directly related to $\mathcal{H}_\infty$ and $\mathcal{H}_2$ concepts. For instance, penalization of the energy of the tracking error and control energy are examples of $\mathcal{H}_2$ control; while penalizing the maximum tracking error subject to control limits is an example of $\mathcal{H}_\infty$ control. Specifically, in [77], loop recovery was achieved by augmenting the original $\mathcal{H}_2$ controller with the additional filter Q. They showed how full or partial loop recovery may be obtained depending if minimum or non-minimum phase plants are considered. Improvements over standard loop recovery techniques were obtained.

- Q-online optimization: Offline optimization evolved to an online modification of Q without any identification algorithm. This is the idea presented in [78]. Q's optimization process is based on root-mean-square signals measures. A state-space relationship between a nominal plant with disturbances and an observer-based feedback controller $K(Q)$ is obtained. The order of Q should be fixed depending on the application. A steepest descent algorithm is used to obtain the parameter values of the predefined YK parameter Q, so the error is minimized from the disturbances on the system. However, the method is valid when the uncertainty is limited but unknown.

An identification algorithm is needed when there is a large model-plant mismatch. This identification algorithm is directly related to the dual YK parametrization in three different methods: Iterated, nested and indirect adaptive control designs.

For iterated and nested solutions [7], $K(Q)$ is seen as a controller where Q changes online, as well as $G(S)$ is seen as a nominal plant with an augmentation related to unmodeled dynamics. The process is as follows: First, a nominal controller K is designed for a nominal plant G. Plant-model mismatch is identified through the dual YK parameter S, and then the augmented controller Q is designed to optimally control S to some performance criteria.

- In iterative control design, unmodeled dynamics represented by S are identified by using the Hansen scheme with Q inclusion presented in section 2.4. It avoids bias problems in the identification process. S is used in an iterative manner for finding the Q that improves the performance criteria. Iteration is needed as the value of S is not initially reliable or due to new deficiencies in the model. In each iteration the order of the controller increases as S includes the applied Q, followed by a control update step.

- In nested control design, successive S are identified on the residual mismatch between model and plant. An external signal needs to be

injected in order to identify the new S. In each step the model of the system is updated. This new model is then taken into consideration for obtaining a new Q, until the performance criteria is fulfilled. This kind of structure is practical when a plant is described by different recursive fractional forms [79].

Although, iterated and nested solutions look sufficient for any system uncertainty, algorithms are conceived for a time-invariant Q property. In order to deal with a time-variant Q, an adaptive version of nested control was proposed in [80], called in literature indirect adaptive control.

- In indirect adaptive control design, a fixed structure of Q is created. Parameters in Q are the changing ones, depending on the model-plant mismatch identified by S. As Q varies with time, the unbiased identification provided in the iterated solution is no longer available. External excitation signals are needed in order to identify S, and this could compromise the control performance. For solving so, two different solutions were targeted: two time scales in the adaptive algorithm was proposed in [81], a faster one for the identification of S, and a much slower for the adaptation of Q; and Q augmentation with a filter in the frequency of the excitation signals needed for the identification of S in [7].

2.5.2 Applications

(Q,S)-based adaptive control solutions were used in solving different systems control problems': [82] used direct Q adaptive control in a hard disk servo system to minimize the maximum position error signal, which is the deviation of the read/write head from the center of the track.

Simulation results of the direct adaptive-Q controller were presented in [83] to illustrate their performance enhancement capabilities when disturbances appear on the system. Part of these results were previously validated in a 55th order aircraft model with a $\mathcal{H}_2$ controller design with Q augmentations for achieving resonance suppression [7].

Experimental results are in [84] for laboratory-scale model of a district heating system. In the district heating system, as consumers are not happy with the variable supply rate, differential pressure sensors are added to examine the problem. That revealed a performance problem, so control capabilities are added to another pump, improving the initial $\mathcal{H}_2$ controller through the corresponding augmented Q.

2.6 (Q,S)-based fault tolerant control

The key idea of using Fault Tolerant Control (FTC) strategy is to keep the closed-loop system stable while possibly accepting a reduced performance

when critical faults occur in the system (i.e. loss of sensors and/ or actuators). FTC architectures are mainly based on fault detection and controller reconfiguration techniques [85].

Both YK parameter Q and dual YK parameter S have been used in different FTC schemes to handle controller reconfiguration and fault diagnosis respectively.

2.6.1 Control implementation

Different FTC schemes only based on YK parameter Q are proposed in the literature [86]; in that case, Q is applied to the controller reconfiguration, while the fault detection part is developed based on some coprime factors. In the FTC scheme depicted in Fig. 2.6, f is the fault diagnosis signal calculated as:

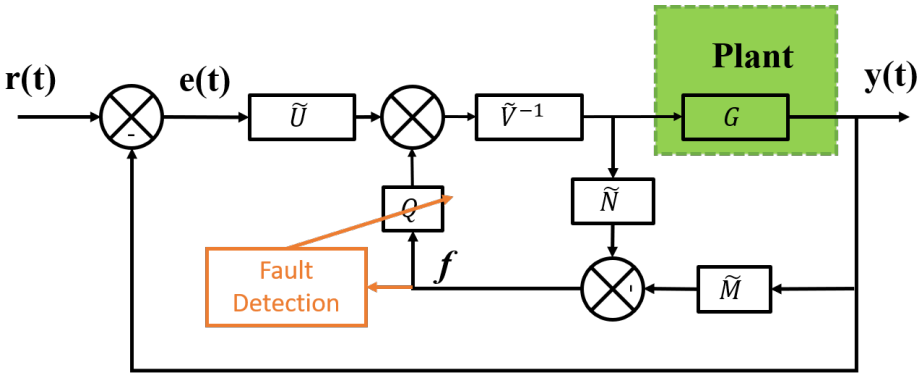

Figure 2.6: Q-based fault tolerant control scheme.

$$f = \tilde{N}u - \tilde{M}y \tag{2.20}$$

When there is no fault, the plant has the same response as the nominal model, which yields to $f = 0$ and the system is controlled by the nominal controller $K = \tilde{v}^{-1}\tilde{u}$ providing adequate performance. Otherwise, the residual signal f is analysed to detect the current fault [87, 88], and then design the suitable YK parameter Q that modifies the controller in the loop in order to manage the current fault.

Another scheme based on YK parameter Q is proposed in [89]. A FTC architecture is designed to tolerate three possible multiplicative faults. Three Q filters are designed offline according to each fault, when a fault occurs the controller switches smoothly from the nominal one to the fault tolerant one by activating the adequate parameter Q. The extension of this architecture where the number of faults can be changed is proposed in [90].

Q-based FTC architectures handle systems with additive faults, and the controller is directly changed with Q, without consideration of S, and with-

out affecting the closed-loop stability. When it comes to parametric faults S plays a key role, obtaining the value of Q that makes stable the control loop.

In (Q, S) based FTC structure the dual YK parameter S is used in the fault diagnosis part. When a fault appears in a system, a nonzero S results. If S is unstable, the fault makes the closed-loop system unstable. Then, controller reconfiguration needs to be carried out to recover stability. This reconfiguration is done through Q. A connection with different additive and parametric faults is in [90] where the optimization of Q is done offline, so only fault diagnosis will be needed in order to choose the proper value of Q. This method is restricted to closed-loop systems with a fault. The fault diagnosis method based on dual YK is extended in [91] to deal with open-loop systems and closed-loop systems with a feedback controller different from the nominal one. The latter is important in fault tolerant control, as fault diagnosis should be running after the first fault has been detected and the controller has been reconfigured. A novel fault tolerant control based control structure to deal with different operational modes (i.e. Start-up or safe mode, normal, full performance, reduced performance and closed-down modes) is proposed in [92]. Fault detection based on dual YK parametrization determines which mode is applied through the corresponding Q.

2.6.2 Applications

In the last two decades YK and dual YK based FTC controllers have been used in different applications. In [90] a servo control system with tacho gain fault that leads to instability is successfully handled using (Q,S)-based FTC scheme. Another approach using an observer based controller is proposed in [93]. The method is applied to a drag racing vehicle control based on a set of observers parametrized with Q , where each observer responds to one or more faults. In [94] a fault tolerant control structure is proposed without requiring any model information or identification procedure. It is applied in weakly stochastic environments using a learning of the YK-parameter Q, the effectiveness of the proposed method is demonstrated in simulation of a DC motor. In [95] YK parametrization is applied in the case of a non-linear faulty system. A fault detection scheme is investigated to estimate and detect the stability performance degradation. To recover the system performance, a performance-based FTC strategy is proposed. Specifically, a generalization of the YK parametrization to non-linear systems is carried out by replacing right and left coprime factors by stable image representation and stable kernel representation respectively. An initial controller K is designed to ensure the system stability, and Q is added to enlarge the stability performance margin in the case of fault. There will be 2 different thresholds one activating the Q, and other one re-configuring the initial K in order to ensure stability. An example with a T-S fuzzy controller as a

nominal controller is also given in the review and applied to a simulation example with a faulty three tank-system.

2.7 (Q,S)-P&P and Multi Model Adaptive Control

P&P investigates control problems for complex systems with a modular structure. Contrary to the FTC field, P&P control tackled the problem of control loop reconfiguration when a new component (i.e. sensor, actuator) is added. It is based on two stages: 1) detection and identification of the additional components to the system; 2) controller reconfiguration to exploit new sensors or actuators to keep the closed-loop stability and improve the overall performance [96].

YK framework is exploited in P&P control as follows: 1) dual YK parameter S is used in the identification part, the added component is usually identified within the closed-loop through the Hansen scheme, since some plants are not permitted to operate in open loop; 2) YK parameter Q is used to modify smoothly the current controller to maintain the system stable and achieve optimal performance. The general theory is explained in [84].

The applicability of P&P control using YK framework is illustrated on different practical systems. In [97] a supermarket refrigeration system with the possibility of adding display cases is controlled with a P&P controller based on YK framework, showing the potential of the approach in maintaining stability and performance of the closed-loop. In [75] two experimental applications of P&P control are presented: a laboratory-scale model of a district heating system, where the control task is to maintain constant differential pressure between the two valves in the heating system. The system has an additional differential pressure sensor, the proposed P&P controller used the added information and improved the pressure regulation.

The second application is a livestock stable climate control system where a real-life experiment is reported, the initial temperature control loop contained a temperature sensor, but the livestock stable is not completely airtight due to cracks in the walls, an additional temperature sensor is added in the cracks area, the P&P controller is extended version of the initial controller taking into account the two temperature information with a variable weighting factor since it is not trivial to attend zero steady state error on both measurements using one actuator.

YK is also employed in the area of Multi Model Adaptive Control (MMAC). MMAC is a supervisor that chooses the proper controller among pre-designed candidates controllers once more information is known about the plant. Controllers are designed based on a predefined set of linear models. Once the closer model in the set is known, the switching is direct [98]. In [9] a MMAC approach using YK framework is proposed to deal with systems subject to significant uncertainties, as noise correlation problem in closed-loop is sup-

pressed by employing the dual YK parametrization. A LPV simulation example with a total of five predefined linear-quadratic-regulator controllers is provided; the closer model in the set to the real system is chosen, switching to the corresponding controller through the correct Q. Finally, as in MMAC the switching is based on the closer model in a predefined set, the CL stability when switching controllers with a real plant is not guaranteed. This situation is analyzed in [99].

2.8 YK and Dual-YK Time Evolution

This sections presents some final remarks of the different YK aplications accordingly to the research institution where they took place. They are temporaly cited to understand the scientific work evolution in the field, providing some insights about the future research directions.

The YK-based applications are mainly developed in four different institutions: Technical University of Danemark, Aalborg University, Grenoble University and University of California. Figure 2.7 shows a timeline evolution of YK research in the last two decades classified by application type in columns. Different color marks are used for research institutions.

Disturbance and noise rejection applications are in the first column of the timeline in Fig.2.7. Research in the area has evolved to deal with disturbances and noise with increasingly complex characteristics, showing experimental results in high-precision systems (i.e. semiconductor manufacturing, active suspension and hard disk drive). In 1999 an experimentation rejecting a single sinusoidal disturbance in an acoustic duct using an adaptive YK parameter Q is described in [53]. In 2005, the YK based control structure evolved to cancel a single narrow band vibration in an active suspension [50]. After that, a repetitive and multiple narrow band disturbance were handled in [39, 40]. And lately, in 2019 YK based control structure is proposed to handle a broad band noise signal [43]. Research in this field are mainly developed by two teams in the University of California and University of Grenoble (blue and red marks respectively in Fig. 2.7). The practical importance of the use of YK parameter in adaptive disturbance and noise rejection have formed a rich research field and new challenges and applications remain to be explored considering multiple frequency noise signal, and large variations in the plant model by including the dual YK parametrization.

YK-based controller reconfiguration is in the second column of the timeline in Fig.2.7 shows the evolution of research using YK parametrization in controller reconfiguration. From 2000 to 2010, papers reported results on YK based controller reconfiguration for LTI systems. In 2004, Technical University of Denmark (marked in pink in Fig.2.7) studied the implementation of multi-variable controller based on the YK parametrization, in order to handle the start-up and the shut down of multi-variable systems [100].

In 2006, they extended the controller architecture to handle systems with additional sensors and/or actuators in stable way, proposing different implementation structures [101]. Those results were used in fault tolerant control field. In 2008, YK based controller reconfiguration technique was used to implement a multi-objective controller accommodating the controller to time-domaine specification with illustrative simulation examples [24]. In 2009, Alborg University (marked in green in Fig.2.7) presented an experimentation of controller reconfiguration based on YK parametrization handling the online introduction of a new sensor in the control loop, providing stability guarantees. In 2010, simulation results on using YK parametrization in controller interpolation of LPV system were provided in [21, 32], extending the initial development on LPV coprime factors studied in 2004 [22]. In 2018 and 2019, developments have been carried out handling controller reconfiguration on ITS systems by the team RITS at INRIA. YK parameter is used to accommodate both longitudinal and lateral behavior of an autonomous vehicle to environment specifications, showing promising experimental results. Latest research on using YK parametrization for controller reconfiguration are more focused on studying the transient behavior while switching between LTI controllers [102, 103].

YK and dual YK based P&P and MMAC control applications are in the third column of the timeline in Fig.2.7. Initial research were conducted in 2000, by the Technical University of Denmark (marked in pink in Fig.2.7) introducing dual YK based closed loop identification [8]. After that, using the contemporary results on controller reconfiguration and closed loop identification, University of Aalborg (marked in green in Fig.2.7), through its project P&P control developed a novel concept for process distributed control, which allows the control system to self reconfigure once an instrumental change is introduced [96]. In 2015, a new dual YK based identification scheme is proposed in order to avoid the use of indirect excitation signals in the reference and feedforward inputs modifying the one proposed in 2003 [68] by the Technical University of Denmark, and in 2018 they showed experimental results on using the proposed scheme. In 2019, experimental results are shown using YK based MMAC in ITS systems [104].

YK and dual YK based FTC control applications are in the forth column of the timeline in Fig. 2.7. Collaboration between Technical University of Denmark and Alborg University significantly contributed on the development of a fault tolerant controller based on both YK and dual YK parametrizations. They proposed first a passive FTC controller [89], then an active FTC controller [105]. In 2012, Technical University of Denmark proposed a model-based FTC controller [92]. In 2015, they extended the active FTC to cover sampled data systems. In 2017, the concept of fault tolerant margin for nonlinear systems is introduced, it plays a key role in detecting system performance degradation caused by some faults [106]. In 2019, this concept is used in a novel FTC scheme by applying the Takagi–Sugeno fuzzy

dynamic modeling technique in desgning YK parameter Q [107]. In 2018, a YK based FTC control scheme is introduced using reinforcement learning technique to adapt the YK parameter when some faults occur. As shown, the latest results on YK based FTC are more oriented on using intelligent control techniques to design the adequate YK parameter Q dealing with nonlinear systems.

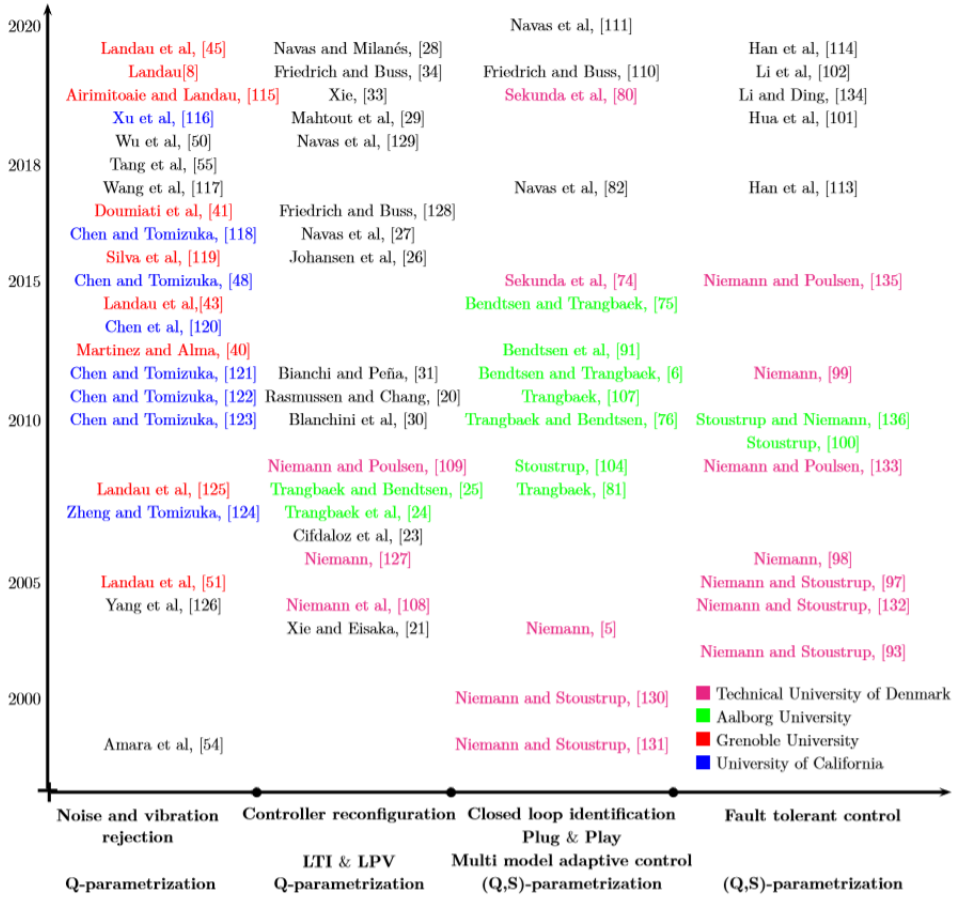

Figure 2.7: Timeline with important applications of YK parametrization Q and dual YK parametrizartion S

2.9 Discussion

This chapter reviewed the use of YK and dual YK parametrizations in different control fields. Different experimental control applications developed during the last 20 years are reported showing the efficiency of YK framework

in controlling complex systems.

Origins of YK parametrization Q describing the set $K(Q)$ of all stabilizing controllers for a given plant, and dual YK parametrization S describing the set of the plants $G(S)$ stabilized by a given controller are explained.

A state-of-the-art classification of YK and dual YK based applications is provided with respect to different control fields as follows:

- In controller reconfiguration field: The use of the Q-based parametrization in both frameworks LTI and LPV allows performance enhancement of the system performance while keeping closed-loop stability. This strong property has been proven through different experimental applications. However, the depicted Q-based controllers implementation does not guarantee the closed-loop performance during the switching instant, which remains a practical implementation problem. In [108] and [103] a design method of the YK parameter Q is proposed to maintain a level of performance during the transition between LTI controllers. In [109] the enhancement of the transition behavior is analyzed with respect to the choice of the full range LPV initial controller.

- In noise rejection and vibration control field: YK parametrization Q is used to reject different types of disturbances, the parametrization of the controller allows the system to cope with a large frequency range. It has been compared to different robust techniques [110], [40] in several experimentation proving its efficiency against multiple disturbance types (known/unknown, narrow/broad band). Current challenge is to insure noise rejection while important variations in the plant model occur. When designing an adaptive controller to cancel an unknown narrow band disturbance, the uncertainties linked to the plant can lead to instability. This problem is addressed in the literature using the dual YK parameter to model the plant uncertainties [111]. However, this solution needs to satisfy stability conditions which cannot be fulfilled for all systems especially when the uncertainty is large. A recent work [112] showed that this difficulty can be overcome by increasing the order of the filter Q. This solution is called YK overparametrization.

  Another possible improvement is to use dual YK parametrization in the identification of disturbance path instead of using auto-regressive methods [113].

- In closed loop identification: The dual YK parametrization S is used to cope with closed-loop identification limitations in an open-loop identification framework. This solution plays a key role when there are system variations and controller could not be disconnected due to stability, physical or economical reasons. This type of identification is also important when controller needs to be adapted online to a

new situation in the system. Current challenges are associated to degree reduction of the resulting identified model for its use in iterative adaptive controllers; its application to system with non-linear dynamics [72] [73]; and extension of the modified Hansen scheme solving the excitation signals problem and the approach adding sensors/actuators to LPV systems.

- In adaptive control field: Offline and online YK parameter Q optimization, and dual YK based methods was used to cope with system variations in adaptive control field. Current challenges are associated to the non-linear extension of the YK parameterization; order reduction of the identified S to avoid degree explosion in nested/iterated applications; integration of intelligent control systems as fuzzy control, genetic algorithm or neuronal networks in this adaptive frameworks; and extension of P&P to a more general control structure, because it is only based in observer-based feedback controllers.

- In fault tolerant control field: Both Q-based and (Q,S)-based FTC architectures are reviewed, handling different fault types (additive, multiplicative or parametric). Current challenges are associated to system performance enhancement and multi objective control in FTC scheme. The goal is not only to properly control the plant when the fault occurs and avoid instability but also to optimize the closed-loop response for both LTI and LPV plants, an initial implementation is proposed in [114], where the performance of a LTI plant is automatically optimized and the controller is adapted to the faulty situation.

  Finally, structural changes are also considered in connection with both YK and dual YK [115] in P&P control technique. It is demonstrated how it is possible to introduce new sensors/actuators into the system, and use them in the YK parameterization to keep a given performance and the closed loop stability.

The most successful experimental applications are represented in a timeline 2.7 with respect to the used parameter (Q, S or both), control fields and research teams. Once the state-of-the-art of YK and dual YK parametrizations has been carried out, Some challenges for potential applications are associated to the integration of intelligent control system as fuzzy control, model predictive control, genetic algorithm or neuronal networks. The issue of order explosion of Q and S which is a real practical problem in adaptive control applications, Combination of YK-based fault tolerant control and Plug & Play to a more general control structure.

Two challenges related to the controller reconfiguration and noise rejection fields are studied in this thesis: Limitation of the use of the scalar factor γ regulating the switch and its frequency; Maximum level of distur-

bance that could be rejected when dealing with conflicting control objectives, and comparison to classical robust control.

Dealing with different control objectives is a real issue when designing controllers for engineering systems. Specially in controlling ITS that evolve in a non-structured environment and need high performance control.

A first thesis studied the use of YK parametrization in ITS [116]. It explored the use of YK parametrization to keep longitudinal vehicle control stability when traffic conditions change. It showed the improvement of the Cooperative Adaptive Cruise Control (CACC) system when non available communication link with the preceding vehicle. It also proposed a MMAC algorithm based on YK parametrization to deal with heterogeneity in CACC systems.

In this thesis, YK parametrization is used to enhance lateral control performance of autonomous vehicles when dealing with different lateral maneuvers (i.e. lane change, obstacle avoidance, lane keeping). Longitudinal control is also explored, YK parametrization is used to handle measurement noise that could appear in the embedded vehicle sensors used in ACC application.

Chapitre 3

Théorie et principes de la parametrisation de YK.

Below is a French summary of chapter 3.

Ce chapitre présente la théorie et les principes sur lesquels se base la parametrisation de YK pour la construction des structures multi-contrôleurs stable. Comme déjà présenté dans le chapitre précédent, le paramétrisation de YK décrit l'ensemble de tous les contrôleurs qui stabilisent un système donné. Cette paramétrisation est basé sur la factorisation coprime. L'ensemble des régulateur est exprimé en fonction du paramètre de YK Q, qui peut être n'importe quelle fonction de transfert stable. La reconfiguration d'un contrôleur stable est effectuée entre différents contrôleurs dans la structure paramétrée en utilisant un signal externe γ, appelé signal de commutation. Il permet l'activation du contrôleur approprié pour l'objectif de contrôle actuel.

Un positionnement général de la paramétrisation de YK dans les techniques de contrôle multi-objectifs est fourni par rapport aux techniques de contrôleurs multi-objectifs simples, et aux techniques de contrôleurs commutants.

La structure de contrôle multi-objectif basée sur la paramétrisation de YK s'appuie sur la factorisation coprime. Le principal avantage de la paramétrisation YK est qu'elle garantit la stabilité de la boucle fermée sous n'importe quel signal de commutation. Le présent chapitre etudie en profondeur les aspects suivants : 1) Détails sur la façon de calculer les coprime facteurs nécessaires pour l'implémentation de la structure de contrôle basée sur la paramétrisation de YK ; 2) La stabilité de la boucle fermée incluant le contrôleur basé sur la paramétrisation de YK.

Un exemple numérique est donné dans ce chapitre, prouvant comment le paramétrisation de YK stabilise une commutation entre deux contrôleurs où la simple combinaison linéaire résulte instable. Un autre exemple numérique illustrant les étapes de la construction d'un contrôleur basé sur la paramétrisation de YK est également décrit dans ce chapitre.

Chapter 3

Youla-Kucera parametrization: Theory and principles

3.1 Introduction

This chapter presents the theory and principles in which YK parameterization relies on for making stable multi-controller structure. As already presented in the previous chapter, YK parameterization describes the set of all controllers that stabilize a given plant model. This parameterization is based on the doubly coprime factorization. The set of the stabilizing controllers is a function of the YK parameter Q, that can be any stable transfer function. Stable controller reconfiguration is carried out between different controllers in the parametrized structure by using an external signal γ, called switching signal. It allows the activation of the suitable controller for the current control objective. A general positioning of YK parametrization in multi-objective control techniques is provided with respect to single multi-objective controller techniques, and switched multi-controller techniques. The multi-objective control structure based on YK parametrization relies on the doubly coprime factorization framework. The main advantage of YK parametrization is that it guarantees the closed loop stability under any arbitrary switching signal. This chapter carries out a deep review in the following aspects: 1) Details on how to compute the needed factors; 2) The stability of the closed loop including YK parametrized controller.

The chapter is structured as follows: Section 3.2 describes a general positioning of YK parametrization in multi-objective control techniques, providing an example of state dependent switching. Section 3.3 presents doubly coprime factorization and the associated Bézout identity and the multi-controller structure design. The closed loop stability analysis under arbitrary switching is included in this section. A numerical example is illus-

trated in section 3.4. Finally, some concluding remarks are given.

3.2 Single controller limitations

A single loop controller may results in an unacceptable performance. Any practical design must be able to cope with load disturbance, plant saturation, measurement noise, process lag, plant parameter uncertainty, sensitivity and also incorporate suitable criteria delimiting transient behavior and steady state performance. The desired performance in control system applications may also temporally evolve based on multiple reasons as sudden sensor failures or a noise signal that appears and disappears. Furthermore, the stability of the closed loop can also be affected when the system deviates from its nominal model.

Let's briefly illustrate some limitations of a single LTI controller in a control design problem. The control of the roll angle of aircraft in different operational conditions is considered. The plant model is taken from [19]:

$$G = \frac{-1000}{s(s+0.875)(s+50)} \tag{3.1}$$

Three controllers are designed to satisfy different control criteria:

- controller K_1 designed to achieve fast closed loop reference tracking and large bandwidth.

$$K_1 = \frac{6.694(s+0.9446)(s+50.01)}{(s^2+13.23s+9.453^2)(s+50.05)} \tag{3.2}$$

- controller K_2 designed to be robust to plant parameter variations.

$$K_2 = \frac{-7.1623\cdot 10^8(s+10^4)(s+50)(s+0.875)(s-3.493\cdot 10^{-7})}{(s+1.113\cdot 10^4)(s+1.002\cdot 10^4)(s+0.009)(s^2+3536s+6.468\cdot 10^6)} \tag{3.3}$$

- controller K_3 designed to cope with measurement noise and ensure small closed loop bandwidth.

$$K_3 = \frac{2187^2(s+0.9977)(s+66.28)}{(s^2+467.2s+486.2^2)(s+507)} \tag{3.4}$$

Figure 3.1 depicts the behavior of the aircraft responding to a step reference in the roll angle, controlled by the controllers K_1, K_2 and K_3 in three different operational conditions. The first line graphs show the behavior of the different closed loops in a clean environment, and with nominal plant model. In this case, the controller K_1 is the suitable one, since it is the

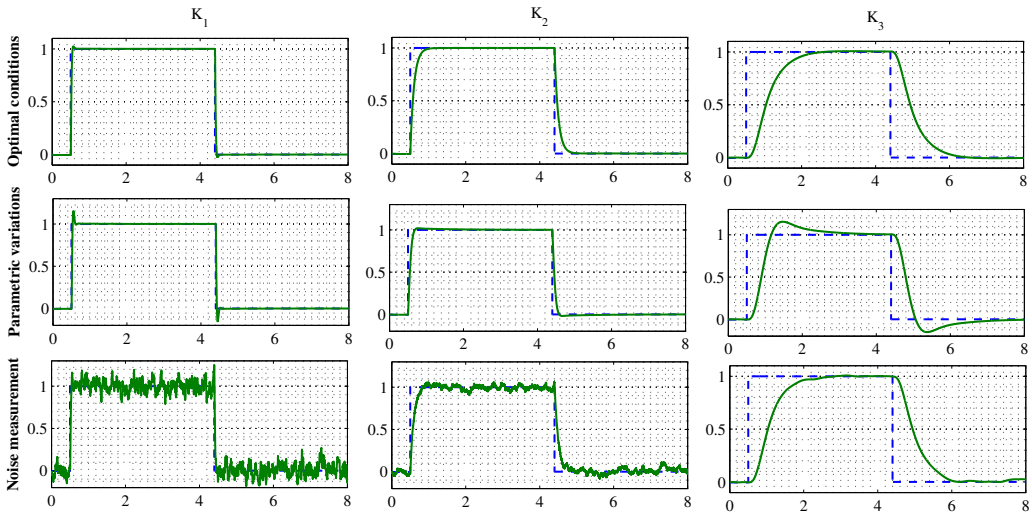

Figure 3.1: Aircraft roll angle control in different operational conditions

fastest one and it causes an admissible overshot (2%). Both controllers K_2 and K_3 present slow responses.

In the second line, parameter variation is caused in the plant model by moving the pole at -50 to -30. In this case, both controllers K_1 and K_3 present an inadmissible overshoot of 20% and 13% respectively. However, controller K_2 remain robust to the parameter variation and shows the best behavior with respect to the response time and overshot.

In the third line, a noise measurement is added in the feedback output, simulated as a random signal. Controllers K_1 and K_2 are sensitive to the noise measurement and show noisy behavior. The controller K_3 is the less sensitive one and exhibits smooth behavior.

As showed in the aircraft roll angle control design, it is a key aspect the ability of the system to provide the best response in all circumstances. Thus, managing the trade-off between different conflicting objectives (i.e. performance/robustness) or satisfying variable performance metrics appears mainly in all control design requirements.

Many solutions are proposed in the literature either by designing a single multi-criteria controller or a multi-controller with different control objectives. In both solutions the controller behavior is adapted to accommodate the operating conditions and enhance the closed loop performance.

In single multi-criteria solution, the controller can be adapted using direct or indirect adaptive control techniques. In multi-controller structure, the local controllers are interpolated using switching/interpolation techniques. The interpolation signal should select the suitable fraction of each

local controller that can satisfy the required performance metrics.

In the following, both solutions are discussed and compared using a simulation example.

3.2.1 Single multi-criteria controller

Multiple techniques have tackled multi-objective controllers using tools of optimal, robust and adaptive control theory: Linear-Quadratic-Gaussian (LQG), H_∞, Model-Reference Adaptive Control ($MRAC$). However, techniques from robust control theory [117] [118] incorporate both robustness and performance objectives in an offline optimization algorithm, leading to the so-called worst case control strategy [7] [119]. In the following, the most used multi-criteria control techniques are presented:

- Linear Quadratic Regulator: This approach is based on the minimization of a quadratic performance cretiria under the assumption that the plant for which it is designed is linear. The result is a linear state feedback controller. This controller is optimal with respect to defined performance metrics, and the resultant closed loop is robust to certain plant variations [7]. In case the plant states are not measurable, they are replaced by estimated stated using an optimal estimator, and the resulting controller including the estimator is named LQG controller.

- H_∞ controller: This approach was originated to solve a fundamental problem of sensitivity in a feedback loop, constraining signals in the loop to achieve a desired requirement, expressed in terms of a ∞-norm. The H_∞ framework aims to minimize the relation between external input signals w (representing disturbances, reference signals, noises, ...) and output z containing tracking errors, control actions and other signals of interest. To achieve this goal, the measurement y is used to derive an input signal u. This mapping between y and u is given by a dynamic controller K guaranteeing the closed loop stability.

- Model Reference Adaptive Control: This approach offers a solution for problems related to Adaptive Control in real world. In MRAC control loop, the real system output is compared to a model reference output, with the controller adjusting errors between both outputs. The mismatch between the plant and reference model can be caused by the variation of the plant parameters or by external signals affecting the control loop. The MRAC controller is able to adjust it self based on the system inputs and outputs. The MRAC control is classified into direct and indirect type: 1) Direct approach minimizes the output error by directly adjusting the controller parameters; 2) Indirect approach estimates the unknown plant parameters using a defined plant model, then the controller input is chosen, [120].

The main disadvantage of these techniques is that the controlled system has a lower performance even if it is new and fully operational. For adaptive control techniques [121] [122], the performance can be enhanced online taking into account the operating conditions. However, the number of parameters to adapt online can easily reach tens. The more parameters to adapt, the slower the adaptation rate. The more inputs and outputs, the more problems can arise concerning uniqueness of controller solution and local minimum [123]. Additionally, the control signal must sufficiently excite system dynamics to ensure a proper online identification or parameter adjustment, which can be in conflict with the control objectives and robustness.

3.2.2 Linear controller switching

The concept of controller switching or blending among controllers is widely studied in the literature [124]. In the last decades different techniques have been investigated as Ad Hoc approaches, gain scheduling control, bumpless transfer and others. The goal of the switching controller design is to satisfy a desired level of closed loop performance according to the switching signal. The crucial issue in switching between controllers is to ensure the system stability under arbitrary switching signal. Also the multi-objective controller must be able to recover the suitable controller according to the operating conditions. The following discusses switching/interpolation techniques with respect to the closed loop stability aspect, closed loop performance metric and switching/interpolation signals under consideration.

- Ad-Hoc approaches: Many forms of *ad hoc* switching / interpolation controllers are motivated by gain scheduling. The *ad hoc* controller is formed by interpolating local controllers. The local controller behavior is described by control parameters (i.e gains, poles and zeros, balanced realizations). Those control parameters are interpolated to reach the desired behavior of the *ad hoc* controller and define its type (i.e. gains interpolation, local controller output interpolation, poles and zeros interpolation ...). The closed loop stability based on *ad hoc* controller approaches is not generally guaranteed even for static switching signal between two stabilizing controllers [100]. Advanced control techniques investigated the stability of the *ad hoc* controllers: small-gain theorem has been used to verify stability of LPV systems with hidden coupling induced by the gain scheduled controller for static interpolation signals [125]; Linear Matrix Inequalities (LMIs) are used to search a common Lyapunov functions for the closed loop controlled by the interpolated controller and ensure the stability. To sum up, the ad-hoc switching/interpolating control techniques allow the interpolation of different local controllers designed separately, and the interpolation

signal interpolates local controllers parameters but it do not ensure closed loop stability.

- Self-Scheduled approaches: In these techniques, both local controllers and switching/interpolation signals are designed simultaneously to form the interpolated controller [15]. The advantage of self-scheduled technique is that the closed loop stability is guaranteed since it is a design requirement. Another benefit is performance metric that can also be handled as a design criteria (i.e. quadratic H_∞ performance metric [126]). However, the design of local controllers are coupled one to the other, so any change in one local controller can affects all the other local controllers from stability and performance aspect. Furthermore, the self-scheduled technique is restricted to switch/interpolate local controllers with common structure (i.e. all proportional controllers, all H_2 controllers, ...). Other disadvantage is that the switching can only depend on the open loop parameters (i.e. plant and controller parameters) and can't be arbitrary.

- Bumpless-Transfer approaches: This technique is more dedicate to design switched/interpolated controllers for switched plants [17]. The controller switching occurs to reach a target response characterizing the ideal closed loop behavior in l_2 sens after the plant switching. As such, bumpless-transfer design is concerned with a specific class of interpolation signals and performance metrics. Thus it can not guarantee stability under arbitrary switching signal.

- Controller Parametrization: Rather than directly interpolating a set of controllers, those can be mapped into a single controller based on YK parameter [5, 6]. This parametrization allows stable interpolation between a set of controllers designed and tuned independently to stabilize a given system with multiple control objectives and under any arbitrary interpolation signal [19]. Besides the stability aspect, YK parametrization allow the switching/interpolation among controller structures (i.e. a Proportional-Integration-Derivative controller with an H_∞ controller).

Table 3.1 shows a comparative study of the presented controller switching techniques. The approaches are compared with respect to initial controller design (either it can be designed separately using different control techniques and structures or not), also from the possibility of using arbitrary switching signal (i.e. based on parameters that are external to the closed loop), and finally from the switching stability point of view.

An illustrative example is presented below, where a state depending switching between two stable closed loops is implemented. The example

Table 3.1: Switching control design techniques

Approaches	Initial controllers designed separately	Arbitrary switching signals	Switching stability guarantee
Ad-hoc [125]	✓	✓	X
Self scheduled [126]	X	X	✓
Bumpless transfer [17]	X	X	✓
Controller parametrization [19]	✓	✓	✓

compares Ad-hoc and controller parametrization techniques to show that using controller parametrization technique, the switching stability is regardless of the switching signal.

Example 3.2.1 *Let's have two stable feedback loop, where a LTI plant G is stabilized by two different state feedbacks K_1 and K_2, resulting in two stable closed loops as follows:*

$$\dot{x}_{cl1} = \begin{bmatrix} -1 & 10 \\ -1 & -1 \end{bmatrix} x_{cl1} \tag{3.5}$$

and

$$\dot{x}_{cl2} = \begin{bmatrix} -1 & 1 \\ -10 & -1 \end{bmatrix} x_{cl2} \tag{3.6}$$

In the following, a state dependent switching between the two stable systems will be designed, a switching signal γ is defined as follows:

$$\gamma = \begin{cases} 1 & x_1 x_2 \leq 0 \\ 0 & x_1 x_2 > 0 \end{cases}$$

The switched controller is build using two different techniques:

- *An Ad-Hoc technique where the control signal is a linear combination of the two controllers outputs $u = -(1-\gamma)K_1 x - \gamma K_2 x$.*
- *Using a parametrized controller based on YK parametrization, when the switching signal $\gamma = 0$ the controller K_1 is activated and when $\gamma = 1$ the controller K_2 is activated.*

As it can be noticed in Example.3.2.1, switching between two stable closed loops (see Figure.3.2) can yield to either an unstable behavior (see Figure.3.3a), or to a stable switched system (see Figure.3.3b). In the case of arbitrary switching signal, the stability of the switched system rely on the switching technique. In the following sections, the YK principles are detailed and the stability of the related closed loop is analysed.

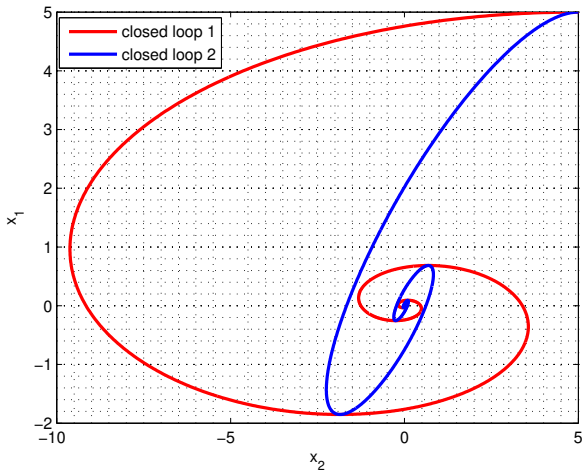

Figure 3.2: State trajectories for both stable closed loops from an initial value $x' = \begin{bmatrix} 5 & 5 \end{bmatrix}$.

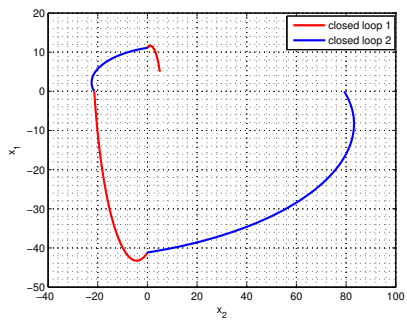

(a) State trajectories for switched system using Ad-Hoc technique.

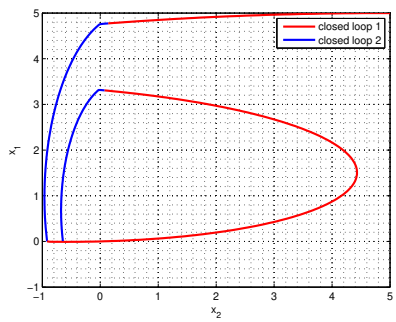

(b) State trajectories for switched system using YK parametrized controller.

Figure 3.3: State depending switching.

3.3 YK: definition and stability

This section presents the basis and principles on designing the YK parametrization of all stabilizing controllers for a given plant [7] [127] [128].

Let R_p be the set of all linear, real, rational and proper transfer functions with appropriate dimensions in continuous or discrete time. Similarly, let RH_∞ be the set of all stable transfer functions in R_p.

Additionally, let's consider the negative stable feedback of the plant transfer function $G \in R_{m\times n}$, mapping n inputs to m outputs. and the stabilizing controller $K \in R_{n\times m}$:

$$G(I + KG)^{-1} = (I + GK)^{-1}G \tag{3.7}$$

3.3.1 Doubly Coprime Factorization

The first step in characterizing the class of all stabilizing controller is the coprime factorization of the plant model and the controller. For scalar transfer functions, the plant model and controller are written as a ratio of two stable transfer functions. In the case of MIMO systems the plant model and controller matrix transfer functions are factorized to a product of a stable transfer function matrix and a transfer function matrix with a stable inverse. The factorization is called coprime when the two factors have no common unstable zeros. The coprimeness excludes unstable pole/zero cancellation in the fractional representation.

Definition 3.3.1 *Left and Right coprime factorization over RH_∞*
The transfer function matrix pair (N, M) are right-coprime over RH_∞ if N, $M \in RH_\infty$ and transfer function matrices $X, Y \in RH_\infty$ exist such that:

$$XN + YM = I \tag{3.8}$$

Similarly, the function function matrix pair $(\tilde{N}, \tilde{M})$ are left-coprime if $\tilde{N}$,$\tilde{M}$ $\in RH_\infty$ and transfer function matrices $X, Y \in RH_\infty$ exist such that:

$$\tilde{N}X + \tilde{M}Y = I \tag{3.9}$$

The coprimeness of the factors M and N means that $\begin{bmatrix} M \\ N \end{bmatrix}$ has full column rank in $|z| > 1$ in discrete time or in $Re(s) < 0$ in continuous time. Correspondingly, coprimeness of $\tilde{M}$ and $\tilde{N}$ means that $\begin{bmatrix} \tilde{M} & \tilde{N} \end{bmatrix}$ has full rank in $|z| > 1$ in discrete time or in $Re(s) < 0$ in continuous time.

Example 3.3.1 *For SISO system: Let's consider the LTI SISO transfer function $G = \frac{5}{s+5}$, the right coprime factorization of G can be $M = \frac{s+5}{s+2}$ and $N = \frac{5}{s+2}$ with $X = \frac{0.2(s+2)}{(s+1)}$ and $Y = \frac{s(s+2)}{(s+5)(s+1)}$, the left coprime factorization can be $\tilde{M} = \frac{s}{(s+1)}$ and $\tilde{N} = \frac{5s}{(s+5)(s+1)}$ with $X = \frac{0.2(s+5)}{s}$ and $Y = 1$.*

Let's consider the coprime factorization of the plant transfer function $G \in R_{m\times n}$ and the controller $K \in R_{n\times m}$.

$$G = NM^{-1} = \tilde{M}^{-1}\tilde{N} \qquad N, M, \tilde{N}, \tilde{M} \in RH_\infty \tag{3.10}$$

$$K = UV^{-1} = \tilde{V}^{-1}\tilde{U} \qquad U, V, \tilde{U}, \tilde{V} \in RH_\infty \tag{3.11}$$

Assuming that the controller K stabilizes the plant G, the coprime factors must satisfy the so called *Bezout* identity or *Diophantine* equations.

Lemma 3.3.1 *Consider the plant $G \in R_{m\times n}$ and $K \in R_{n\times m}$. Then K stabilizes G if and only if there exist M, N, U, V, $\tilde{M}$, $\tilde{N}$, $\tilde{U}$, $\tilde{V} \in RH_\infty$ such that the following Diophantine equations are satisfied:*

$$\tilde{V}M - \tilde{U}N = I, \tag{3.12}$$

$$\tilde{M}V - \tilde{N}U = I, \tag{3.13}$$

Or equivalently, the Bezout identity is satisfied:

$$\begin{bmatrix} \tilde{V} & -\tilde{U} \\ -\tilde{N} & \tilde{M} \end{bmatrix} \begin{bmatrix} M & U \\ N & V \end{bmatrix} = \begin{bmatrix} M & U \\ N & V \end{bmatrix} \begin{bmatrix} \tilde{V} & -\tilde{U} \\ -\tilde{N} & \tilde{M} \end{bmatrix} = \begin{bmatrix} I & 0 \\ 0 & I \end{bmatrix} \tag{3.14}$$

To calculate those factors [7], a state space descriptions of the plant model G and controller K is considered:

$$\begin{aligned} \dot{x}_G(t) &= A_G x_G(t) + B_G u(t) \\ y(t) &= C_G x_G(t) + D_G u(t) \end{aligned}, \qquad G : \left[\begin{array}{c|c} A_G & B_G \\ \hline C_G & D_G \end{array}\right] \tag{3.15}$$

$$\begin{aligned} \dot{x}_K(t) &= A_K x_K(t) + B_K y(t) \\ u(t) &= C_K x_K(t) + D_K y(t) \end{aligned}, \qquad K : \left[\begin{array}{c|c} A_K & B_K \\ \hline C_K & D_K \end{array}\right] \tag{3.16}$$

A key step in computing the coprime factorization, is to first construct state feedback gains F_G and F_K to stabilize the pairs (A_G, B_G) and (A_K, B_K) respectively. Under the controllability assumption of the pairs (A_G, B_G) and (A_K, B_K), constant state feedback matrices F_G and F_K can be easily obtained by performing a state feedback design such that $(A_G + B_G F_G)$ and $(A_K + B_K F_K)$ have all eigenvalues within the unity circle in discrete time domain or in the left half plane in continuous time domain. State space descriptions of stable right and left coprime factors for G and K are given as follows :

$$\begin{bmatrix} M & U \\ N & V \end{bmatrix} = \left[\begin{array}{cc|cc} A_G + B_G F_G & 0 & B_G & 0 \\ 0 & A_K + B_K F_K & 0 & B_K \\ \hline F_G & C_K + D_K F_K & I & D_K \\ C_G + D_G F_G & F_K & D_G & I \end{array}\right] \tag{3.17}$$

$$\begin{bmatrix} \tilde{V} & -\tilde{U} \\ -\tilde{N} & \tilde{M} \end{bmatrix} = \left[\begin{array}{cc|cc} A_G + B_G Y D_K C_G & B_G Y C_K & -B_G Y & B_G Y D_K \\ B_K Z C_G & A_K + B_K Z D_G C_K & -B_K Z D_G & B_K Z \\ \hline F_G - Y D_K C_G & -Y C_K & Y & -Y D_K \\ Z C_G & -(F_K - Z D_G C_K) & Z D_G & Z \end{array}\right] \tag{3.18}$$

where $Y = (I - D_K D_G)^{-1}$ and $Z = (I - D_G D_K)^{-1}$. Then, coprime factors can be calculated using the standard transformation from state space description to transfer function matrix.

$$P : \left[\begin{array}{c|c} A_P & B_P \\ \hline C_P & D_P \end{array}\right], \qquad P = C_P(sI - A_P)^{-1} B_P + D_P \tag{3.19}$$

Doubly coprime factorization plays a central role in obtaining stabilizing controllers for different systems. Initially, coprime factors have been developed for an LTI plant controlled by a fully observer-feedback controller [129], then it has been extended to factorize a reduced-order observer based controller [130, 131]. The LTI coprime factorization framework have been enlarged to include numerous LTI systems controlled by arbitrary feedback controllers: continuous as well discrete time systems; one dimensional and multidimensional systems [132]. Latest researchers studied coprime factorization for nonlinear feedback control systems presenting a promising framework for nonlinear systems analysis, control design and stabilization [133–136].

3.3.2 The class of all stabilizing controllers

According to Youla-Kucera [4] [5], [6], all stabilizing controllers for a given plant G stabilized by a nominal controller K, can be parametrized using a stable filter Q so called YK parameter.

Theorem 3.3.2 *Let $K \in R_{n\times m}$ be a nominal controller stabilizing the plant $G \in R_{m\times n}$, with coprime factorizations given in (3.17), (3.18) satisfying the double Bezout equation (3.14). Consider also the following class of controllers $K(Q)$ parametrized in terms of $Q \in RH_\infty$ in right factored form:*

$$K(Q) = U(Q)V(Q)^{-1}, \tag{3.20}$$

$$U(Q) = U + MQ, \qquad V(Q) = V + NQ; \tag{3.21}$$

Or in the left form:

$$K(Q) = \tilde{V}(Q)^{-1}\tilde{U}(Q), \tag{3.22}$$

$$\tilde{U}(Q) = \tilde{U} + Q\tilde{M}, \qquad \tilde{V}(Q) = \tilde{V} + Q\tilde{N}; \tag{3.23}$$

Then, the factorization of the class of controllers $K(Q)$ with the factorization of the plant G satisfy the Bezout identity in (3.14), so that $K(Q)$ stabilizes G for all $Q \in RH\infty$.

Proof: Let's assume that K factorized in (3.11) stabilizes G factorized in (3.10). Thus it satisfies the *Bezout* identity. Now, let's analyse the *Bezout* identity when G is controlled by the class of controllers $K(Q)$ factorized in (3.22) and (3.23):

$$\begin{bmatrix} \tilde{V}(Q) & -\tilde{U}(Q) \\ -\tilde{N} & \tilde{M} \end{bmatrix} \begin{bmatrix} M & U(Q) \\ N & V(Q) \end{bmatrix} = \begin{bmatrix} \tilde{V} + Q\tilde{N} & -(\tilde{U} + Q\tilde{M}) \\ -\tilde{N} & \tilde{M} \end{bmatrix} \begin{bmatrix} M & U + MQ \\ N & V + NQ \end{bmatrix} \tag{3.24}$$

$$= \begin{bmatrix} (\tilde{V} + Q\tilde{N})M - (\tilde{U} + Q\tilde{M})N & (\tilde{V} + Q\tilde{N})(U + MQ) - (\tilde{U} + Q\tilde{M})(V + NQ) \\ -\tilde{N}M + \tilde{M}N & -\tilde{N}(U + MQ) + \tilde{M}(V + NQ) \end{bmatrix} \tag{3.25}$$

$$= \begin{bmatrix} \tilde{V}M - \tilde{U}N & \tilde{V}U - \tilde{U}V \\ -\tilde{N}M + \tilde{M}N & -\tilde{N}U + \tilde{M}V \end{bmatrix} + \begin{bmatrix} Q(\tilde{N}M - \tilde{M}N) & H(Q) \\ 0 & (-\tilde{N}M + \tilde{M}N)Q \end{bmatrix} \tag{3.26}$$

The expression $H(Q)$ is noted in the equation (3.26) for sake of space, it includes the following terms:

$$H(Q) = Q\underbrace{(\tilde{N}U - \tilde{M}V)}_{-I} + \underbrace{(\tilde{V}M - \tilde{U}N)}_{I}Q + Q\underbrace{(\tilde{N}M - \tilde{M}N)}_{0}Q \tag{3.27}$$

Since K stabilizes G, their coprime factors satisfies the *Bezout* identity and give:

$$\begin{bmatrix} \tilde{V}M - \tilde{U}N & \tilde{V}U - \tilde{U}V \\ -\tilde{N}M + \tilde{M}N & -\tilde{N}U + \tilde{M}V \end{bmatrix} = \begin{bmatrix} I & 0 \\ 0 & I \end{bmatrix} \tag{3.28}$$

Thus, $K(Q)$ stabilizes G and their coprime factors satisfies the *Bezout* identity:

$$\begin{bmatrix} \tilde{V}(Q) & -\tilde{U}(Q) \\ -\tilde{N} & \tilde{M} \end{bmatrix} \begin{bmatrix} M & U(Q) \\ N & V(Q) \end{bmatrix} = \begin{bmatrix} I & 0 \\ 0 & I \end{bmatrix} \tag{3.29}$$

The class of all stabilizing controllers can be implemented using a Linear Fractional Transformation (LFT) separating the nominal part of the controller and the YK parameter Q:

$$K(Q) = F(J_K, Q) \tag{3.30}$$

$$K(Q) : \begin{bmatrix} u \\ r \end{bmatrix} = J_K \begin{bmatrix} y \\ s \end{bmatrix}, s = Qr \tag{3.31}$$

Using the *Bezout* identity the controller $K(Q)$ can be expressed as follows:

$$\begin{aligned} K(Q) &= (U + QM)(V + QN)^{-1} \\ &= (U + \tilde{V}^{-1}(I + \tilde{U}N)Q)(V + NQ)^{-1} \\ &= (UV^{-1}(V + NQ) + \tilde{V}^{-1}Q)(V + NQ)^{-1} \\ &= K + \tilde{V}^{-1}Q(I + V^{-1}NQ)^{-1}V^{-1} \end{aligned} \tag{3.32}$$

From the LFT controller form in (3.31) and the equation (3.32), J_K can be deduced:

$$J_K = \begin{bmatrix} UV^{-1} & \tilde{V}^{-1} \\ V^{-1} & -V^{-1}N \end{bmatrix} \tag{3.33}$$

The LFT form of the class of stabilizing controllers shows that the final control signal consists on a signal generated by the nominal controller K and a signal from a control loop involving the YK parameter Q.

Based on the strong property of guaranteeing the closed loop stability using different filters $Q \in RH_\infty$, the class of stabilizing controllers $K(Q)$ for a given plant G have been used in different control fields, ranging from controller reconfiguration [128] to fault tolerant control [106] passing by noise rejection and active vibration control [38].

3.3.3 Controller transition

YK parametrization has been used in the field of controller reconfiguration to switch from a given controller K_1 stabilizing a feedback control loop to another one $K2$ stabilizing the same control loop and showing different performance [19].

The main objective is to design the YK parameter $Q \in RH_\infty$ to switch from $K1$ to $K2$. In this case the nominal controller is $K1$ and Q must be designed to make $K(Q) = K2$.

The first step to design the YK filter is to properly factorize the plant G and both controller $K1$ and $K2$ using the state space formulation in (3.17) and (3.18) such as :

$$\begin{aligned} G &= NM^{-1} = \tilde{M}^{-1}\tilde{N} \\ K1 &= U_1V_1^{-1} = \tilde{V}_1^{-1}\tilde{U}_1 \\ K2 &= U_2V_2^{-1} = \tilde{V}_2^{-1}\tilde{U}_2 \end{aligned} \tag{3.34}$$

Considering $K1$ as a nominal controller stabilizing the plant G, the class of stabilizing controllers can be expressed as follows:

$$K(Q) = K1 + \tilde{V}_1^{-1}Q(I + V_1^{-1}NQ)^{-1}V_1^{-1} \tag{3.35}$$

$K2$ is one of the stabilizing controllers in the set $K(Q)$, the YK parameter Q can be designed to satisfy $K(Q) = K2$.

$$K2 = K1 + \tilde{V}_1^{-1}Q(I + V_1^{-1}NQ)^{-1}V_1^{-1} \tag{3.36}$$

then,

$$\begin{aligned} K2 - K1 &= \tilde{V}_1^{-1}Q(I + V_1^{-1}NQ)^{-1}V_1^{-1} \\ \tilde{V}_1(K2 - K1)V_1 &= Q(I + V_1^{-1}NQ)^{-1} \end{aligned} \tag{3.37}$$

and,

$$Q = (\tilde{V}_1^{-1} - (K2 - K1)N)^{-1}(K2 - K1)V_1 \tag{3.38}$$

Using the *Bezout* identity, the expression of Q can be simplified as follows:

$$
\begin{aligned}
Q &= (\tilde{V}_1^{-1} - \tilde{V}_2^{-1}\tilde{U}_2 N + \tilde{V}_1^{-1}\tilde{U}_1 N)^{-1}(K2 - K1)V_1 \\
Q &= ((\tilde{V}_1^{-1}(I + \tilde{U}_1 N) - \tilde{V}_2^{-1}\tilde{U}_2 N)^{-1}(K2 - K1)V_1 \\
Q &= ((\tilde{V}_1^{-1}(\tilde{v}_1 M) - \tilde{V}_2^{-1}\tilde{U}_2 N)^{-1}(K2 - K1)V_1 \\
Q &= (M - \tilde{V}_2^{-1}\tilde{U}_2 N)^{-1}(K2 - K1)V_1 \\
Q &= (\tilde{V}_2 M - \tilde{U}_2 N)^{-1}\tilde{V}_2(K2 - K1)V_1 \\
Q &= \tilde{V}_2(K2 - K1)V_1
\end{aligned}
\tag{3.39}
$$

Notice that: $K(0) = K1$ and $K(Q) = K2$ when $Q = \tilde{V}_2(K2 - K1)V_1$.

Thanks to YK parametrization, two controllers can be involved in the same control structure as shown in Fig.3.4. The stability of the closed loop is guaranteed by the stability of Q.

A scalar factor $\gamma \in [0, 1]$ is considered to guarantee smooth transition when moving from the nominal controller to another one. The class of all stabilizing controllers is expressed using the scalar factor γ, and that does not affect the stability of the closed loop showed in (3.29) and satisfies the *Bezout* identity:

$$K(\gamma Q) = (U_1 + \gamma QM)(V_1 + \gamma QN)^{-1} \tag{3.40}$$

When $\gamma = 0$ the control signal is completely generated by K_1. $0 < \gamma < 1$ generates a control signal combination of K_1 and K_2 responses. When $\gamma = 1$ the control signal is completely generated by $K2$.

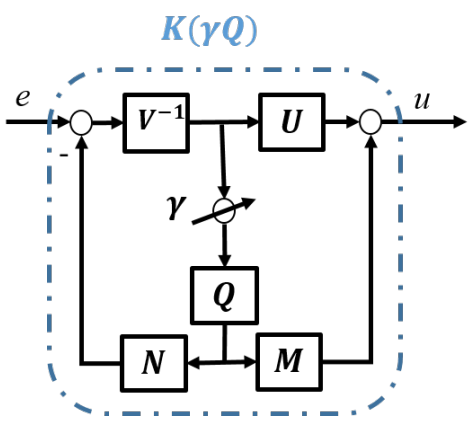

Figure 3.4: Youla-Kucera control structure

The controller transition adjusted using γ allow the adaptation of the controller response to the different operating conditions (as sensors failures, noise, ...), playing a key role in the smoothness of the final control response.

3.3.4 Youla-Kucera controller stability analysis

This section analyzes the stability of the closed loop including the YK controller K(γQ), by checking the uniform asymptotic stability of the closed loop system for every switching signal γ using notions of stability of systems with impulse effects.

System with impulse effects

Let's consider a finite set of controller transfer matrices $\mathcal{K} = \{K_i, \quad i \in \mathcal{P}\}$, each K_i stabilizes the system transfer matrix G. The general multi-controller problem is to build a control structure that switches among the transfer function in the set $\mathcal{K}$. In this context, the multi-controller K_γ is a dynamical system with two inputs; control error signal e_T and switching signal $\gamma : [0, \infty) \to \mathcal{P}$ which is a piecewise constant selecting a controller K_γ with $\gamma \in \mathcal{P}$. While γ remains constant, the multi-controller K_γ behaves like the transfer function K_i for $\gamma = i$ from its input e_T to its output u_c. The time at which the signal γ is discontinuous is called the switching time of γ. For simplicity, let's consider the signal γ continuous from above to the switching times: if t_1 and t_2 are two consecutive switching times of γ, then the signal γ is constant on $[t_1, t_2)$.

Each controller K_i in $\mathcal{K}$ is assumed to have a stabilizable and detectable realization $\{A_i, B_i, C_i, D_i\}$. Over any interval where the switching signal γ is constant, the multi-controller K_γ is defined by a dynamical system:

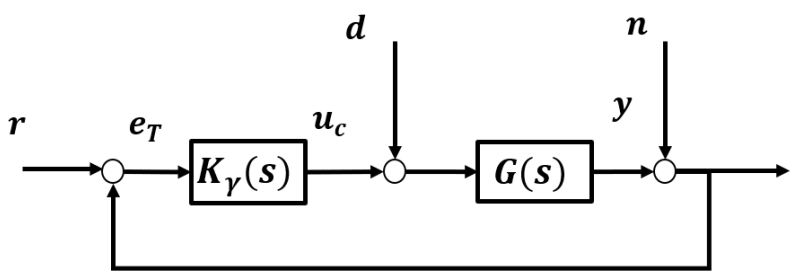

Figure 3.5: Feedback connection between the controller with impulse effects $K_\gamma(s)$ and the LTI system $G(s)$.

$$\dot{x}_c = A_\gamma x_c + B_\gamma e_T, \qquad u_c = C_\gamma x_c + D_\gamma e_T \tag{3.41}$$

And a rule to describe the controller state immediately after the switching:

$$x_c = R_c(\gamma(t), \gamma(t^-))x_c(t^-) \tag{3.42}$$

where the $R_c(i, j) \in \mathbb{R}^{n_c * n_c}, i, j \in \mathcal{P}$ is the state reset matrix. Equations (3.41)-(3.42) define a system with impulse effects [137].

When a controller $K_\gamma(s)$ with impulse effects is connected to a system $G(s)$ described by a stabilizable and detectable realization $\{A, B, C\}$ as shown in Fig.3.5, the closed loop system resulting from the feedback connection between K_γ switching from the controller K_j to K_i and $G(s)$ can be formulated as follows:

$$\dot{x} = A_{cl(\gamma)}x + B_{cl(\gamma)}w, \qquad y = C_{cl(\gamma)}x \tag{3.43}$$

with $x := \begin{bmatrix} x_G' & x_c' \end{bmatrix}'$, $w := \begin{bmatrix} d' & r' - n' \end{bmatrix}$ and:

$$A_{cl(\gamma)} := \begin{bmatrix} A - BD_iC & BC_i \\ -B_iC & A_i \end{bmatrix}, \; B_{cl(\gamma)} := \begin{bmatrix} B & 0 \\ 0 & B_i \end{bmatrix}, \; C_{cl(\gamma)} = \begin{bmatrix} C & 0 \end{bmatrix}, \; \gamma = i; \tag{3.44}$$

And at the switching time:

$$x(t) = R_{cl}(\gamma(t), \gamma(t^-))x(t^-) \tag{3.45}$$

with:

$$R(i,j) := \begin{bmatrix} I & 0 \\ 0 & R_c(i,j) \end{bmatrix}, \qquad i, j \in \mathcal{P} \tag{3.46}$$

Since each transfer function in the set $\mathcal{K}$ stabilizes the system $G(s)$, the closed loop in (3.43) is asymptotically stable for each constant value of $\gamma(t) = i \in \mathcal{P}$. However, this is not enough to guarantee that the state of the closed loop system in (3.43)-(3.45) remain bonded for every value of $\gamma(t)$ and every bounded piecewise continuous exogenous inputs r, n and d (see Example.3.2.1). Thus, the aim is to analyse the asymptotic stability where the state vector x is required to decay to zero when $r = d = n = 0$.

When $w = 0$, the autonomous solution of the closed loop state equations (3.43)-(3.45) can be written as:

$$x(t) = \phi(t, t_0; \gamma)x(t_0) \quad t, t_0 \in \mathbb{R}, \tag{3.47}$$

Where,

$$\phi(t, t_0; \gamma) := e^{(t-t_m)A_{cl(\gamma(t_m))}} \prod_{k=1}^{m-1} R_{cl}(\gamma(t_{k+1}), \gamma(t_k))e^{(t_{k+1}-t_k)A_{cl(\gamma(t_k))}}. \tag{3.48}$$

Here $\{t_1, t_2, ..., t_m\}$ are the switching times of γ in the interval $(t_0, t]$. The closed loop system in (3.43)-(3.45) is exponentially stable, if there exist positive constants c, λ such that for every γ,

$$\|\phi(t, t_0; \gamma)\| \leq ce^{-\lambda(t-t_0)} \quad \forall t, t_0 \geq 0, \tag{3.49}$$

The state transition matrix $\phi(t, t_0; \gamma)$ of a system with impulse effects has the following properties:

For any γ in $\mathcal{P}$ and $\tau \in \mathbb{R}$:

$$\begin{aligned} &(i) \quad \phi(\tau,\tau;\gamma) = I_n. \\ &(ii) \quad \frac{d}{dt}\phi(t,\tau;\gamma) = A_{cl(\gamma(t))}\phi(t,\tau;\gamma) \\ &(iii) \quad \phi(t,\tau;\gamma) = R_{cl}(\gamma(t),\gamma(t^-))\phi(t^-,\tau;\gamma) \end{aligned} \tag{3.50}$$

Property (ii) is valid in the interval where $\gamma(t)$ is constant, and property (iii) for each switching time t.

When $w \neq 0$, the solution of the closed loop state equations (3.43)-(3.45) can be written as:

$$x(t) = \phi(t,t_0;\gamma)x(t_0) + \int_{t_0}^{t} \phi(t,\tau)B_{cl(\gamma(\tau))}w(\tau)d\tau, \quad t,t_0 \in \mathbb{R}, \tag{3.51}$$

For each bounded piecewise continuous signal $w(t)$, and for every $\gamma(t)$, x(t) in (3.51) remains bounded as long as the autonomous closed loop system in (3.43)-(3.45) with $w = 0$ is exponentially stable and the condition in (3.49) is satisfied.

In the following, the stability condition for systems with impulse effects will be derived using *Lyapunov* theory.

Suppose now that, on any interval where $\gamma(t)$ is constant and equal to $i \in \mathcal{P}$, there exist symmetric, positive definite matrices $\{S_i \in \mathbb{R}^{n\times n} : i \in \mathcal{P}\}$, such that $V_i(x) := x'S_ix$ is a positive definite *Lyapunov* function. $V_i(x)$ decreases exponentially along the solution of the autonomous system in equation (3.43) with $w = 0$ if :

$$S_iA_{cl(i)} + A'_{cl(i)}S_i < 0, \qquad i \in \mathcal{P} \tag{3.52}$$

Indeed, on such an interval and for sufficiently small $\lambda > 0$.

$$\frac{d}{dt}V_i(x(t)) \leq -2\lambda V_i(x(t)). \tag{3.53}$$

And when $\gamma(t)$ switches from the controller K_j to K_i, that means when $\gamma(t^-) = j$ and $\gamma(t) = i$. The matrices S_j and S_i must satisfy the following condition:

$$R'_{cl}(i,j)S_iR_{cl}(i,j) \leq S_j, \qquad i,j \in \mathcal{P} \tag{3.54}$$

Indeed, the evolution of the *Lyapunov* function $V_i(x(t))$ in the switching time can be expressed as follows:

$$\begin{aligned} V_i(x(t)) &= x'(t)S_ix(t) = x'(t^-)R'_{cl}(i,j)S_iR_{cl}(i,j)x(t^-) \\ &\leq x'(t^-)S_jx(t^-) =: V_j(x(t^-)). \end{aligned} \tag{3.55}$$

From the resulting dynamic equations (3.53) and (3.55), the following can be deduced:

$$V_{\gamma(t)}(x(t)) \leq e^{-2\lambda(t-t_0)} V_{\gamma(t_0)}(x(t_0)), \qquad \forall t \geq t_0. \tag{3.56}$$

which yields to:

$$\|x(t)\| \leq ce^{-\lambda(t-t_0)} \|x(t_0)\|, \quad c = max_{i,j\in\mathcal{P}} \|S_i\| \|S_j\| \tag{3.57}$$

Remark 3.1 *It can be noticed that $V_{\gamma(t)}(x(t))$ may be discontinuous at the switching times but its value is always decreasing as shown in (3.55). As long as the conditions in (3.52) and (3.54) remain satisfied.*

Two special cases considering the stability conditions in (3.52) and (3.54) can be analyzed:

- A complete state reset: $R_{cl}(i,j) = 0$, for all $i,j \in \mathcal{P}$. In this case, the condition in (3.54) is trivially satisfied, and the only remaining stability condition for the switched system is the asymptotic stability of each closed loop $A_{cl(i)}$ for all $i \in \mathcal{P}$. Therefore, in this case the existence of $\{S_i : i \in \mathcal{P}\}$ that holds (3.52) is enough.
- Absence of state reset: $R_{cl}(i,j) = I$, for all $i,j \in \mathcal{P}$. In this case, the condition in (3.54) requires that all S_i to be equal, because it demands both $S_i \leq S_j$ and $S_j \leq S_i$ for all $i,j \in \mathcal{P}$. Therefore, to satisfy both conditions in (3.52) and (3.54) needs the existence of a common *Lyapunov* function for the family of the closed loops $A_{cl(i)}$, which is the sufficient exponential stability condition for the switched system in (3.43)-(3.45).

From the analysis of the two specific cases, it can be noticed that it is possible to choose a multi-controller realization that allow the existence of a common *Lyapunov* function for the closed loop switched systems. This avoids to reset the controller states.

In the following, the stability of a multi-controller switched system based on YK parametrization will be analyzed using the concept of system with impulse effects.

Youla-Kucera multi-controller stability

Let's consider a LTI feedback loop where a nominal controller $K_0(s)$ stabilizes the plant $G(s)$. K_0 and G are strictly proper transfer matrices with appropriate dimensions.

Let's $\{A, B, C\}$ and $\{A_{K_0}, B_{K_0}, C_{K_0}, D_{K_0}\}$ be minimal realizations of G and K_0, respectively, and F_G, F_{K_0} matrices such that $A + F_G C$ and $A_{K_0} + F_{K_0} C_{K_0}$ are asymptotically stable.

The matrices $A_E, B_E, C_E, D_E, F_E, G_E$ can be defined as follows:

$$A_E := \begin{bmatrix} A + F_G C & 0 \\ 0 & A_{K_0} + F_{K_0} C_{K_0} \end{bmatrix}, B_E := \begin{bmatrix} B \\ -F_{K_0} \end{bmatrix}, D_E := \begin{bmatrix} -F_G \\ -B_{K_0} - F_{K_0} D_{K_0} \end{bmatrix},$$

$$C_E := \begin{bmatrix} C & 0 \end{bmatrix}, \quad F_E := \begin{bmatrix} 0 & -C_{K_0} \end{bmatrix}, \quad G_E := D_{K_0},$$

The matrix A_E is asymptotically stable. $G(s)$ and $K_0(s)$ transfer matrices can be expressed as follows:

$$\begin{aligned} G(s) &= C_E(sI - (A_E + D_E C_E))^{-1} B_E \\ K_0(s) &= F_E(sI - (A_E - B_E F_E))^{-1}(D_E - B_E G_E) + G_E \end{aligned} \tag{3.58}$$

Based on that, right coprime factorization can be deduced for the plant $G(s) = X_p^{-1} Y_p$ and the controller $K_0(s) = X_c^{-1} Y_c$ as follows:

$$\begin{bmatrix} X_c & -Y_c \\ Y_p & X_p \end{bmatrix} := \begin{bmatrix} F_E \\ C_E \end{bmatrix} (sI - A_E)^{-1} \begin{bmatrix} B_E & -D_E \end{bmatrix} + \begin{bmatrix} I & -G_E \\ 0 & I \end{bmatrix}. \tag{3.59}$$

and the YK controller for a Q_i parameter:

$$K_i = (X_c - Q_i Y_p)^{-1}(Y_c + Q_i X_p) \tag{3.60}$$

Let's now consider a state space realisation $\left\{\bar{A}_i, \bar{B}_i, \bar{C}_i, \bar{D}_i\right\}$ for Q_i. Using the YK controller expression in (3.60) and the state space realization of the coprime factors in (3.59), the following system of equations can be realized:

$$\dot{x} = \bar{A}_i x + \bar{B}_i e_Q, \qquad v = \bar{C}_i x + \bar{D}_i e_Q, \tag{3.61}$$

$$\dot{x}_E = A_E x_E + B_E u_c - D_E e_T, \qquad e_Q = C_E x_E + e_T, \tag{3.62}$$

$$u_c = -F_E x_E + G_E e_T + v, \tag{3.63}$$

Equations (3.61), (3.62) and (3.63) describe the realization of the controller K_i as shown in the block diagram in Fig.3.6. It's important to notice that only (3.61) changes from controller to controller in the set of stabilizing controllers.

In following, the asymptotic stability of closed loop will be analyzed when the YK parameter changes from Q_j to Q_i using the formulation described below. For this purpose, the Youla Kucera parameter Q is considered as a system with impulse effects and can be described as follows:

$$\dot{x} = \bar{A}_{\gamma(t)} x + \bar{B}_{\gamma(t)} e_Q, \quad v = \bar{C}_{\gamma(t)} x + \bar{D}_{\gamma(t)} e_Q \tag{3.64}$$

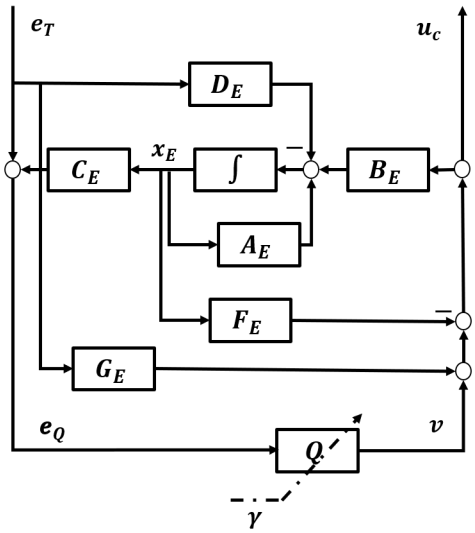

Figure 3.6: Youla-Kucera parametrized controller $K(Q)$

with,

$$x(t) = \bar{R}(\gamma(t), \gamma(t^-))x(t^-), \tag{3.65}$$

The reset matrices $\left\{\bar{R}(i,j) : i,j \in \mathcal{P}\right\}$ should be chosen so that there exist symmetric, positive definite matrices $\left\{\bar{S}_i \in \mathbb{R}^{n\times n}, i \in \mathcal{P}\right\}$, such that:

$$\bar{S}_i\bar{A}_i + \bar{A}_i'\bar{S}_i < 0, \quad \bar{R}(i,j)'\bar{S}_i\bar{R}(i,j) \geq \bar{S}_j, \quad i,j \in \mathcal{P}. \tag{3.66}$$

Using the state equations in (3.62), (3.63) and the representation of the YK parameter $Q_{\gamma(t)}$ as a system with impulse effects in (3.64) and (3.65). The state space realization of the multi-controller based on YK parametrization, including the impulse effects can be deduced as follows:

$$\dot{x}_{K(Q_i)} = A_{K(Q_i)}x_{K(Q_i)} + B_{K(Q_i)}e_T, \quad u_c = C_{K(Q_i)}x_{K(Q_i)} + D_{K(Q_i)}e_T. \tag{3.67}$$

and

$$x_{K(Q_i)}(t) = R_{K(Q_i)}(\gamma(t), \gamma(t^-))x_{K(Q_i)}(t^-) \tag{3.68}$$

with

$$A_{K(Q_i)} = \begin{bmatrix} A_E - B_EF_E + B_E\bar{D}_iC_E & B_E\bar{C}_i \\ \bar{B}_iC_E & \bar{A}_i \end{bmatrix}, \quad B_{K(Q)} = \begin{bmatrix} -D_E + B_E(\bar{D}_i + G_E) \\ \bar{B}_i \end{bmatrix}$$

$$C_{K(Q_i)} = \left[-F_E + \bar{D}_iC_E\bar{C}_i\right], \qquad D_{K(Q)} = \bar{D}_i + G_E \tag{3.69}$$

$$R_{K(Q)}(i,j) = \begin{bmatrix} I & 0 \\ 0 & \bar{R}(i,j) \end{bmatrix}. \tag{3.70}$$

Now, let's analyse the stability of the overall closed loop switched system controlled by the YK multi controller built above expressed by following state space matrix:

$$A_{cl(K(Q_i))} = \begin{bmatrix} A_E + D_E C_E - B_E(\bar{D}_i + G_E)C_E & -B_E F_E + B_E \bar{D}_i C_E & B_E \bar{C}_i \\ D_E C_E - B_E(\bar{D}_i + G_E)C_E & A_E - B_E F_E + B_E \bar{D}_i C_E & B_E \bar{C}_i \\ -\bar{B}_i C_E & \bar{B}_i C_E & \bar{A}_i \end{bmatrix} \tag{3.71}$$

Theorem 3.3.3 *There exist symmetric matrices $\{S_i : i \in \mathcal{P}\}$ for which (3.52) and (3.54) hold with $\left\{A_{cl(K(Q_i))}, R_{cl(K(Q))} : i, j \in \mathcal{P}\right\}$ as in (3.43) and (3.45), Where the process realization $\{A, B, C\}$ is given by*

$$A := A_E + D_E C_E, \qquad B := B_E, \quad C := C_E \tag{3.72}$$

The controller realization $\{A_i, B_i, C_i, D_i : i \in \mathcal{P}\}$ are given by (3.69), and the controller reset matrices $\{R_c(i,j), i, j \in \mathcal{P}\}$ are given by (3.70). The closed loop system with impulse effects in (3.43) and (3.45) is therefore exponentially stable, uniformly over $\mathcal{P}$.

To prove Theorem 3.3.3 on the closed loop state matrix $A_{cl(K(Q_i))}$, the transformation matrix $T := \begin{bmatrix} I & 0 & 0 \\ 0 & 0 & I \\ -I & I & 0 \end{bmatrix}$ is defined yielding to:

$$TA_{cl(K(Q_i))}T^{-1} = \begin{bmatrix} A_E + D_E C_E - B_E F_E - B_E G_E C_E & B_E \bar{C}_i & -B_E F_E + B_E \bar{D}_i C_E \\ 0 & \bar{A}_i & \bar{B}_i C_E \\ 0 & 0 & A_E \end{bmatrix} \tag{3.73}$$

In the following, the aim is to prove the existence of the symmetric matrices $S_i, i \in \mathcal{P}$ for the transformed matrix $TA_{cl(K(Q_i))}T^{-1}$, the diagonal elements of the matrix S_i will be constructed one by one.

First, knowing that the nominal controller K stabilizes G with the stabilizable and detectable realizations in (3.58), the matrix

$$\bar{A}_E = \begin{bmatrix} A_E + D_E C_E - B_E G_E C_E & B_E F_E \\ -(D_E - B_E G_E)C_E & A_E - B_E F_E \end{bmatrix} \tag{3.74}$$

is asymptotically stable. Therefore,

$$T_E \bar{A}_E T_E^{-1} = \begin{bmatrix} A_E + D_E C_E - B_E F_E - B_E G_E C_E & B_E F_E \\ 0 & A_E \end{bmatrix} \tag{3.75}$$

with $T_E = \begin{bmatrix} I & 0 \\ I & I \end{bmatrix}$, is also asymptotically stable. As a result, the matrices $A_E + D_E C_E - B_E F_E - B_E G_E C_E$ and A_E are asymptotically stable and there exist positive definite symmetric matrices S_1 and S_2 such that:

$$S_1(A_E+D_E C_E-B_E F_E-B_E G_E C_E)+(A_E+D_E C_E-B_E F_E-B_E G_E C_E)' S_1' = -I, \tag{3.76}$$

$$S_2 A_E + A_E' S_2' = -I. \tag{3.77}$$

In addition, each YK parameter Q_i is stable, so there exist:

$$P_i = -\bar{S}_i \bar{A}_i - \bar{A}_i' \bar{S}_i', \quad i \in \mathcal{P} \tag{3.78}$$

which is a positive definite. Therefore, there must exist a positive constant ϵ, sufficiently small, such that:

$$P_i - \epsilon \bar{S}_i \bar{B}_i C_E C_E' \bar{B}_i' \bar{S}_i > 0, \forall i \in \mathcal{P}, \tag{3.79}$$

which guarantees that each matrix R_i is also positive definite such as:

$$R_i = \begin{bmatrix} P_i & -\bar{S}_i \bar{B}_i C_E \\ -C_E' \bar{B}_i' \bar{S}_i & \epsilon^{-1} \end{bmatrix}, \quad i \in \mathcal{P} \tag{3.80}$$

Now, the positive definite symmetric matrix can be defined to hold (3.52) and (3.54) for the closed loop system state matrix $A_{cl(K(Q_i))}$ in (3.71) as follows:

$$S_{cl(K(Q_i))} = T' \begin{bmatrix} \epsilon_1 S_1 & 0 & 0 \\ 0 & \epsilon \bar{S}_i & 0 \\ 0 & 0 & S_2 \end{bmatrix} T \tag{3.81}$$

with:

$$\epsilon_1 = \frac{1}{2}(\max_{i \in \mathcal{P}} \|S_1 W_i R_i^{-1} W_i' S_1\|)^{-1} \tag{3.82}$$

where, for each $i \in \mathcal{P}$,

$$W_p = \begin{bmatrix} B_E \bar{C}_i & -B_E F_E + B_E \bar{D}_i C_E \end{bmatrix} \tag{3.83}$$

From (3.71) and (3.81), we have:

$$S_{cl(K(Q_i))} A_{cl(K(Q_i))} + A_{cl(K(Q_i))}' S_{cl(K(Q_i))}' = -\epsilon_1 T' \begin{bmatrix} I & -S_1 W_i \\ -W_i' S_1 & \epsilon_1^{-1} R_i \end{bmatrix} T, \quad i \in \mathcal{P} \tag{3.84}$$

From (3.82) we have $I - \epsilon_1 S_1 W_i R_i^{-1} S_1 W_i > 0$ for each $i \in \mathcal{P}$, that makes the determinant of $\begin{bmatrix} I & -S_1 W_i \\ -W_i' S_1 & \epsilon_1^{-1} R_i \end{bmatrix}$ positive, thus:

$$\begin{bmatrix} I & -S_1 W_i \\ -W_i' S_1 & \epsilon_1^{-1} R_i \end{bmatrix} > 0, \quad i \in \mathcal{P}. \tag{3.85}$$

From (3.84) and (3.85) it can be concluded that the first stability condition in (3.52) is hold for $A_{cl(K(Q_i))}$. Let's now consider the second stability condition (3.54) for the closed loop reset matrix:

$$R(i,j)'S_iR(i,j)-S_j = \begin{bmatrix} 0 & 0 & 0 \\ 0 & 0 & 0 \\ 0 & 0 & \epsilon(\bar{R}(i,j)'\bar{S}_i\bar{R}(i,j)) - \bar{S}_j) \end{bmatrix}, \quad i,j \in \mathcal{P} \quad (3.86)$$

The non zero element of the matrix (3.86) is negative because of the design condition in (3.66). Thus, the second stability condition is hold for the closed loop reset matrix because (3.86) is negative semi-definite. This proves the Theorem 3.3.3.

3.4 Numerical example

This section presents a numerical example of switching between two different controller using YK parametrization.

Let's consider a second order completely controlable and observable plant $G(s)$ with it's correspondent state space realization:

$$G(s) = \frac{1}{s^2+2s+2}, \quad \left[\begin{array}{c|c} A_G & B_G \\ \hline C_G & D_G \end{array}\right] = \left[\begin{array}{cc|c} -2 & -2 & 1 \\ 1 & 0 & 0 \\ \hline 0 & 1 & 0 \end{array}\right] \quad (3.87)$$

Two controllers K_1 and K_2 are designed to perform two different closed loop performance.

$$K_1(s) = \frac{-400s^2-5500s-800}{s^2+100s}, \quad \left[\begin{array}{c|c} A_{K_1} & B_{K_1} \\ \hline C_{K_1} & D_{K_1} \end{array}\right] = \left[\begin{array}{cc|c} -100 & 0 & 256 \\ 1 & 0 & 0 \\ \hline 134.8 & -3.125 & -400 \end{array}\right] \quad (3.88)$$

And:

$$K_2(s) = \frac{-100s^2-200s-200}{s^2+100s}, \quad \left[\begin{array}{c|c} A_{K_2} & B_{K_2} \\ \hline C_{K_2} & D_{K_2} \end{array}\right] = \left[\begin{array}{cc|c} -100 & 0 & 128 \\ 1 & 0 & 0 \\ \hline 76.56 & -1.563 & -100 \end{array}\right] \quad (3.89)$$

To design the YK multi controller, the first step is to compute the coprime factors of the plant $G(s)$, $K_1(s)$ and $K_2(s)$. The right coprime factors M, N, U, V and the left coprime factors $\tilde{M}, \tilde{N}, \tilde{U}, \tilde{V}$ are computed using the formulas in (3.17) and (3.18) respectively. For the plant, the feedback gain is $F_G = \begin{bmatrix} 0.5 & 0.4375 \end{bmatrix}$ resulting in the following stable factors:

$$\begin{bmatrix} M & \tilde{M} \\ N & \tilde{N} \end{bmatrix} = \begin{bmatrix} \frac{s^2+2s+2}{s^2+1.5s+1.563} & \frac{s^2+2s+2}{(s+96.37)(s+0.1424)} \\ \frac{1}{s^2+1.5s+1.563} & \frac{1}{(s+96.37)(s+0.1424)} \end{bmatrix} \quad (3.90)$$

For the controllers $F_{K_1} = \begin{bmatrix} 0.3692 & -0.2277 \end{bmatrix}$ and $F_{K_2} = \begin{bmatrix} 0.7383 & -0.4553 \end{bmatrix}$ resulting in the following stable coprime factors:

$$\begin{bmatrix} U_1 & \tilde{U}_1 \\ V_1 & \tilde{V}_1 \end{bmatrix} = \begin{bmatrix} \frac{-400(s+13.6)(s+0.147)}{(s^2+5.492s+58.28)} & \frac{-400(s+0.147)(s+13.6)(s^2+1.5s+1.563)}{(s+96.37)(s+0.1424)(s^2+5.492s+58.28)} \\ \frac{s(s+100)}{(s^2+5.492s+58.28)} & \frac{s(s+100)(s^2+1.5s+1.563)}{(s+96.37)(s+0.1424)(s^2+5.492s+58.28)} \end{bmatrix} \tag{3.91}$$

$$\begin{bmatrix} U_2 & \tilde{U}_2 \\ V_2 & \tilde{V}_2 \end{bmatrix} = \begin{bmatrix} \frac{-100(s^2+2s+2)}{(s^2+5.492s+58.28)} & \frac{-100(s^2+1.5s+1.563)}{(s+98.99)(s+1.01)} \\ \frac{s(s+100)}{(s^2+5.492s+58.28)} & \frac{s(s+100)(s^2+1.5s+1.563)}{(s+98.99)(s+1.01)(s^2+2s+2)} \end{bmatrix} \tag{3.92}$$

YK parameter $Q(s)$ is computed using the formula in (3.39):

$$Q = \frac{300s(s+0.1139)(s+17.55)(s+100)(s^2+1.5s+1.563)}{(s+98.99)(s+1.01)(s^2+2s+2)(s^2+5.492s+58.28)} \tag{3.93}$$

The multi-controller based on Q is implemented using the structure illustrated in Figure 3.4, the scalar factor γ is varying in $[0,1]$ to show the evolution of the closed loop behavior. In the following, the behavior of the closed loop controlled by the YK parametrized controller $K(\gamma Q)$ is analyzed in the temporal space as well as in the frequency space.

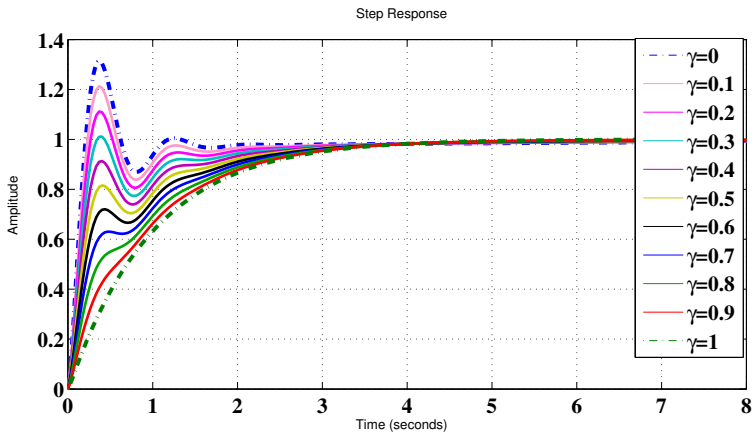

Figure 3.7: step response evolution with γ varying from 0 to 1

Figure 3.7 depicts the step responses of the plant $G(s)$ controlled first by the controller K_1 (dashed blue line), then by the controller K_2 (dashed green line) and finally, by the parametrized controlled $K(\gamma Q)$ with different values of $\gamma \in [0,1]$ (solid colored lines). The dashed blue line shows the step response of the first closed loop (CL_1) with an 31.4% overshoot and a rise time 0.154 seconds, the dashed green line shows the step response of the

Table 3.2: YK closed loop temporal response characteristics

γ	0	0.1	0.2	0.3	0.4	0.5	0.6	0.7	0.8	0.9	1
Overshoot (%)	31.4	21.3	11.2	1.1	0	0	0	0	0	0	0
Rise time (sec)	0.154	0.17	0.194	0.228	0.309	1.73	1.85	1.95	2.01	2.12	2.17

second closed loop (CL_2) without overshoot and a rise time of 2.17 seconds. YK based closed loop controller responses evolve from K1 to k2 reducing the overshoot and increasing the rise time. Table 3.2 reports the values of the overshoot and rise time for each value of γ. The value of the overshoot decreases when γ goes from 0 to 1 while the value of the rise time increases, which can be justified by the fact that the YK controller $K(\gamma Q)$ evolves from K_1 to K_2 and CL_1 presents the most important overshoot and the smallest rise time. It is important to notice that the values of the temporal characteristics are bounded by the values of the temporal characteristics of CL_1 and CL_2 and presents a monotonous evolution with respect to γ as shown in Figure 3.7 (solid colored lines).

Table 3.3: YK closed loop zero's evolution with respect to γ

	Z_1	Z_2	Z_3	Z_4
$\gamma = 0$	X	-13.6030	X	-0.1470
$\gamma = 0.1$	-98.9111	-13.2485	-1.1264	-0.1465
$\gamma = 0.2$	-98.8191	-12.8215	-1.2723	-0.1460
$\gamma = 0.3$	-98.7101	-12.2957	-1.4617	-0.1455
$\gamma = 0.4$	-98.5789	-11.6284	-1.7191	-0.1450
$\gamma = 0.5$	-98.4182	-10.7432	-2.0941	-0.1445
$\gamma = 0.6$	-98.2165	-9.4720	-2.7130	-0.1441
$\gamma = 0.7$	-97.9559	-7.1172	-4.2043	-0.1436
$\gamma = 0.8$	-97.6064	-5.0627+ 3.1833j	-5.0627- 3.1833j	-0.1432
$\gamma = 0.9$	-97.1132	-4.1797 + 5.1861j	-4.1797 - 5.1861j	-0.1428
$\gamma = 1$	P_2	P_3	P_4	P_6

Regarding the frequency analysis of the parametrized closed loop CL_{YK}, the poles and zeros of the closed loops resulting from each value of γ are presented in Table 3.3 and Table 3.4 respectively. The poles corresponding to the different values of $0 < \gamma < 1$ remain the same, and are in $\{CL_1$ pole's $\cup\, CL_2$ pole's $\}$. The zeros move with respect to γ from the zeros of CL_1 to the poles of CL_1 to compensate them when γ is equal to 1 and the system is entirely controlled by K_2. Table 3.3 shows how the zero Z_1 moves to compensate of the pole P_2, same for Z_2 that moves from a zero of CL_1 to

Table 3.4: YK closed loop pole's evolution with respect to γ

	P_1	P_2	$P_{3,4}$	P_5	P_6
$\gamma = 0$	X	-96.3659	-2.7458± 7.1233j	X	-0.1424
$\gamma = 0.1$	-98.9898	-96.3659	-2.7458± 7.1233j	-1.0102	-0.1424
$\gamma = 0.2$	-98.9898	-96.3659	-2.7458± 7.1233j	-1.0102	-0.1424
$\gamma = 0.3$	-98.9898	-96.3659	-2.7458± 7.1233j	-1.0102	-0.1424
$\gamma = 0.4$	-98.9898	-96.3659	-2.7458± 7.1233j	-1.0102	-0.1424
$\gamma = 0.5$	-98.9898	-96.3659	-2.7458± 7.1233j	-1.0102	-0.1424
$\gamma = 0.6$	-98.9898	-96.3659	-2.7458± 7.1233j	-1.0102	-0.1424
$\gamma = 0.7$	-98.9898	-96.3659	-2.7458± 7.1233j	-1.0102	-0.1424
$\gamma = 0.8$	-98.9898	-96.3659	-2.7458± 7.1233j	-1.0102	-0.1424
$\gamma = 0.9$	-98.9898	-96.3659	-2.7458± 7.1233j	-1.0102	-0.1424
$\gamma = 1$	-98.9898	X	X	-1.0102	X

compensate P_3, and Z_3 to P_4, finally Z_4 moves to compensate P_6.

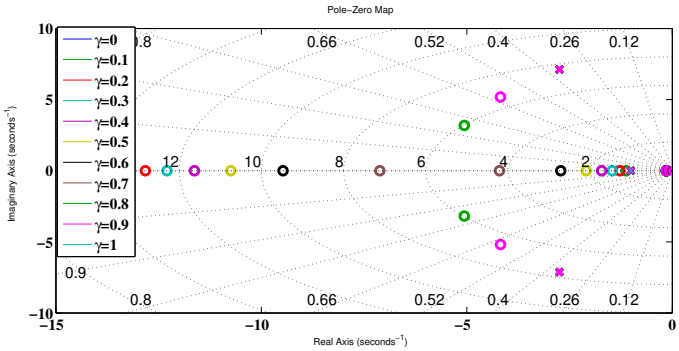

(a) Zeros' motion from Z_2 and Z_3 to P_3 and P_4 respectively

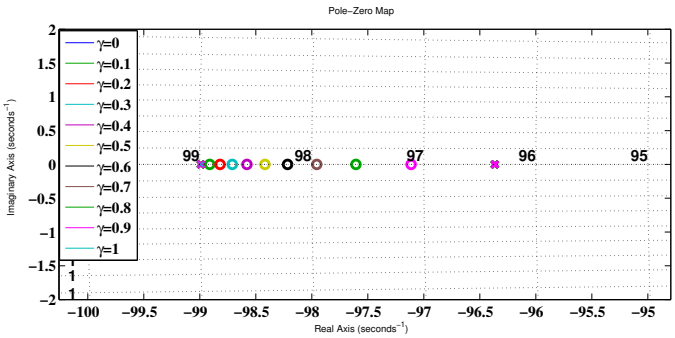

(b) Zeros' motion from Z_1 to P_2

Figure 3.8: Zeros and poles map

Figure 3.8 shows the poles and zeros of the CL_{YK} for different values

of γ in a pole-zero map, the poles are represented by crosses and zeros with circles. Figure 3.8a describes the motion of Z_2 and Z_3 to P_3 and P_4 respectively, and figure 3.8b shows the convergence of Z_1 to P_2.

3.5 Conclusion

This chapter presented the basis on building a multi-objective controller based on YK parametrization. The mathematical framework of doubly coprime factors is described showing its key role in designing the YK parameter Q. The set of all stabilizing controllers $K(\gamma Q)$ is build using the plant model $G(s)$ and a nominal controller K_0. The final controller is re-configurable and can switch within the set all stabilizing controllers without loosing the stability of the closed loop. The switching is supervised by the signal $\gamma(t)$ designed to accommodate the controller reconfiguration to the operating conditions by activating the suitable controller at each instant. Thus, the closed loop performance is enhanced in all circumstances. The stability of the closed loop is a key aspect in this context, since arbitrary switching between stabilizing controllers can yield to unstable behavior. A deep stability analysis of YK parametrized controller is provided using stability notions of system with impulse effects; It's proved that YK paramterization allows to perform stable arbitrary switching within the entire set of stabilizing controllers.

A numerical example is given, proving how YK parameterization stabilizes a transition between two controllers where direct linear change results unstable, having a state dependent switching signal. Another numerical example showing the steps to build a YK based controller, while moving from a second order closed loop response to a first order closed loop response is also depicted in this chapter.

Different structures are derived in the literature from the common multi-controller definition $K(\gamma Q)$. Stability property remains preserved within the different implementations, but the transition performance can be sensitive to the multi-controller implementation. Next chapter analyses the transient behavior with respect to different design criteria: the placement of the switching signal in the control loop; the dynamic of the nominal controller; and the switching frequency.

Chapitre 4

Analyse du comportement transitoire des structures de contrôle de YK.

Below is a French summary of chapter 4.

Ce chapitre explore le comportement transitoire des structures de contrôle basées sur la paramétrisation de YK lorsqu'elles transitent entre deux contrôleurs différents. Comme indiqué dans le chapitre précédent, le paramétrage YK permet de connecter tous les régulateurs stabilisant un système donné en utilisant le paramètre de YK Q dans une structure de contrôle, garantissant ainsi une commutation stable entre les différents régulateurs. Cependant, la transition entre deux régulateurs peut dégrader les performances de la boucle fermée dans une implémentation réelle du système. Ainsi, le comportement transitoire des différentes implémentations YK est étudié en fonction de différents paramètres de conception.

Plus précisément, huit structures de contrôle différentes basées sur YK sont comparées en fonction de trois paramètres principaux : 1) placement du signal de commutation dans la structure ; 2) configuration du contrôleur en fonction de la dynamique de la boucle fermée de chaque contrôleur indépendant; et 3) relation entre la fréquence du signal de commutation et la réponse du système en boucle fermée. La comparaison est effectuée à l'aide de deux régulateurs différents: des réponses en boucle fermée de premier et de second ordre afin d'évaluer le comportement transitoire. Ensuite, quelques lignes directrices sur la façon de concevoir les contrôleurs basés sur la paramétrisation de YK en fonction du cahier de charge sont fournies.

Chapter 4

Transient behavior analysis for YK control structures

This chapter explores the temporal evolution of YK-based control structures when transiting between two different controllers. As stated in the previous chapter, YK parametrization allows the connection of all stabilizing controllers for a given plant using the YK parameter Q in one control structure, guaranteeing stable switching between the different stabilizing controllers. However, the transition between two controllers may degrade the closed loop performance in a real implementation of the system. Thus, the transient behavior of the different YK implementation is studied according to different design parameters.

Specifically, eight different YK-based control structures are compared according to three main parameters: 1) switching signal placement on the structure; 2) controller configuration according to the closed-loop bandwidth of each independent control response; and 3) relationship between switching signal frequency and closed-loop system response. The comparison is carried out using two different controllers: first and second order closed-loop responses in order to evaluate the transient behavior. Then, some guidelines about how to design YK-based controllers according to the requirements are provided.

The rest of this chapter is structured as follows: Section 4.1 introduces the different YK-based control structures. Section 4.2 presents the different transient behavior analysis and guidelines on implementing the different structures. To finish, concluding remarks are given in section 4.3.

4.1 YK control structure implementations

YK parametrization provides all stabilizing controllers by connecting a plant G with an initial controller K_0 and the YK parameter Q, which can be any stable system with appropriate dimensions. Eight different YK control structure implementations are used in the literature as shown from Fig. 4.1a to Fig. 4.1h. Each new structure tries to overcome a limitation of the former one.

The standard structure is $S1$ presented in [138], it has been modified to avoid some drawbacks: matrix inversability [139], plant disconnection [25] [26], or to reduce the complexity of the YK transfer function [101], giving a total of eight different YK structures for controller reconfiguration. There are few studies that compare the different structures and the benefits/drawbacks of each of them. In [140] the different YK control structures are identified and compared in function of their benefits/drawbacks and the transient behavior when doing controller reconfiguration. Even if a stable transition and closed-loop poles positions are maintained, transient responses resulted different depending on the employed YK control structure. Structures 2, 6 and 8 are the fastest one without oscillations.

Table 4.1 presents results of a study conducted about different YK structures [140]. It shows structures 1 to 8 (S1 to S8) with their benefits/drawbacks, specific Q calculation and main reference where the structure could be found. It is important to remark that the scalar factor γ is responsible of the transition between the two controllers. u is the control signal and y the output of the system G.

Table 4.1: Summary Table YK structure for controller reconfiguration.

	K^1	C^2	MI^3	Q^4	S^5	Ref^6
S1	✓	↑	✓	$M_0^{-1}M_1(\tilde{U}_1V_0 - \tilde{V}_1U_0)$	✓	[138]
S2	✓	↑	✓	$M_0^{-1}M_1(\tilde{U}_1V_0 - \tilde{V}_1U_0)$	✓	[138]
S3	X	↑	X	$M_0^{-1}M_1(\tilde{U}_1 - \tilde{V}_1\tilde{U}_0\tilde{V}_0^{-1})$	✓	[26]
S4	X	↑	X	$\mathrm{M}_0^{-1}M_1(\tilde{V}_0^{-1}(\tilde{U}_1V_0 - \tilde{V}_1U_0))$	✓	[26]
S5	✓	↑	X	$M_0^{-1}M_1(\tilde{U}_1V_0 - \tilde{V}_1U_0)$	✓	[139] [101]
S6	✓	↑	X	$M_0^{-1}M_1(\tilde{U}_1V_0 - \tilde{V}_1U_0)$	✓	[139] [101]
S7	✓	↓	✓	-	X	[101]
S8	✓	↓	✓	-	X	[101]

[1]K_0 disconnection [2]Complexity [3]Matrix inversability [4]YK parameter Q
[5]System variation through dual YK parameter S [6]Structure reference

In the following, the eight structures are compared by evaluating three different parameters design: 1) switching signal placement within the struc-

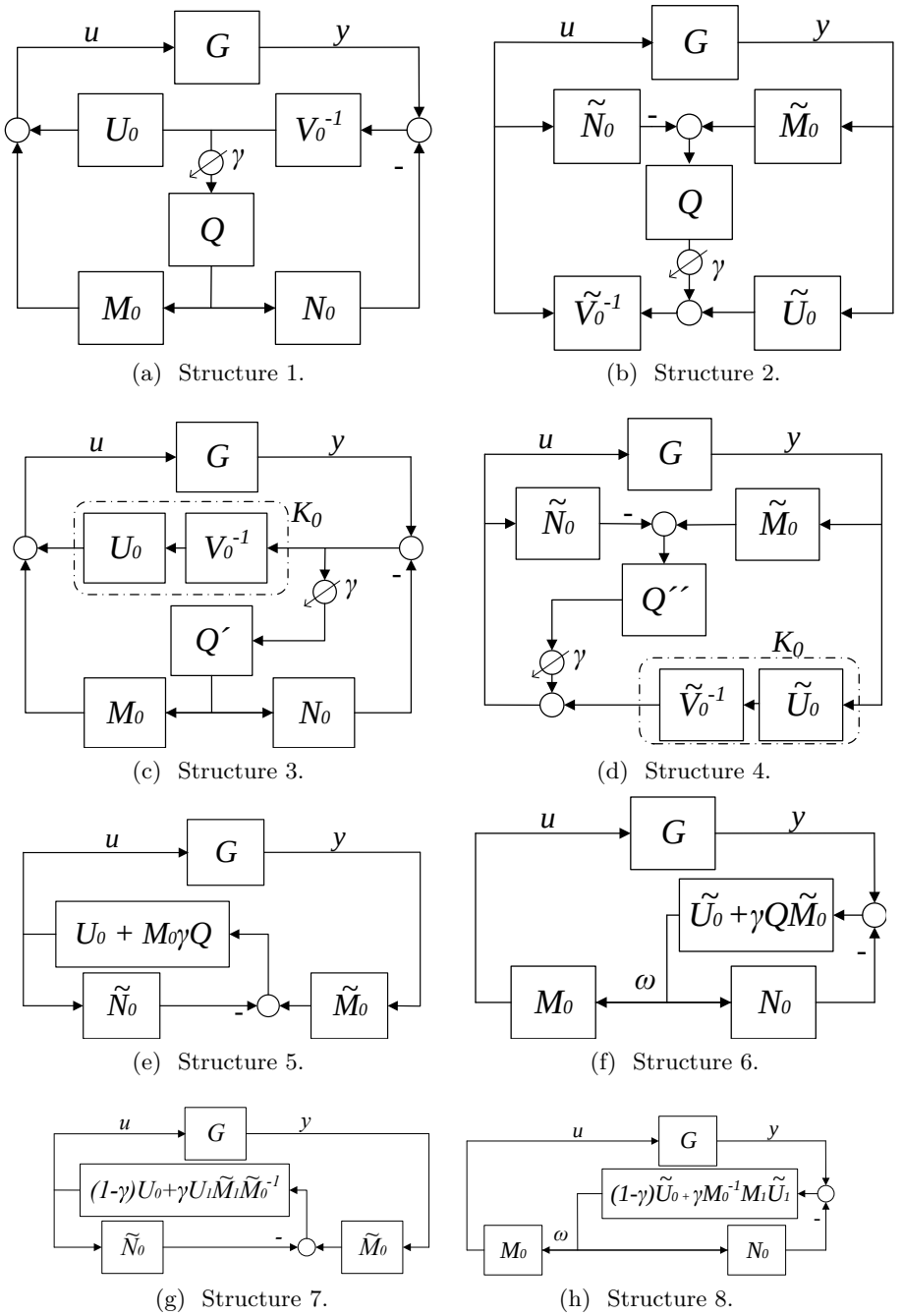

(a) Structure 1. (b) Structure 2.

(c) Structure 3. (d) Structure 4.

(e) Structure 5. (f) Structure 6.

(g) Structure 7. (h) Structure 8.

Figure 4.1: Youla-Kucera structures.

ture; 2) controller configuration according to the closed-loop bandwidth of each independent control response; and 3) relationship between switching signal frequency and closed loop system response.

4.2 Transient behavior

The transient comparative analysis is carried out from the time to convergence point of view. Having this in mind, three different situations are considered:

- γ placement: according to the eight structures and the way of implementing them in reality, gamma may be located either after or before the Q, affecting the whole system performance.
- Initial and final control dynamics: YK paramerization guarantees stability when evolving between two controllers. However, there are no guidelines in how transition changes when different initial and final control dynamics are employed. The objective is to analyze the benefit of going first from the faster to the slower or vice-versa.
- γ switching frequency: the maximum allowed frequency to transit between two controllers may also be critical to guarantee a given performance during the transition.

4.2.1 γ placement

According to the YK parametrization, the class of all stabilizing controllers in function of the YK parameter Q and the scalar factor γ is expressed as follows:

$$K(\gamma Q) = (U_0 + M_0\gamma Q)(V_0 + N_0\gamma Q)^{-1} \tag{4.1}$$
$$= (\tilde{U}_0 + \gamma Q\tilde{M}_0)(\tilde{V}_0 + \gamma Q\tilde{N}_0)^{-1} \tag{4.2}$$

The scalar factor $\gamma \in [0, 1]$ is the one in charge of doing the control reconfiguration in any of the eight existing structures in the literature provided in section 4.1. γ plays a key role in selecting the proportion of each controller (K_0 or K_1) in the final control signal:

- When $\gamma = 0$ the control signal is the one corresponding to K_0.
- $0 < \gamma < 1$ generates a mixed control signal between K_0 and $K1$ responses.
- When $\gamma = 1$ the control signal is the one corresponding to $K1$.

As it is a scalar factor multiplying a transfer function, it could be either implemented before or after Q without affecting the mathematical approach. However, this may degrade the performance in a real implementation of the system. The impact of its placement in the transient behavior is firstly analyzed. Original γ placement in the literature for the eight YK-based

structure is compared with the other option, seeking to improve system transition.

The effect of γ placement on the transient behavior of the different YK-based control structures is carried out using a numerical example.

Let's consider a plant G that may be stabilized using two different controllers K_1 and K_2. Their closed-loop responses correspond to:

$$Cl_{K_1} = \frac{1}{(\frac{4}{3}s+1)(2s+1)} \tag{4.3}$$

$$Cl_{K_2} = \frac{1}{s+1} \tag{4.4}$$

A step change in the signal γ is generated in order to check if its placement affects the transition. This is evaluated from the time-to-convergence point of view.

Figure 4.2 depicts the transient behavior of each structure with different γ positions: before or after YK parameter Q. A step in γ from 0 to 1 is generated at second 3 (pink solid line). Initial and final responses of controllers K_1 and K_2 are plotted in blue and green dotted lines respectively. System responses during transition when γ is before Q are shown in the top graph. The middle graph represents system responses when γ is placed after Q. The bottom graph depicts responses with the optimal γ placement.

When γ is placed before YK parameter Q, structures $S1$, $S2$, $S4$, $S5$, $S6$ and $S7$ present the same transient behavior (black solid line); response converges to K_2 after 2.6 seconds with a small overshoot. Structure $S3$ (red solid line) converges after 3.4 seconds from the switching instant without overshoot. Structure $S8$ presents an important overshoot with a time to converge of 10 seconds (blue solid line).

When γ is placed after YK Q, structures $S1$, $S2$, $S3$, $S6$, and $S8$ (blue solid line) present the same transient behavior: Time to converge is 1.8 seconds, without overshoot. Structures $S5$ and $S7$ (black solid line) present the same behavior, time to converge is 2.1 seconds without overshoot. Structure $S4$ (cyan solid line) shows an important overshoot with a long time to converge of 10 seconds.

Similar tests were carried out with different closed loops systems, concluding that the behavior is reproducible even if closed loop changes. From a practical implementation point of view, one can clearly appreciate the impact of the placement in the closed-loop system response.

An optimal γ placement is deduced for each structure (see table 4.2). The response of the eight control structures using the optimal γ location is depicted in the bottom graph of Fig. 4.2.

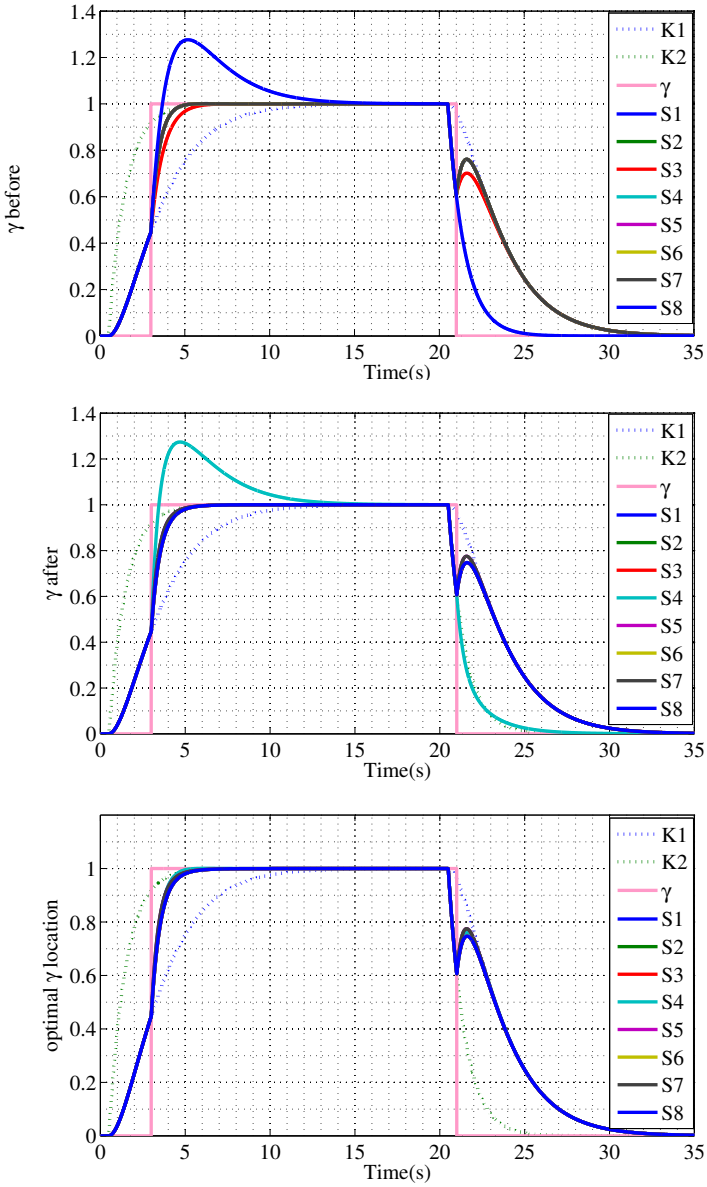

Figure 4.2: Transient behavior analysis with respect to γ placement.

Table 4.2: Optimal γ placement in YK structures.

	S1	S2	S3	S4	S5	S6	S7	S8
γ	after	after	after	before	after	after	after	after

4.2.2 Initial and final controllers dynamics

The eight YK control structures presented in section 4.1 allow stable controller reconfiguration. Stability is ensured independently of the sense of

switching of γ (i.e. from 0 to 1 or 1 to 0). However, the choice of initial and final controller affects the transition behavior. This section analyses how the transient behavior changes in each structure depending on dynamics of initial and final controllers (i.e. from slow to fast control dynamics or vice-versa).

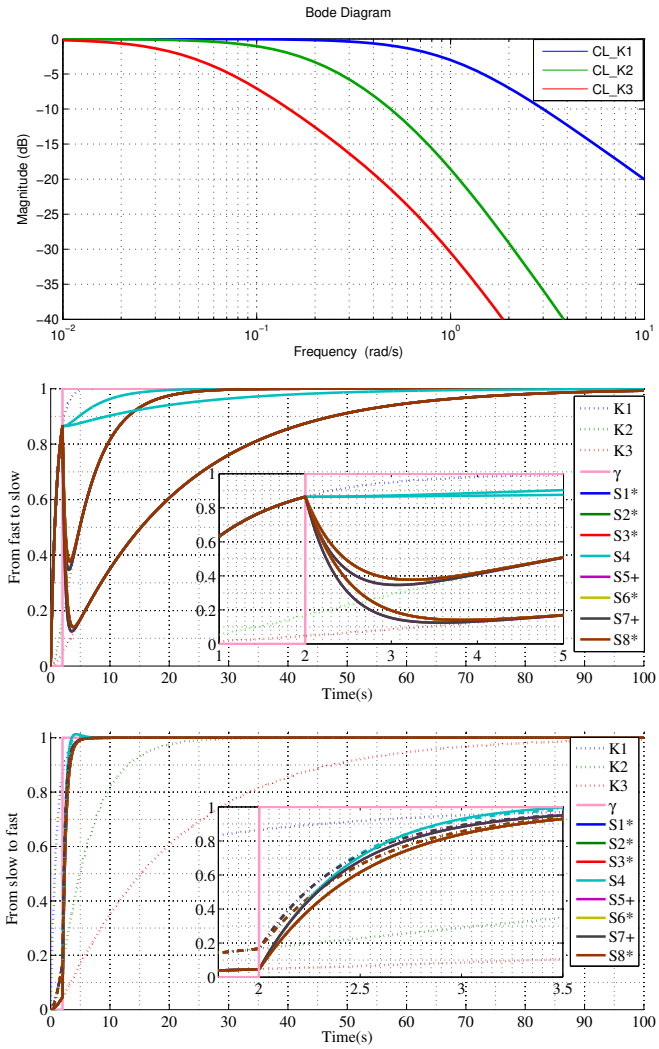

Figure 4.3: Transient behavior analysis with respect to the nominal controller dynamic

To evaluate the different structures behavior with respect to the initial and final controller dynamics, different closed-loop responses are tested.

The top graph of figure 4.3 shows three different closed loops frequency responses, controllers K_1, K_2 and K_3 are designed to provide the following bandwidths: $1rad/s$ (blue solid line), $0.1rad/s$ (green solid line) and

$0.05rad/s$ (red solid line) respectively.

YK parameter Q is computed in each structure using mathematical expressions indicated in Table 4.1 together with the optimal γ placement indicated in the previous section. Those are calculated for switching from K_1 to K_2, K_1 to K_3, K_2 to K_1 and K_3 to K_1, so fast-slow or slow-fast modifications with small and large dynamics differences are tested.

Middle graph depicts responses when the initial controller is the faster one K_1 (blue dotted line) and the final one is either K_2 (green dotted line) or K_3 (red dotted line). The switching signal γ is plotted in pink solid line. Structures $S5$ and $S7$ (black solid line) converge from K_1 to K_2 or K_3 response in 2 seconds; the time to converge of structures $S1$, $S2$, $S3$, $S6$ and $S8$ (brown solid line) is 2.2 seconds as shown in the zoomed part of the graph; $S4$ (cyan solid line) took the same time to converge from $K1$ to $K2$ response that the $K2$ took to converge to the reference (it is similar to the response time of the closed-loop $K2$); the same result is shown while switching from $K1$ to $K3$ (time to converge is equivalent to the closed-loop response time with K_3). The slower the final controller the slower the transition from initial to final controller when using $S4$.

Bottom graph plots responses in Fig. 4.3 show the scenario when the initial controller is the slow one K_3 and the final the faster one (either K_1 or K_2). Structures $S1$, $S2$, $S3$, $S5$, $S6$, $S7$ and $S8$ (brown solid line) present a similar result than in the previous case, time to converge is 2 seconds. Only $S4$ has a different behavior (cyan solid line), it converges after 6 seconds, which is again similar to the response time of the closed loop with K_1.

These tests were carried out with different closed loops systems, concluding that structures $S1$, $S2$, $S3$, $S5$, $S6$, $S7$ and $S8$ present the same transition behavior no matter the dynamic of the initial and final controllers; and structure $S4$ takes the same time to converge that the response time of the final controller closed-loop response. Thus, in order to ensure the transition convergence using $S4$, especially in applications with high frequency switching, it is recommended to compute the YK parameter in order to switch from the slow to the fast controller.

4.2.3 Switching frequency

It has been already stated that the use of YK parametrization with an arbitrary switching signal will not affect the stability of the system [19] (see section 3.3.4 for more details). However, the switching frequency defined as the number of transitions from 0 to 1 and from 1 to 0 per second could degrade the YK controller performance. Different switching frequencies are tested below, using the eight control structures.

The effect of γ frequency in the transient behavior of the different YK-based control structures is carried out using the same closed-loop control response presented in section 4.2.1 for two different controllers K_1 and K_2.

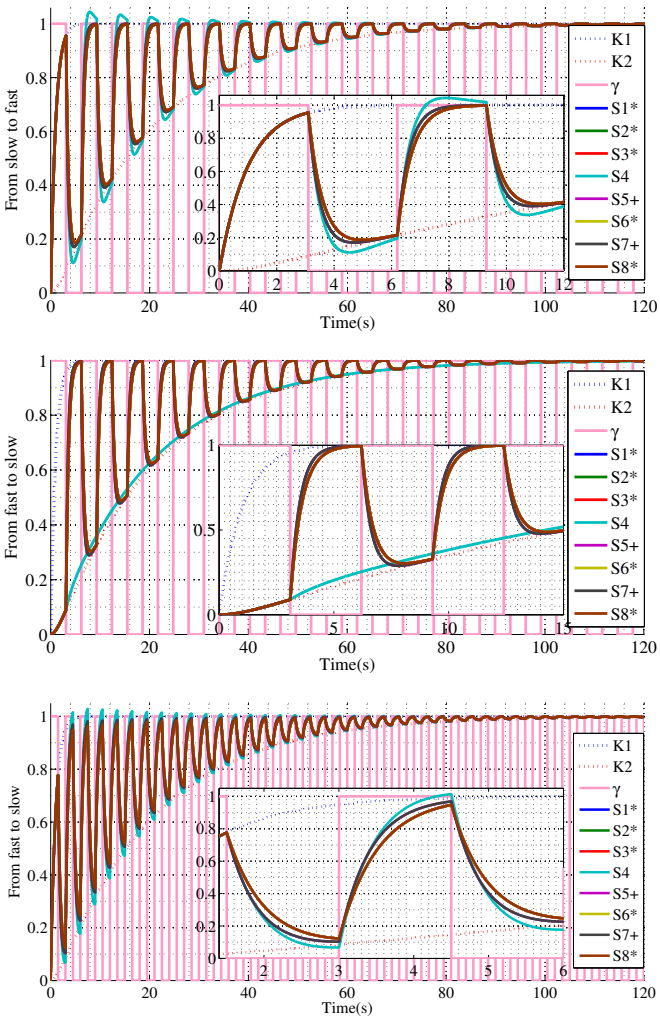

Figure 4.4: Transient behavior analysis with respect to switching frequency

The switching signal γ is placed in its optimal placement as indicated in table 4.2. Again, the time-to-convergence will be studied to evaluate γ frequency impact.

Responses of the different YK-based control structures with different frequency switching signals are presented in Fig. 4.4. γ is a square signal between [0,1] with a given frequency (pink solid line). Responses corresponding to controllers K_1 and K_2 are plotted in dotted blue and red lines. Different YK parameters Q are obtained to switch from $K1$ to $K2$ or vice-versa.

First plot corresponds to the case where switching is performed from $K2$ to $K1$ (from slow to fast) with γ's frequency equal to $1rad/s$ (this is equal to the bandwidth of the fast closed loop CL_{K_1}). Results show that

all structures (brown and grey solid lines) reach the final controller (in both cases γ: 0 => 1 or 1 => 0), except structure $S4$ (cyan solid line) that requires more time to reach convergence. Second plot corresponds to the case where switching is carried out from fast K_1 to slow K_2 controllers with the same switching frequency. Under this situation, the results show that all structures (brown and grey solid line) except $S4$ performed the switching properly. Structure $S4$ (cyan solid line) could not switch at this frequency, as structure $S4$ takes the same time that the slow controller to converge as shown in Fig.4.3. Bottom graph shows the same design configuration that in the first graph (from K_2 to K_1) but with a switching frequency of $2rad/s$. Results show how all structures can not perform a complete switch since this frequency is higher than the bandwidth of the fast closed loop ($1rad/s$).

Thus, all structures except $S4$ converge to their final solution when the switching frequency is below the bandwidth of the fast closed-loop independently of the direction of switching. The more the frequency of the switching signal γ is high the more the performance is degraded since the control structure has less time to converge from one controller response to the other one.

4.3 Conclusion

This chapter presented a study of the potential different implementations of YK-based control structures and their impact during the transient behavior. Specifically, three main parameters are evaluated: switching signal placement, closed-loop bandwidth capabilities of each controller; and switching signal frequency. The evaluation is carried out from the time-to-convergence point of view by using a numerical example. A comparison between the implementation complexities of each of them is included.

Next guidelines that can be deduced from the provided study are: γ placement after the YK Q provides better responses in all control structures except in $S4$ where it must be placed before. When possible, the second controller must be the fastest one in all structures. When switching frequency is not a design requirement, the frequency transition must be carried out slower than the slow closed-loop response while using $S4$. All structures except $S4$ can reach the final controller response for all switching frequencies up to fast closed loop bandwidth. Transient behavior response is degraded when the switching signal is higher than the faster closed-loop response.

In the next chapters, YK based lateral and longitudinal controllers are designed for autonomous vehicles, following the resulting implementation guidelines.

Chapitre 5

Contrôle latéral

Below is a French summary of chapter 5.

Ce chapitre explore l'utilisation de la paramétrisation de YK pour traiter le problème du contrôle latéral des véhicules automatisés, avec un accent particulier sur le contrôle du comportement du véhicule lorsque les circonstances d'opération changent. Des résultats de simulation et d'expérimentation utilisant une Renault ZOE sont présentés.

La paramétrisation YK est utilisée pour explorer le problème des erreurs latérales importantes dues soit à des changements de voie soudains, soit à des problèmes de positionnement potentiels ou à tout autre problème. Grâce à la paramétrisation YK, le contrôleur proposé permet une reconfiguration automatique et stable du contrôleur lorsque la situation de conduite change par rapport à l'erreur latérale.

Cette structure de contrôle basée sur YK comprend deux contrôleurs (T&C): un pour le suivi de la trajectoire souhaitée en utilisant une petite distance d'anticipation, et un pour le changement de voie présentant des réponses plus lisses et utilisant une plus grande distance d'anticipation. La reconfiguration du contrôle est basée sur un système de décision, mesurant l'erreur latérale et activant l'un des deux contrôleurs ou une partie des deux pour améliorer la performance du contrôle.

Les résultats expérimentaux ont prouvé que la structure de contrôle proposée est une bonne façon de faire face à ces situations. Elle améliore les performances en n'utilisant qu'un seul contrôleur dans les deux cas. Le principal avantage de la structure de contrôle proposée est qu'elle peut être considérée comme un cadre de contrôle général, qui reconfigure les différents contrôleurs de manière automatique et stable afin de maximiser les performances de contrôle possibles.

Chapter 5

Lateral Control

This chapter explores the use of Youa-Kucera (YK) parametrization to deal with lateral control problem of automated vehicles, with a special emphasis on controlling the vehicle behavior when the operating circumstance changes. Both simulation and experimental results using a Renault ZOE are presented.

YK parametrization is used to explore the problem of large lateral errors due to either sudden lane changes, potential positioning problems or any other issues. Thanks to YK parametrization, the proposed controller allows stable controller reconfiguration when the driving situation changes with respect to the lateral error. Different controllers based on a look-ahead distance are designed for each driving situation (i.e. lane change, lane tracking) and embedded in a re-configurable YK controller. The controller reconfiguration is based on a decision taking into account the lateral error corresponding to the driving situation.

The chapter is structured as follows: Experimental platform and its different functional components used to validate the proposed lateral controller is described in section 5.1. Section 5.2 presents the lateral control problem when facing different driving situations such as lane change and lane tracking scenarios and how this can impact the control performance. A brief lateral control review is provided in section 5.3. Section 5.4 explains the motivations behind using YK parametrization to handle the driving situations changes. The vehicle model and controller design are provided in 5.5. Section 5.6 shows simulation results of the proposed controller in different scenarios. The experimental results of the proposed controller and its performance are provided in section 5.7. Finally, some concluding remarks are giving in section 5.8 on the use of YK parametrization for the autonomous vehicle lateral control.

5.1 Experimental platform description

The control structures developed in this thesis has been tested in real scenarios. The experimental platform is a computer-controlled Renault ZOE. The vehicle is completely robotized, enabling the control of the steering wheel, throttle and brake pedals for the control part. In this section, the embedded architecture is described with a brief explication for each functional component.

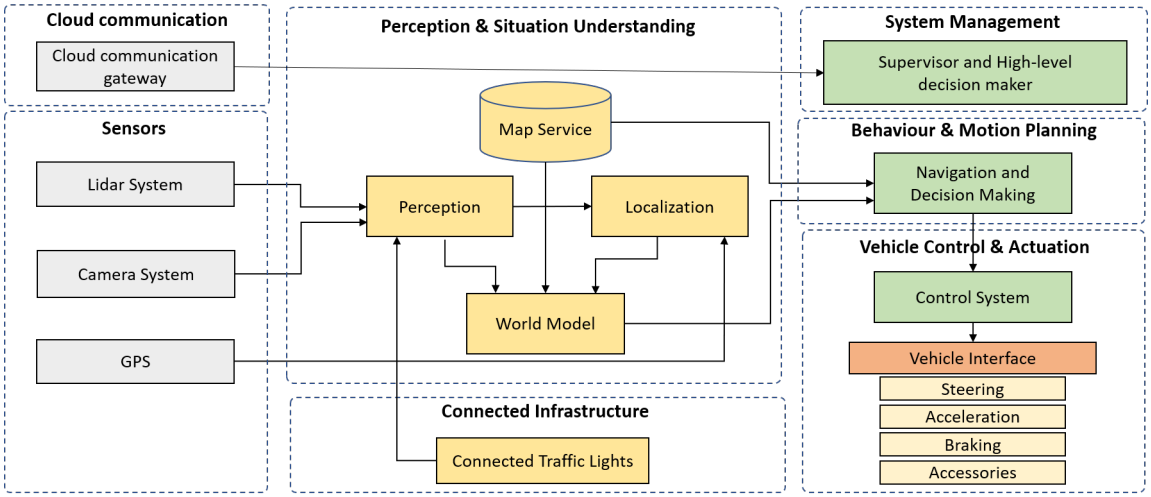

Figure 5.1: Functional component of the automated ZOE

Autonomous driving is a complex task, it requires the management of different sensors such as cameras, Laser Imaging Detection And Ranging system (LIDAR) and Global Positioning System (GPS), also different actuators such as steering system, throttle and brake pedals. Thus, different functions like perception, map service, localization, world model, navigation and decision-making, and vehicle control are integrated into an unified system that exhibits rational behavior. The arrangement and interaction of different functional components play a crucial role on the robustness and reliability of the vehicle operation. Figure 5.1 shows different components of the vehicle.

- Cloud Communication: This component handles the communication between the autonomous vehicles and the cloud server. The cloud communication is added to allow remote tracking and map visualization of all autonomous vehicles in real time, providing them safety alerts and warnings such as, slippery zone or civil work in progress. This component provides also remote control option during critical situation like priority vehicle approaching. It uses cellular technology to connect the vehicles to the cloud.

- Supervisory System: This component monitors and controls all the components to ensure the safety and robustness of the operational modules. It selects the discrete behavior which each functional component must have at each moment. It maintains different operational modes (e.g. autonomous, manual, standby) and sends signals to the appropriate operational components to switch their states accordingly.

- Perception: The main functionality of the perception system is to detect, locate, measure, classify and predict the motion of the obstacles and road features in the external environment in which the vehicle operates. It provides a first level scene understanding that is then enriched with contextual data in world model system with the help of localization system and map service. The vehicle is set up with multi-sensor configuration that comprises cameras and lidars.

- Localization: The main objective of the localization system is to provide position, heading, velocity and timing information, together with integrity information. The navigation of autonomous vehicles requires vehicle position accuracy exceeding the available one from GPS-based inertial guidance systems. Thus, localization system requires local map data with lane information close to the vehicle in order to precisely locate itself within the lane.

- Map service: This component is responsible for gathering and centralizing all map related information, aiding to localize the vehicle within the available map. The map database stores the map of the operational area in a proprietary format that enables faster access. Communication with map service is implemented in query pattern. Requesting modules send a query to the map service component for receiving relevant information.

- World Model: This component is added to enhance the situation understanding capabilities and help the decision making system to provide a coherent decision. It receives input from perception, localization, and map service components, and provides enriched data to navigation and decision making component. It provides a contextualization of the perception data, identifying the maneuvers that the ego vehicle is allowed to perform with respect to the perceived surroundings and traffic rules by identifying the surrounding objects that concern each maneuver, and their intentions.

- Navigation and Decision Making: The main goal of navigation and decision making system is to compute a safe itinerary ensuring that the vehicle reaches its desired destination while avoiding obstacles, following road regulation rules (e.g. maximum speed). The navigation system computes the global path for the ego vehicle in order to execute

the mission provided by the supervisory control, defining a smooth real maximum speed which takes account of the safety constraints of the vehicle (maximum lateral acceleration, maximum steering wheel, width of the road, etc.).

- Vehicle Control System: This component is responsible for carrying out the switching of physical relays from manual driving mode to autonomous driving mode and conversely. It computes the necessary control signals that will assure that the ego vehicle follows a given real-time computed trajectory (both path and speed). When in autonomous driving mode, the system also controls and monitors a set of vehicle accessories such as lights, wipers, horn and warning light. It also monitors continuously the health state of the surrounding systems and inner modules and executes specific fail-safe policies or emergency actions triggered using vehicle safety devices (emergency stop button, override key, etc.).

  The control algorithms are embedded in a MicroAutoboxII (MABx) using MatLab Simulink turning at 100Hz. The MABx is connected to the vehicle via a CAN network. Signals such as vehicle localization, vehicle speed or longitudinal acceleration are provided by on-board sensors. Communications with actuators are done at their maximum capacity, i.e. 100 Hz. The low level actuators for the steering wheel and the throttle/brake pedals are off-the-shelf systems.

5.2 Problem description

Automated vehicles are getting more and more attention because of their potential to improve drivers' life, insuring road safety, increasing highway capacity or reducing carbon emission. When it comes to conceive autonomous vehicles, assuring its stability plays a key role. The vehicle motion stability is assured by a control process that is capable to interpret high level decisions (i.e. follow a line, avoid an obstacle) into actions according to a given trajectory. Vehicle control can be divided in longitudinal (i.e. the ability to regulate vehicle speed by controlling brake and throttle actuators) and lateral (i.e. vehicle steering regulation to track and follow a reference path) controllers.

Let's consider the lateral control of autonomous vehicle. Problem formulation focuses on handling different driving situations involving lateral motion with a high performance level and keeping a comfortable feeling in the vehicle.

Two driving situations are showed in figure 5.2. The reference trajectory is represented with the green line in the top graph. At $t = 0$ the vehicle is located at $3m$ from the straight line. Thus, the lateral control needs to

perform a lane change maneuver to reach the reference trajectory. Once the vehicle is in the desired lane, the reference trajectory is curved and the lateral controller should address the turn.

The lane-change maneuver or situations with significant lateral error (i.e. first starting, lane change, localization discontinuity, obstacle avoidance ...) needs a smooth lateral controller, avoiding overshoots and high lateral acceleration and keeping the passenger's comfort.

Figure 5.2 depicts this. Top graph represents the trajectories of the vehicle when controlled with two different lateral controllers C_1 (blue solid line) and C_2 (red solid line) following a desired trajectory (green solid line); Middle and bottom graphs plot controllers steering wheel angle and steering wheel rate responses respectively.

The controller $C1$ is designed to handle the lane-change scenario according to the previous specifications, it performs the blue trajectory. One can notice that the steering angle and the steering rate are smooth in the second and third graphs respectively. However, the controller $C1$ failed in tracking the turn.

The curved line scenario, or in general situations with small lateral errors needs a fast and reactive controller to track the changes in the trajectory and follow it. The controller $C2$ is designed to cope with line-tracking specifications, it performs the red trajectory. one can see that in the turn scenario, the controller $C2$ tracks well the reference. However, in the lane-change the lateral motion is fast and evolves high steering angle and rate which makes the feeling jerky inside the vehicle.

This example shows that one simple controller can't handle lateral motion scenarios with conflicting control objectives. Ideally, the lateral controller should behave like $C1$ in the lane-change, and like $C1$ in turns. Ensuring high control performance and passenger comfort demand to adapt the lateral control response to the driving situation while keeping the system stability.

Autonomous vehicle can face different driving situations that change depending on the road layout and potential interactions with other traffic agents. The main goal of this work is to recognize the driving situation change, and adapt the controller response to satisfy the required vehicle behavior. The main technical challenges are the followings:

- Design a multi-controller structure using YK parametrization to guarantee the stability of the lateral motion.
- Define a decision system able to recognize driving situation changes.
- Define the parameter γ as the decision parameter that selects the adequate controller with respect to the driving situation.
- Keep controllers simple to implement in real time and easy to tune, allowing a transparent interpretation of its parameters.

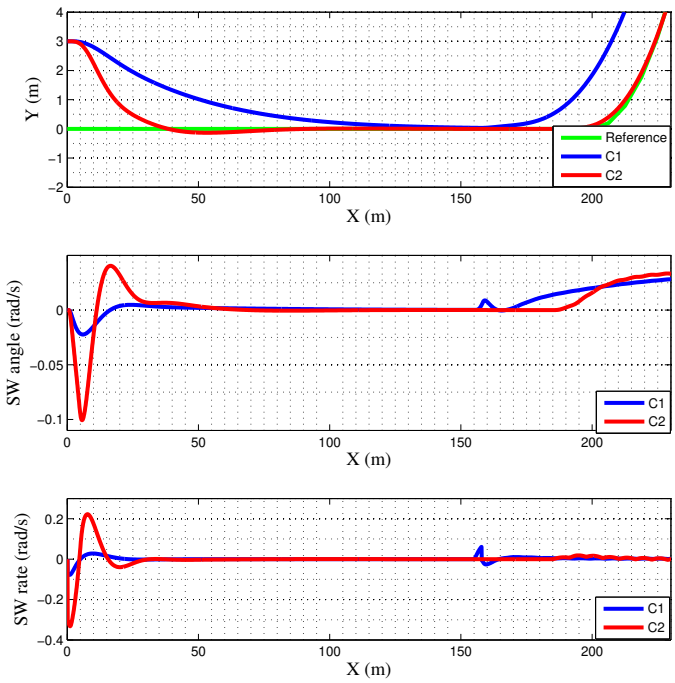

Figure 5.2: Lane change followed by a turn

5.3 Lateral control review

Steering control has been widely studied in the last three decades. The first demonstration was carried out in "No Hands Across America" event in mid 90s. Carnegie Mellon University's researchers [141] presented Navlab car that completed around 5000km in semi-autonomous mode. The steering wheel was controlled by correcting lateral offset and heading error. Curvature was used as feedforward in the control loop. The vehicle was semi-autonomous because the throttle and brake pedals were controlled by the driver.

In 1998 Prof.Broggi et *al* [142] demonstrated the ARGO vehicle, that conducted itself along the Italian highway network. The steering system was based on a proportional controller to correct the vehicle deviation with respect to the center lane.

In 2005, Stanley vehicle won the second DARPA (Defense Advanced Research Projects Agency) Grand Challenge [143]. Its steering controller was based on a nonlinear feedback of the cross-track error by using estimated velocity, UKF pose and measured steering wheel angle. This approach works

well for low speed, but it neglected the steering column dynamics.

In 2012, BRAiVE vehicle was demonstrated in the Intercontinental Autonomous Challenge, developed by Prof. Broggi's team [144]. Its lateral controller included two levels: first, setting a target point in the desired trajectory, at a look ahead distance that vary with respect to the vehicle speed, then converting the curvature in the control point to steering value, by inverting the vehicle dynamic model. To avoid jerky performance, variation in curvature lower than $\pm 5\%$ was not considered. The vehicle was able to drive in urban areas (i.e. roundabouts).

In the same year, the university team of Prof.Sunwoo won the autonomous car competition organized by Hyundai Motor in Korea [145]. The basic idea of the lateral controller is that the vehicle always moves along Ackerman geometry, except for straight movement. The vehicle showed good performance in mixed circuits.

In 2013, Mercedes cooperated with different research labs to make an autonomous journey in memorial Berta Benz road. The lateral controller included two parts: first, a feedforward part that calculates the desired yaw rate using trajectory curvature at a target point. This one is set at a look-ahead distance that varies with respect to the vehicle speed, in order to compensate the steering column dynamics; second, a feedback part, that minimizes the lateral displacement in order to stabilize the lateral position. Finally, the required steering wheel angle is computed from the desired yaw rate using an inverse stationary single track model. For steady state accuracy, a steering angle offset observer is used to compensate both deviation in the inverse single track model as well as a steering angle offset in the steering actuator [146].

The above described systems are part of automated steering wheel demonstration well known in the literature. Below, other proposed lateral control approaches are described.

In [147] a nested PID controller is used to control the vehicle steering angle. The proposed control strategy involves two nested control blocks. The first one has to ensure the tracking of a yaw rate reference signal on the basis of the yaw rate tracking error measured by a gyroscope in spite of constant disturbances and parameter uncertainties; the second one has to generate the yaw rate reference signal on the basis of the lateral offset measured by the vision system in order to drive the lateral offset to zero. The main advantage of using nested control structure with two independent control loops is that it allows to design standard PID controller in a multivariable context (two outputs,one input). An experimental tests, performed by a prototype vehicle, successfully validate the controller in both straight lines and curves, exhibiting good performance.

In [148] an H_∞ approach is used to design a controller for ground vehicle trajectories tracking. The adopted approach is based on the separation between the longitudinal and lateral dynamics. A H_∞ technique with loop

shaping is adopted for the lateral controller synthesis. The H_∞ design gives a good framework to deal with system uncertainties, measurement noises and passenger comfort. The experimental results of testing the controller in a lane tracking and lane changing scenarios are acceptable even at high velocities.

A sliding mode controller is used in [149]. The controller output is the steering angle and the input is the lateral displacement error. The particularity of such a strategy is to take advantage of the robustness of the sliding mode controller against nonlinearities and parametric uncertainties in the vehicle model, while reducing chattering using high order sliding mode. To validate the control strategy, the closed-loop system simulated on Matlab-Simulink has been compared to the experimental data acquired on a robotized platform, according to several driving scenarios. The validation shows robustness and good performance of the sliding mode controller.

To enhance the overall performance of automated steering, more sophisticated control techniques are used. A fuzzy control approach to deal the comfort problem is adopted in [150]. The fuzzy controller is compared to a classic Lyapunov controller and shows effective performance. However, stability proof and performance analysis for this fuzzy control strategy are still difficult to establish.

In [151] human steering skills are used to emulate manual driving. Lateral controller is based on fuzzy logic approach designed in two main steps: first, information about a human driver handling are captured, and processed in order to get relevant data about the attitude of the driver; second, a system able to get the information and return an appropriate fuzzy controller is created using an iterative genetic algorithm. The obtained set of fuzzy controllers have been tested in a private and experimental area, most of them showed good behavior in straight lines, but also bad behavior in curve lines caused by the non-predictive model used in the control without tacking into account the non-immediate reference points of the desired route. The controllers showed very smooth driving, even when they were circulating at relatively high speeds. The major drawback of this approach is the number of driving situations needed to build a representative training data set.

Besides artificial intelligence techniques, model based control methods have been also explored in vehicle lateral control. Model predictive control (MPC) provides interesting results [152]. Thanks to its capabilities, MPC handles efficiently constrained control problems for nonlinear and uncertain systems. A Nonlinear Model Predictive Control (NMPC) approach has been proposed in [153] where they focus on lateral control, while considering a basic longitudinal control to track the reference speed. The main drawback of MPC is that it is computationally expensive techniques and it requires optimization.

In [154], inspired by drivers mechanism, authors developed a T&C con-

troller (*Target and Control Driver Steering Model*). The generated steering rate is simply the target angle error (angle between the vehicle heading and the target point set at a look-ahead distance) scheduled by a gain feedback, it has been successfully implemented on a bus revenue service as a simple linear control loop. In [155] the same approach has been validated on experimental car.

The timeline in figure 5.3 shows the evolution of the control techniques used in autonomous vehicle demonstrations, and others validated experimentally as explained below in this section. The most recent results are shown in automated vehicle demonstration in Rambouillet (France) within the framework of the Tornado project, covering urban and rural areas [156]. The lateral controller combines both $T\&C$ technique and YK parametrization as explained in this chapter [30, 157].

The review of the different techniques shows two different approaches when dealing with steering control: 1) the use of complex vehicle model that includes all dynamics, and design suitable control structure that handles nonlinear behaviors and model parameter variations. In this case, the computation time becomes large for real time operation [158]; and 2) the use of linear controller based on a simplified vehicle model, and tuned for a defined use case (i.e. lane keeping, lane changing), which can't satisfy steering performance in different driving situations.
Automated steering systems should be able to address any circumstances ranging from starting the vehicle fully stopped to activating the function with a significant error with respect to the reference trajectory or performing lane changes. For covering all this situations, a single controller will not satisfy all conditions.

5.4 Motivation on using Youla Kucera

The goal of the controller is to develop a system able to deal with not only trajectory following but also with any other circumstance. When passing from manual to autonomous driving (i.e. autonomous driving activation), the vehicle may have an initial lateral deviation in function of vehicle position with respect to the reference trajectory. The lateral deviation in autonomous driving can also be caused either by a lane change maneuver, avoidance maneuver or even a localization discontinuity. The aim of the lateral controller is to handle these situation providing a human driving performance. However, it will be hard to manage all circumstances with a single controller.

Figure 5.4 shows step response of the expected controller for each situation. In lane-tracking task (solid blue line), the controller must provide fast response to track changes in the desired trajectory (i.e. curved line). Overshoots are tolerated because its maximum value is equal to the initial

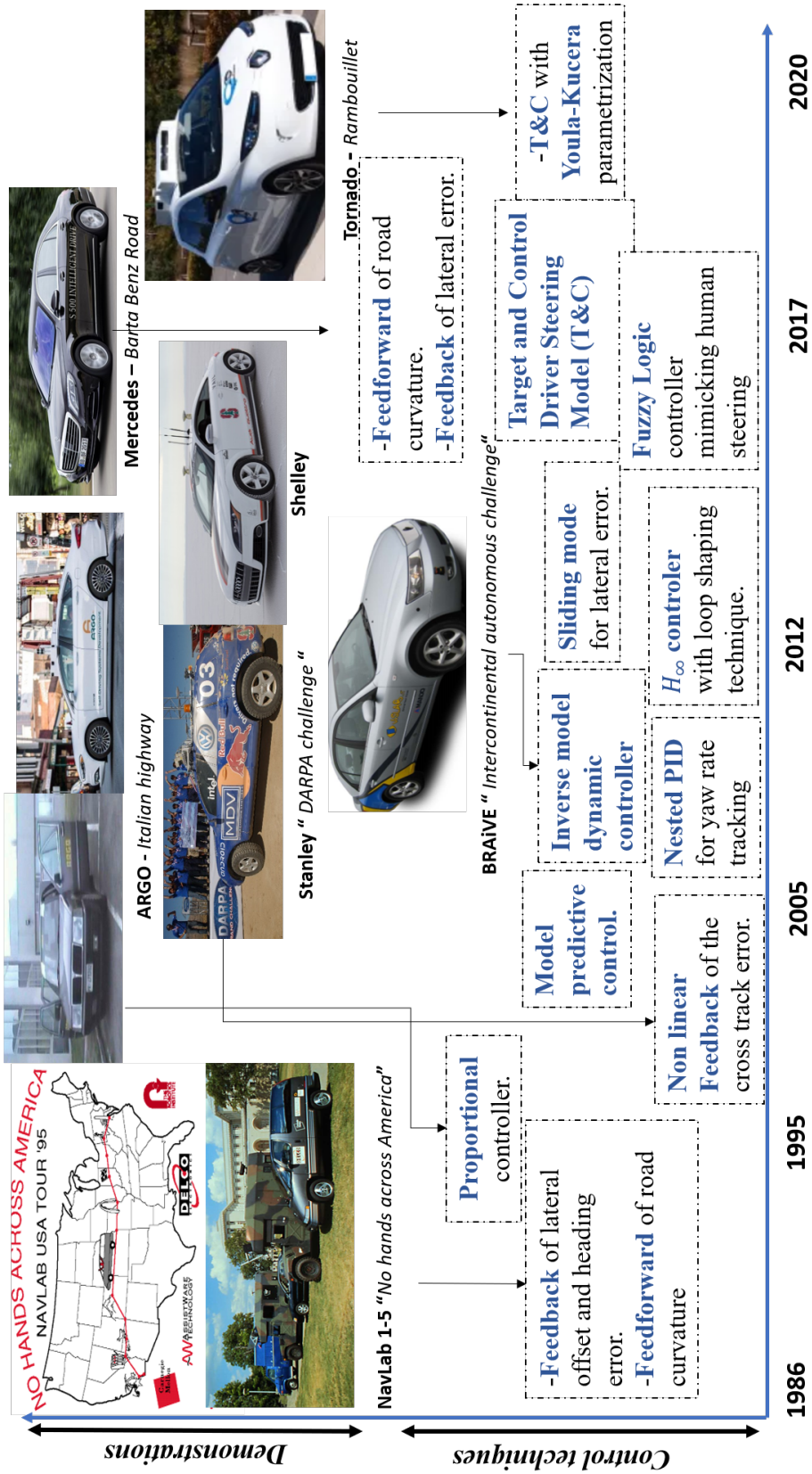

Figure 5.3: Timeline of autonomous vehicle demonstrations with lateral control techniques

lateral error, which is small in this case (the vehicle is already in the lane). While in lane-changing case (solid red line), the initial lateral error is significant. Thus, a smooth response is required, less overshoots are provided while compromising the rising time.

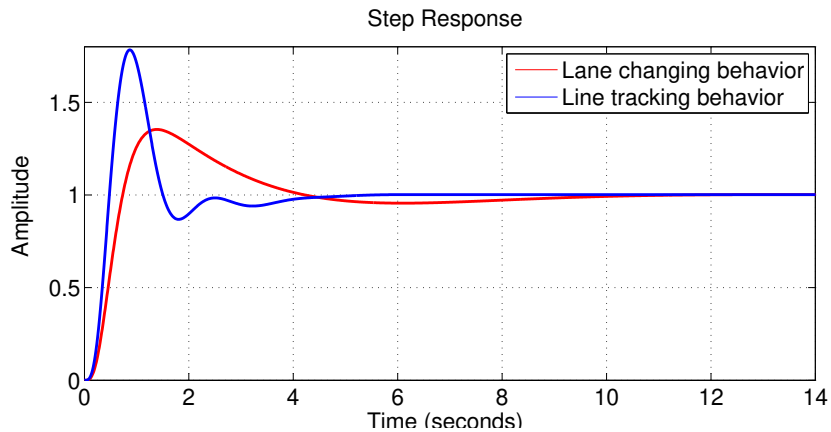

Figure 5.4: Desired control behavior

The proposed lateral control structure can cover the above situations by adapting the controller behavior accordingly to the lateral deviation. The information about the lateral deviation is provided to the controller by the navigation and localisation systems. Thus, for the controller it is considered as a system independent signal. The proposed solution is to design a YK based control structure switching gradually between two different lateral controllers: a lane-tracker controller for small lateral error and lane keeping cases; and a lane change controller for situations with significant lateral deviation. The switching between the two controller is orchestrated using the lateral deviation measured in real time.

The use of YK parametrization in designing the lateral controller is motivated by the following main reasons: 1) YK parametrization guarantees stable transition between the two initial closed loops; 2) It allows to implement several controllers stabilizing a plant with different closed loops behaviors in one control structure; 3) The switching signal γ in YK parametrized controller can handle system independent and external signals which is the la lateral deviation in the proposed solution.

5.5 Control design

The proposed lateral controller is based on YK parametrization, including the two initial controllers and the switching signal.
The control structure is illustrated in Fig. 5.5. It includes two controllers:

lane-changing controller C_1 (dashed red box); lane-tracking controller C_2 (dashed blue box). The switching between controllers is handled by the signal γ based on the lateral error between the vehicle and the desired trajectory.

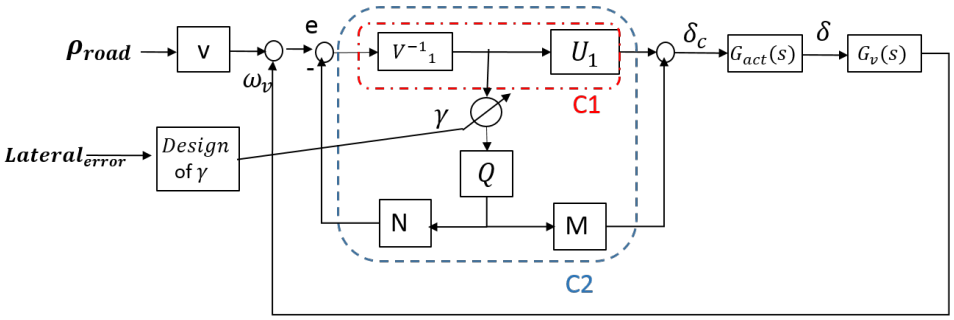

Figure 5.5: Control structure

In the following the design of C_1 and C_2 using the $T\&C$ approach [154] is explained as well as the vehicle model and the steering actuator model.

5.5.1 Vehicle model

A linear bicycle model is used to design the controller and analyze the stability of the lateral motion. The description of vehicle model construction is provided below.

Lateral vehicle kinematics

The vehicle kinematics are used to describe the vehicle motion (rotation and translation) of the vehicle frame $(M, x_{vehicle}, y_{vehicle})$ in the global ground frame $(O, x_{global}, y_{global})$. In the kinematic model, the four vehicle wheels are lumped into a unique mass M located at the center of the gravity of the vehicle as shown in figure 5.6.

The transfer of the motion from the vehicle frame to the global frame is expressed using the *Bour* formula [159] as follows:

$$\left[\frac{d\vec{V}}{dt}\right]_{global} = \left[\frac{d\vec{V}}{dt}\right]_{vehicle} + \Omega_{vehicle/global} \wedge \vec{V} \tag{5.1}$$

where $\vec{V} = \begin{bmatrix} \dot{x} \\ \dot{y} \end{bmatrix}$ represents the vehicle speed vector, and $\Omega_{vehicle/global} = \dot{\psi}$ represents the angular velocity of the vehicle frame with respect to the global frame. Therefore, the acceleration of the vehicle is expressed as follows:

$$\begin{aligned} \ddot{x}_{global} &= \ddot{x} - \dot{\psi}.\dot{y} \\ \ddot{y}_{global} &= \ddot{y} + \dot{\psi}.\dot{x} \end{aligned} \tag{5.2}$$

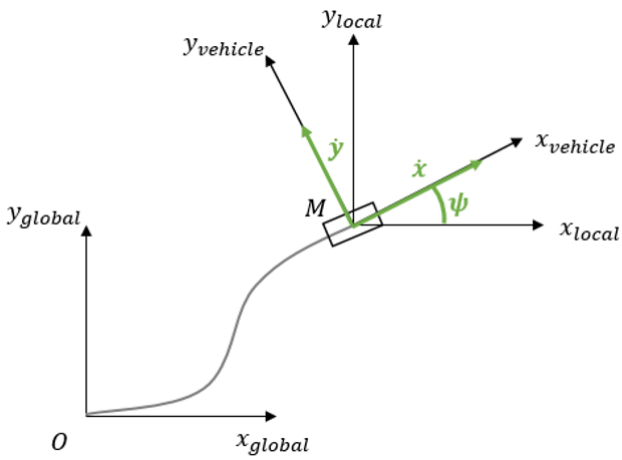

Figure 5.6: Lateral kinematic motion

And the speed is projected in the global frame as follows:

$$\begin{aligned} \dot{x}_{global} &= \dot{x}\cos\psi - \dot{y}\sin\psi \\ \dot{y}_{global} &= \dot{x}\sin\psi + \dot{y}\cos\psi \end{aligned} \tag{5.3}$$

This kinematic model is derived under the assumption that there is no tire slip angle, it is reliable when the velocity vector of each wheel is in the direction of the wheel. This is the reason why the kinematic-based controller has been used for limited low speed situation such as smart parking assist system, but not for performing lateral motion in autonomous driving [160] since the performance of lateral control critically depends on the vehicle parameters, especially the cornering stiffness and the tire-road conditions.

Lateral vehicle dynamics

The description of the dynamic vehicle model is based on Newton's laws, it yields to the following equations for longitudinal and lateral motions:

$$\begin{aligned} ma_x &= F_r^x + F_f^x\cos(\delta) - F_f^y\sin(\delta) \\ ma_y &= F_r^y + F_f^x\sin(\delta) + F_f^y\cos(\delta) \end{aligned} \tag{5.4}$$

where the steering of the two front wheels is assumed to be the same noted δ, the front or rear longitudinal tire forces are the sum of the front or rear left and right longitudinal tire forces (i.e. $F_f^x = F_{fl}^x + F_{fr}^x$, $F_r^x = F_{rl}^x + F_{rr}^x$), also the front or rear lateral tire forces are the sum of the front or rear left and right lateral tire forces (i.e. $F_f^y = F_{fl}^y + F_{fr}^y$, $F_r^y = F_{rl}^y + F_{rr}^y$).

The yaw moment equation is also necessary to describe the lateral motion, the yaw balance is expressed with respect to the center of gravity of the vehicle M.

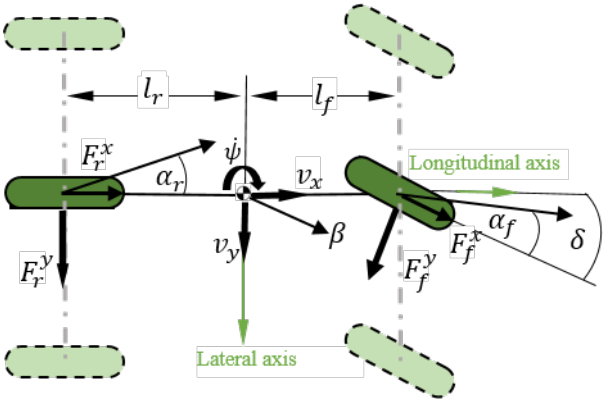

Figure 5.7: Lateral dynamic mode

$$I_z\ddot{\psi} = l_f F_f^x \sin\delta + l_f F_f^y \cos\delta - l_r F_r^y + M_z \tag{5.5}$$

where I_z, l_f and l_r are yaw moment of inertia, distance from the front and rear axle to the vehicle center of gravity M respectively. The yaw moment M_z indicates a direct yaw moment control input, which is generated by independent torque control of in-wheel motors. During the yaw motion, M_z is the low level control law to stabilize the vehicle yaw motion additionally to the steering action, which is the high level control input in the autonomous vehicle lateral controller.

Under small tire sleep angle ($\beta = \arctan\frac{v_y}{v_x}$) assumption, with v_x and v_y represent the longitudinal and the lateral vehicle speed respectively, the lateral tire forces can be expressed linearly as follows:

$$\begin{aligned} F_f^y &= -2C_f\alpha_f = -2C_f(\frac{v_y + \dot{\psi}l_f}{v_x} - \delta) \\ F_r^y &= -2C_r\alpha_r = -2C_r(\frac{v_y - \dot{\psi}l_r}{v_x}) \end{aligned} \tag{5.6}$$

where C_f and C_r are the front and rear tire cornering stiffness respectively.

Using small steering angle, the approximations $\sin\delta = \delta$ and $\cos\delta = 1$ are applied to simplify the lateral dynamic equations as follows:

$$ma_y = m(\dot{v}_y + v_x\dot{\psi}) = F_r^y + F_f^y \tag{5.7}$$

$$I_z\ddot{\psi} = l_f F_f^y - l_r F_r^y + M_z \tag{5.8}$$

State space formulation

The objective of the lateral control design in autonomous vehicle is to track a predefined path, while ensuring yaw stability. The main control actuator

is the steering system and the control input is the steering angle. Using the equations (5.7)(5.8) of the simplified dynamic model and lateral forces expressions in equation (5.6). The following state space form is derived:

$$\begin{aligned} \dot{X}_v &= A_v X_v + B_v u_v \\ Y_v &= C_v X_v \end{aligned} \tag{5.9}$$

where the state vector is:

$$X_v = \begin{bmatrix} y & v_y & \psi & \dot{\psi} \end{bmatrix}^T$$

y is the vehicle lateral position and $u_v = \delta$ is the steering angle in the front tire. The system matrix A_v,B_v and C_v are described below:

$$A_v = \begin{bmatrix} 0 & 1 & 0 & 0 \\ 0 & \frac{-2(C_f+C_r)}{mv_x} & 0 & \frac{-2l_fC_f+2l_rC_r}{mv_x} - v_x \\ 0 & 0 & 0 & 1 \\ 0 & \frac{2(l_rC_r-l_fC_f)}{I_zv_x} & 0 & -2\frac{(l_f^2C_f+l_r^2C_r)}{I_zv_x} \end{bmatrix} \tag{5.10}$$

$$B_v = \begin{bmatrix} 0 & \frac{2C_f}{m} & 0 & \frac{2l_fC_f}{I_z} \end{bmatrix}^T$$

$$C_v = \begin{bmatrix} 0 & 0 & 0 & 1 \end{bmatrix}$$

The vehicle transfer function is deduced from the state space model as follows:

$$G_v = C_v(Is - A_v)^{-1}B_v \tag{5.11}$$

5.5.2 Steering actuator

Exact modeling of the steering actuator involves mechanical and electrical components. The inertial system consists of the steering wheel, the assist motor and the spring system made of the torsion bar and the tire as shown in figure 5.8.

Table 5.1: Steering actuator parameters

Notation	Description
J_c	steering column inertia.
D_c	column damping.
K_c	column stiffness.
R_m	motor reduction ratio.
R_r	rack reduction ratio.
τ_d, τ_m, τ_r	driver, motor and rack torque respectively.
θ_c	steering wheel angle.

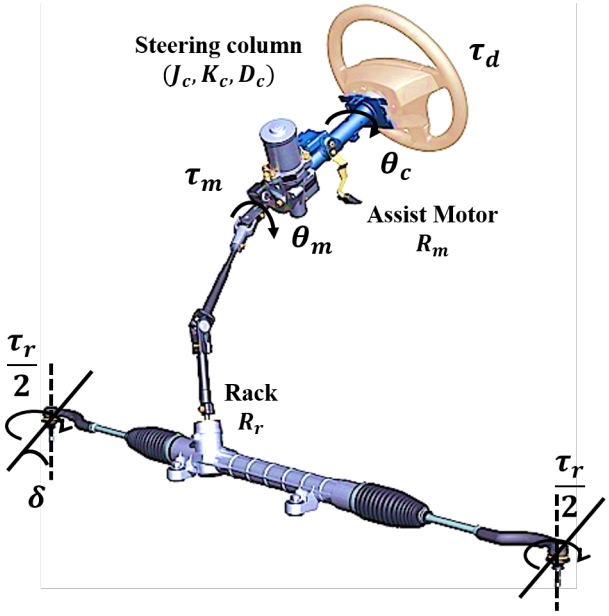

Figure 5.8: Steering actuator model

Using the second Newton's law, the dynamic equations modeling the steering actuator are derived by neglecting the dry frictions in each component.

$$J_c\ddot{\delta} + D_c\dot{\delta} + K_c(\delta - \theta_c) = R_r\tau_d + R_rR_m\tau_m - \tau_r \tag{5.12}$$

where τ_r is the turning torque of the front tire. It depends on the offset d_k (distance between the kingpin and the front wheel) and on the tire stiffness as follows:

$$\begin{aligned} \frac{\tau_r}{2} &= d_kC_f\alpha_f \\ \alpha_f &= \beta + \frac{l_f\dot{\psi}}{v_x} - \delta \end{aligned} \tag{5.13}$$

The lateral controller provides an ideal steering angle that allows the vehicle to turn and follow the desired trajectory. To compute the correspondent steering torque, the steering system should be included. A second order transfer function can be deduced describing the steering column dynamics. However, it should be noted that the turning torque τ_r expressed in equation (5.13) reflects the road reaction and is speed dependent [161]. Besides, the motor torque τ_m representing the EPS assistance provided by a control law that depends on both vehicle speed and driver torque τ_d as explained in [162].

Figure 5.9 shows the response of the steering actuator of the ZOE platform. Different tests have been conducted in different longitudinal speeds

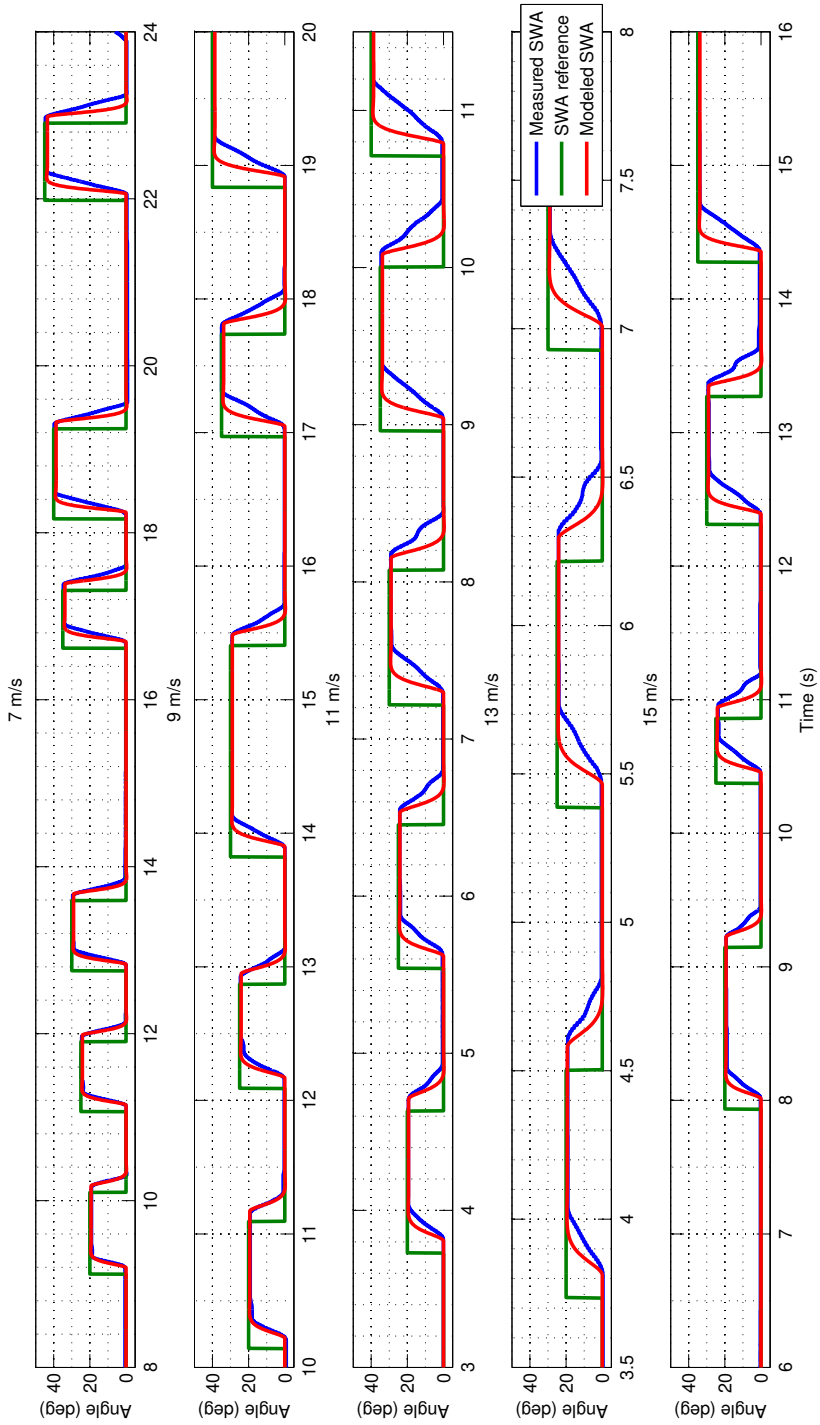

Figure 5.9: Steering wheel behavior for different longitudinal speed

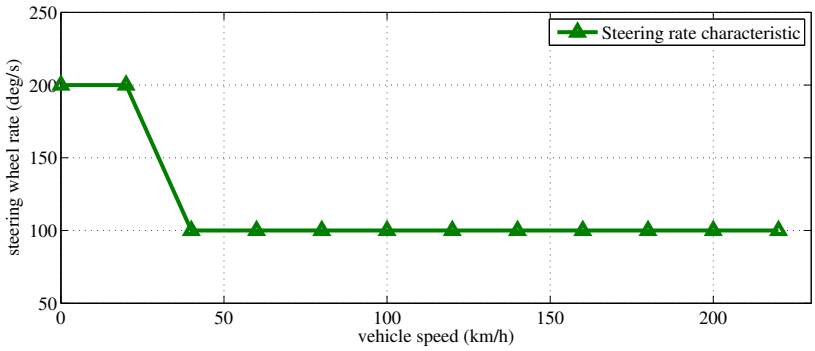

Figure 5.10: Steering rate characteristic

(i.e 7m/s, 9m/s, 11m/s, 13m/s and 15m/s). For each speed, the steering angle reference changes between 20 deg and 45 deg plotted in green solid line. The steering wheel response is plotted in blue solid line. and the red solid line shows the response of a transfer function computed using the identification toolbox of Matlab for the data measured at $7m/s$.

The identified transfer function is as follows:

$$G_{act} = \frac{726.6}{s^2 + 45.06s + 751.6} e^{-0.076s} \tag{5.14}$$

It should be noticed that in the first graph corresponding to $v_x = 7m/s$, the behavior of the steering systems matches the identified transfer function G_{act} for the references $20deg$ and $40deg$, and the more the reference angle is high the more the behavior of the steering system diverges from G_act response. The reason behind this behavior is the control loop inside the EPS, especially the saturation of the regulated steering wheel rate following a steering rate characteristic provided by the steering system supplier as shown in figure 5.10. The steering wheel rate saturation is speed dependent. This can be seen in the steering wheel behavior for different vehicle speeds in figure 5.9, the higher the speed the smaller is the reference angle that generates the saturation of steering rate: for 7m/s, 9m/s and 11m/s the steering rate saturation started from the angles 30 deg, 25 deg and 20 deg respectively.

The analysis of these tests allow to conclude that an accurate steering system model should be an LPV model, since there is different parameters that define the EPS behavior. The characteristics of the controller within the assist motor depend on the vehicle speed and the driver torque. Furthermore, the steering actuator presents non linear behavior due to the friction.

Recent research works presented LPV modelisation and control design for EPS systems. Authors in [163] describe the history of the steering systems and its modelisation including both mechanical and electronic control parts. In [164] an LPV steering model varying with respect to the vehi-

cle speed and the driver requested torque is used to design an H_∞ EPS controller.

In this thesis work, the controller is designed for an LTI vehicle model with a constant longitudinal speed $v_x = 10m/s$. Thus, and for sake of simplification an LTI steering system is identified.

Thus, the general plant to be controlled is $G = G_v G_{act}$ with G_v described in (5.11).

5.5.3 Lateral controller

The design of C_1 (lane-changing controller) and C_2 (lane-tracking controller) is based on T&C approach [154]. Figure 5.11 illustrates the target heading of the vehicle θ_T corresponding to the target point $\mathbf{T}(x_T, y_T)$, the vehicle is located in the point $\mathbf{V}(x_v, y_v)$. The target point $\mathbf{T}$ is set at a distance d named *Look-ahead distance* from the vehicle position $\mathbf{V}$.

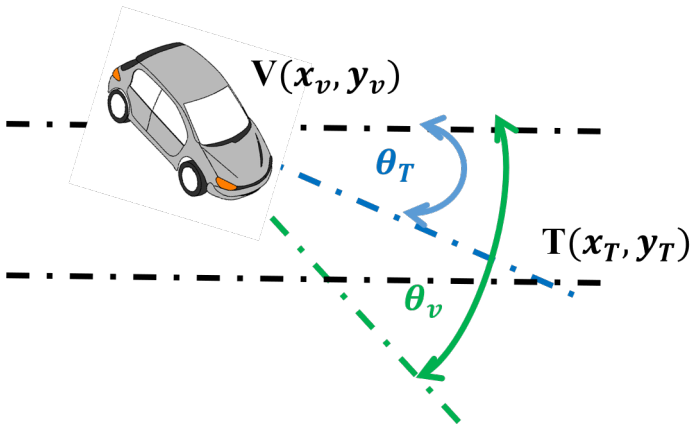

Figure 5.11: Target heading angle

Assuming that at the current instant t the vehicle is in the position $\mathbf{V}$ and it maintains its yaw rate $\dot{\psi}(t)$ and its speed $v_x(t)$, the desired heading angle $\theta_T(t)$ is the heading angle that the vehicle should have to reach the target position $\mathbf{T}$.
Thus, the heading angle error is :

$$\theta_e(t) = \theta_T(t) - \theta_v(t)$$

where $\theta_v(t)$ is the current vehicle heading, and the steering wheel rate is generated by the following control law :

$$\dot{\delta}(t) = k\theta_e(t) \tag{5.15}$$

To design a T&C controller, formulated into a standard state feedback, two intermediate points are defined (see figure 5.12):

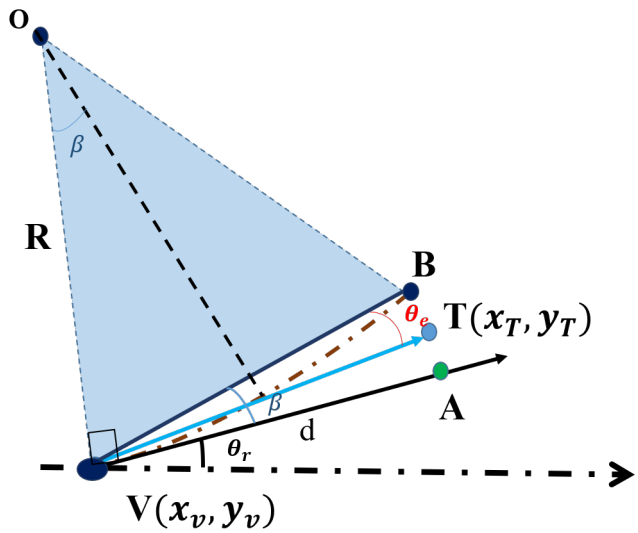

Figure 5.12: Target angle error computation

- **A**(x_A, y_A): the point that the vehicle will reach if it travels the look-ahead distance d without changing the current heading angle θ_r.

- **B**(x_B, y_B): the point that the vehicle will reach if it travels the look-ahead distance d while keeping its current yaw rate $\dot{\psi}$ and speed v_x.

While the vehicle travels d keeping a constant yaw rate $\dot{\psi}$ and longitudinal speed v_x, the resulting trajectory is the arc $\widehat{VB}$. Assuming that the trajectory radius R is much larger then the look-ahead distance d, $\widehat{VB}$ is approximated to the segment VB. Turning this segment VB by the heading angle error θ_e the vehicle reaches the target position **T**.
Thus, the coordinates of **T** can be calculated as follows:

$$\begin{cases} x_T = x_v + d\cos(\theta_r + \beta + \theta_e) \\ y_T = y_v + d\sin(\theta_r + \beta + \theta_e) \end{cases} \tag{5.16}$$

Assuming that both of θ_e and θ_r are small, and $\beta \approx \frac{d}{2R}$, equation (5.16) can be linearized as follows:

$$\begin{cases} x_T = x_v + d(1 - \dfrac{d}{2R}\theta_e - \dfrac{d}{2R}\theta_r - \theta_e\theta_r) \\ y_T = y_v + d(\theta_r + \dfrac{d}{2R}\theta_e\theta_r + \dfrac{d}{2R} + \theta_e) \end{cases} \tag{5.17}$$

By ignoring the higher order term $\theta_e\theta_r$ and replacing $R = \frac{v_x}{\dot{\psi}}$ in (5.17), we

obtain:

$$\begin{cases} x_T = x_v + d(1 - \dfrac{d\dot{\psi}}{2v_x}\theta_e - \dfrac{d\dot{\psi}}{2v_x}\theta_r) \\ y_T = y_v + d(\dfrac{d\dot{\psi}}{2v_x} + \theta_e + \theta_r) \end{cases} \tag{5.18}$$

In the other hand the target point **T** must satisfy the trajectory equation:

$$y_T = d\sin(\beta_{road}) \approx d\left(\frac{d}{2R_{road}}\right) = \frac{d^2\rho_{road}}{2} \tag{5.19}$$

Where, ρ_{road} is the lateral road curvature at the target position **T** and $\rho_{road} = 1/R_{road}$ with $R_{road} >> d$.
By combining (5.18) and (5.19), θ_e can be expressed as follows:

$$\theta_e = \frac{d}{2}\rho_{road} - \left(\frac{1}{d} + \frac{d}{2v_x}\dot{\psi} + \theta_r\right) \tag{5.20}$$

Correspondingly, the control law can be deduced:

$$\dot{\delta} = k\theta_e = k\left(\frac{d}{2}\rho_{road} - \left(\frac{1}{d} + \frac{d}{2v_x}\dot{\psi} + \theta_r\right)\right) \tag{5.21}$$

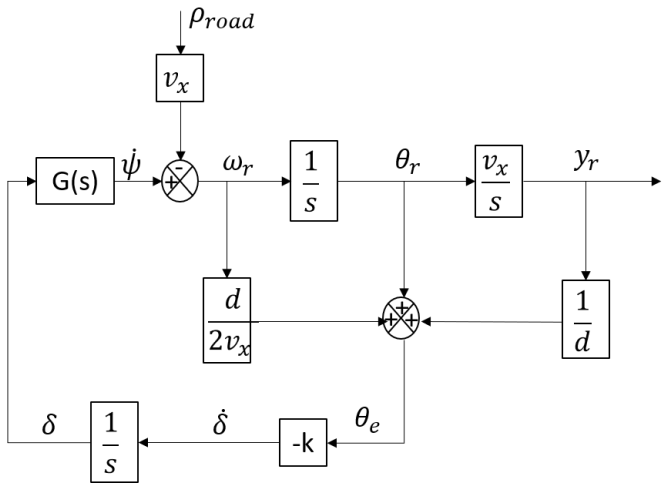

Figure 5.13: Closed-loop of T&C controller

The T&C controller can be seen as a state space feedback control as shown in the diagram in Figure 5.13, since $\omega_r = \dot{\psi} - v\rho_{road}$, $\theta_r = \frac{\omega_r}{s}$ and $y_r = \frac{v}{s}\theta_r = \frac{v}{s^2}\omega_r$, we have:

$$\delta(s) = \frac{-k}{s}\left(\frac{d}{2v_x} + \frac{1}{s} + \frac{v_x}{ds^2}\right)\omega_r(s) \tag{5.22}$$

Thus the controller is expressed in the following parametrized transfer function:

$$C(s) = \frac{-k}{s} \frac{\left(s^2 + 2\frac{v_x}{d}s + 2(\frac{v_x}{d^2})\right)}{2\frac{v_x}{d}s^2} \tag{5.23}$$

The gain k is chosen in order to guarantee the stability of the closed-loop. For doing so, basic pole placement technique is used at a given speed v_x and look-ahead d.

As already precised in section 5.4 two lateral controllers C_1 and C_2 with different behaviors (see Figure 5.4), handling lane changing and line tracking maneuvers respectively are designed.

k and d are designed in order to achieve the expected behaviors of C_1 and C_2, specifically :

- Lane-changing controller C_1: In this case initial lateral error is significant. The controller must be smooth to avoid overshoots and uncomfortable sensation in the vehicle. For solving so, target point is set to $30m$ (i.e. d value).
- Lane-tracking controller C_2: In this case, fast response is required. According to [154], the closer is the target point, the smaller is the tracking error. For doing so, look-ahead distance is fixed to $d = 15m$.

The appropriate feedback gain k is identified using basic pole placement technique as shown in figure 5.14. The resulting controllers are:

$$C_1 = \frac{-1.2s^2 - 1.6s - 1.067}{1.333s^3} \tag{5.24}$$

$$C_2 = \frac{-0.435s^2 - 0.29s - 0.0966}{0.667s^3} \tag{5.25}$$

Both controllers are implemented in a parametrized structure (see Fig. 5.5). As explained in chapter 3, the resultant YK controller switches between C_1 and C_2 without losing the stability of the closed loop. The parameter γ is in charge of the controllers' switching based on the vehicle lateral error with respect to the trajectory as follows:

- When the lateral error $> 3m$, the adequate controller is C_1 so $\gamma = 0$.
- When the lateral error $< 0.2m$, the adequate controller is C_2 so $\gamma = 1$.

Between the two limits γ changes gradually depending on the lateral error values as shown in Figure 5.15.

Then γ changes can be mathematically expressed by the equation below:

$$\gamma = \begin{cases} 0 & |Lat_{error}| > 3 \\ -\frac{1}{2.8}|Lat_{error}| + \frac{3}{2.8} & 0.2 < |Lat_{error}| < 3 \\ 1 & |Lat_{error}| < 0.2 \end{cases} \tag{5.26}$$

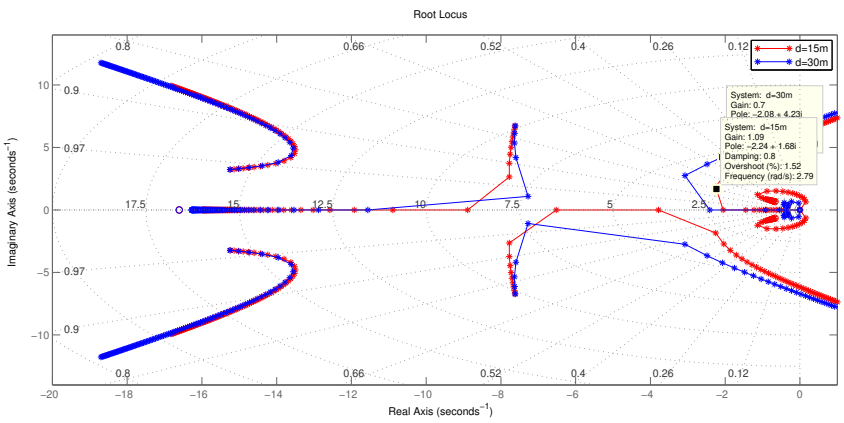

Figure 5.14: Pole placement for different values of k and d.

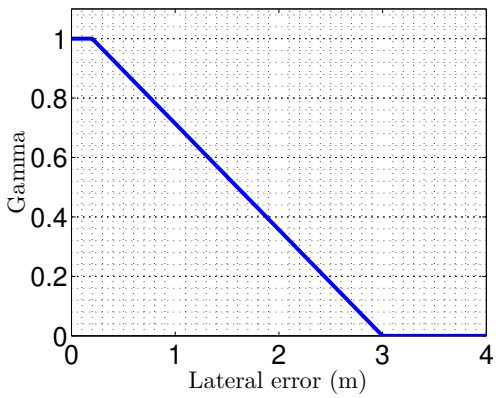

Figure 5.15: The switching parameter γ

5.5.4 Stability Analysis

To illustrate the stability and the behavior of the proposed YK parametrized lateral controller, the closed loop poles and zeros are computed for each value of γ.

The poles of the initial closed loop CL_1 controlled by the lane change controller C_1, and the final closed loop CL_2 controlled by the lane tracking controller C_2 are presented in table 5.2.

During the variation of the parameter γ between 0 and 1, the poles remain the same and are within $\{poles(CL_1) \cup poles(CL_2)\}$. It's notable in the root locus shown in figure 5.16a that all the poles represented by crosses, are superimposed on each other for $0 < \gamma < 1$ and remain in the unity circle, which means that the whole system is stable.

The zeros of the parametrized closed loop are presented in table 5.3.

Contrary to the poles, the zeros move with γ. For $\gamma = 0$, the zeros of the closed loop are composed of: the fixed zeros (i.e. Z_3, Z_4 and Z_5); the zeros offsetting the poles of the final closed loop CL_2 (i.e. $Z6$, $Z7$, $Z8$, $Z9$, $Z10$, $Z11$ and $Z12$) and the pair of zeros (Z_1, Z_2) that move with γ.

For $\gamma = 1$, the zeros of the closed loop are also composed of: the fixed zeros (i.e. Z_3, Z_4 and Z_5); the zeros offsetting the poles of the initial closed loop CL_1 (i.e. $Z1$, $Z2$, $Z6$, $Z7$, $Z8$, $Z9$ and $Z12$) and the pair of zeros (Z_10, Z_11) resulting from the motion of the zeros offsetting the poles of CL_1 for $\gamma = 0$.

For $0 < \gamma < 1$, the zeros of the closed loop are also composed of the fixed zeros (i.e. Z_3, Z_4 and Z_5); and all the moving zeros offsetting the poles of CL_1 and CL_2 for $\gamma = 1$ and $\gamma = 0$ respectively. Thus, Zeros appear and move to compensate C_1 or C_2 effects. The closer γ to one, the closer the zeros to poles of CL_1, and respectively the closer γ to zero the closer the zeros to poles of CL_2.

In Figure 5.16b a part of the root locus is zoomed, zeros and poles are represented respectively by circles and crosses. It shows the motion of Z_6, Z_7 from $P_5(CL_2)$ and $P_6(CL_2)$ to $P_5(CL_1)$ and $P_6(CL_1)$ respectively, and the motion of Z_{12} from $P_7(CL_2)$ to $P_7(CL_1)$ with respect to γ.

Table 5.2: Closed loops poles'

Poles	P_1	P_2	P_3	P_4	P_5	P_6	P_7
CL_1	0.9958+0.0042i	0.9958-0.0042i	0.9670+0.0169i	0.9670-0.0169i	0.8732+0.0375i	0.8732-0.0375i	0.8933
CL_2	0.9911+0.0083i	0.9911-0.0083i	0.9857+0.0383i	0.9857-0.0383i	0.8713+0.0519i	0.8713-0.0519i	0.8692

Table 5.3: YK closed loop zero's evolution with respect to γ

γ	0	0.2	0.4	0.6	0.8	1
Z_1	0.9967+0.0033i	0.9966+0.0034i	0.9964+0.0035i	0.9963+0.0037i	0.9961+0.0039i	$P_1(CL_1)$
Z_2	0.9967-0.0033i	0.9966-0.0034i	0.9964-0.0035i	0.9963-0.0037i	0.9961-0.0039i	$P_2(CL_1)$
Z_3	0.8470	0.8470	0.8470	0.8470	0.8470	0.8470
Z_4	-0.2491	-0.2491	-0.2491	-0.2491	-0.2491	-0.2491
Z_5	-3.4697	-3.4697	-3.4697	-3.4697	-3.4697	-3.4697
Z_6	$P_5(CL_2)$	0.8725+0.0488i	0.8733+0.0459i	0.8738+ 0.0429i	0.8737+0.0401i	$P_5(CL_1)$
Z_7	$P_6(CL_2)$	0.8725-0.0488i	0.8733-0.0459i	0.8738-0.0429i	0.8737-0.0401i	$P_6(CL_1)$
Z_8	$P_3(CL_2)$	0.9817+0.0346i	0.9779+0.0309i	0.9743+0.0270i	0.9708+0.0226i	$P_3(CL_1)$
Z_9	$P_4(CL_2)$	0.9817-0.0346i	0.9779-0.0309i	0.9743-0.0270i	0.9708-0.0226i	$P_4(CL_1)$
Z_{10}	$P_1(CL_2)$	0.9915+0.0082i	0.9919+0.0080i	0.9924+0.0077i	0.9928+0.0073i	0.9933+0.0066i
Z_{11}	$P_2(CL_2)$	0.9915-0.0082i	0.9919-0.0080i	0.9924-0.0077i	0.9928-0.0073i	0.9933+0.0066i
Z_{12}	$P_7(CL_2)$	0.8724	0.8760	0.8804	0.8860	$P_7(CL_1)$

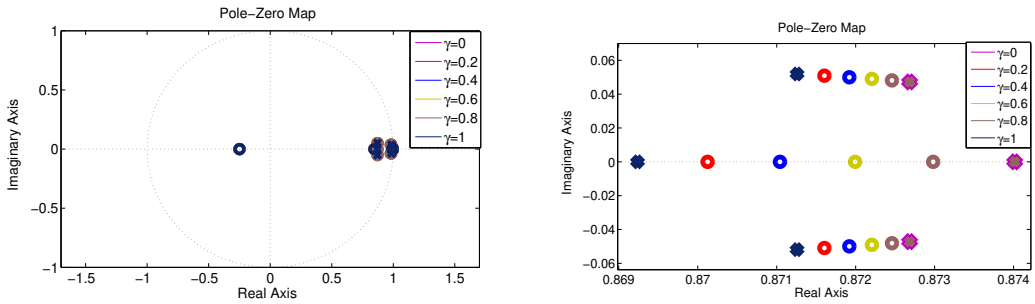

(a) Root locus (b) Dynamics compensation

Figure 5.16: Closed loop root locus with respect to γ

5.6 Simulation results

To validate the proposed control structure, two scenarios was implemented using the vehicle model previously described. In the first one, a straight lane is used as reference trajectory. All simulations are started with an initial deviation of 3 meters from the reference trajectory. In the second scenario, the reference trajectory is a curved lane. The vehicle speed was set to 10m/s.

In Figure 5.17 and Figure 5.18, the performance of the controller C_1 designed for lane-tracking response (solid black line); the controller C_2 designed for lane-change situations (solid blue line) and the proposed YK. one (solid red line) are shown with respect to the reference trajectory (solid green line).

- Straight lane scenario: the vehicle controlled by C_2 (lane-tracker controller) is the first to reach the desired lane, but Figure 5.17b and 5.17c shows that its steering wheel angle is the highest with a brutal steering rate, that causes uncomfortable sensation in the vehicle. The vehicle controlled by C_1 (lane-change controller) has the smoothest steering angle and the lowest steering rate but it takes around 150 m to reach the reference line, while the vehicle controlled by the proposed approach (YK controller) has a correct behavior, it reaches the desired reference line at the same time that the one controlled by C_2 while maintaining smoothness of steering angle and steering rate, it satisfies the required steering performance .

- Curved lane scenario: Figure 5.18a shows that the vehicle controlled by C_1 (lane-change controller) provide an under-steer response, it doesn't track the curved lane, while the vehicle controlled by C_2 tracks well the desired trajectory and the tracking error is insignificant. Finally the vehicle controlled by YK controller provides the same response that the lane-tracking controller.

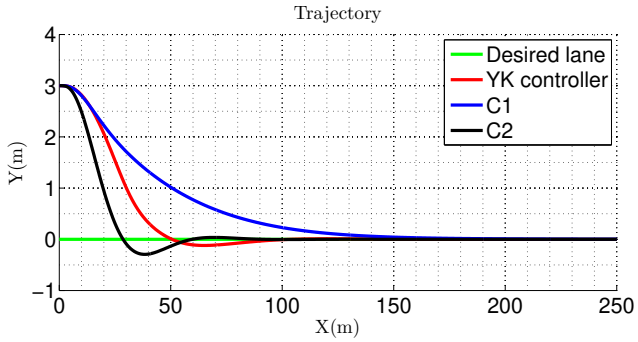

(a) Trajectory response

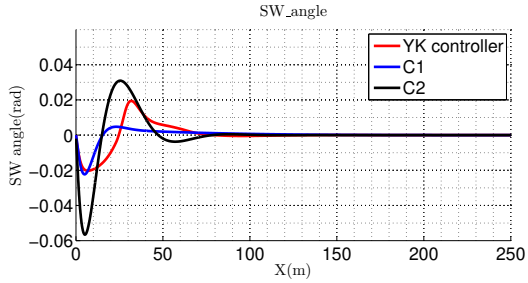

(b) Steering wheel angle

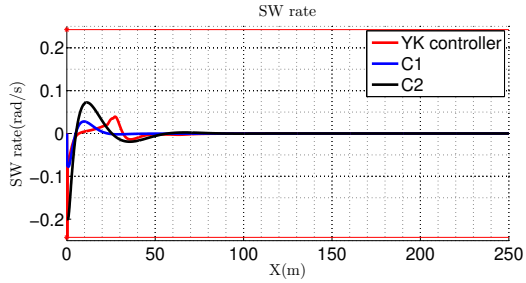

(c) Steering wheel rate

Figure 5.17: Lane-change response

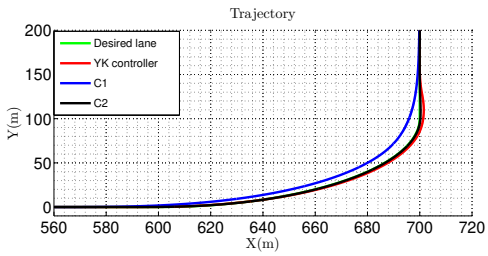

(a) Trajectory response

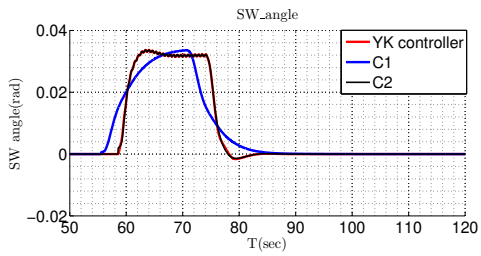

(b) Steering wheel angle

Figure 5.18: Lane tracking response

The simulation results presented in figures 5.17 and 5.18 shows that both lane-changing and lane-tracking maneuvers can be handled by one controller using YK parametrization. The vehicle controlled by YK-controller showed good performances and an appropriate behavior in each scenario which can't be performed by using only C_1 (lane-change controller) or C_2 (lane-tracking controller).

5.7 Experimental results

The proposed approach was tested on an electric Renault ZOE that has been modified for allowing autonomous driving as described in section 5.1. The lateral controller is implemented within the vehicle control system, using the MABx turning at 100Hz. The tests have been conducted in the Satory test track.

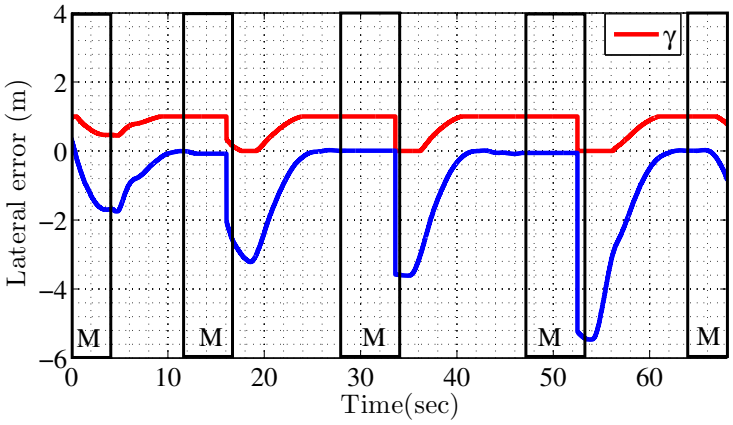

Figure 5.19: Experimental results: lateral error

To validate the proposed control structure, many scenarios have been tested. In each test the vehicle was manually drove from the desired trajectory and the autonomous mode was started at a given lateral error as shown in Fig.5.19. The manual driven phases are denoted by **M**. The vehicle speed is set to 10m/s.
Figure 5.19 shows that the controller switched between C_1 and C_2 gradually according to the lateral error value (see γ). The vehicle was able to reach the desired trajectory in less than 10 seconds in all cases. It performed smooth behavior even for 5m lateral deviation. The correspondent steering angle is presented in Fig 5.20, it shows the smoothness of the vehicle motion.

Figure 5.21 exhibits two trajectories zoomed from figure 5.19. The overshoots remained less than 0.1m no matter the value of the initial lateral error. This two graphics show that YK lateral controller handles different lateral errors with the same control performance. It's also worth to mention that in each test the vehicle maintained comfortable steering as in manual driving.

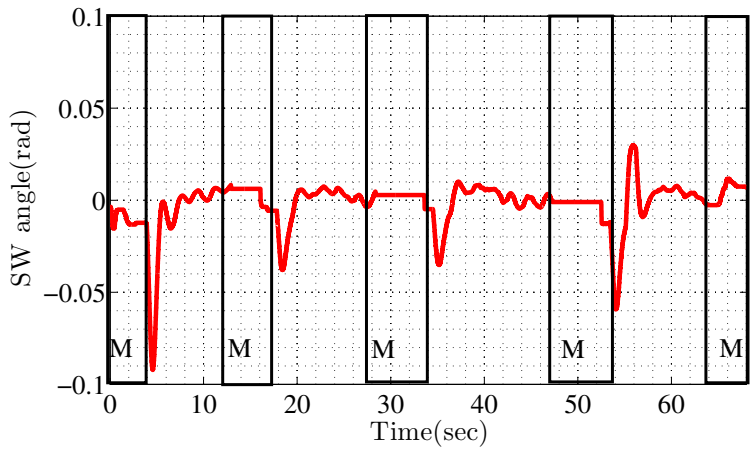

Figure 5.20: Experimental results: steering wheel angle

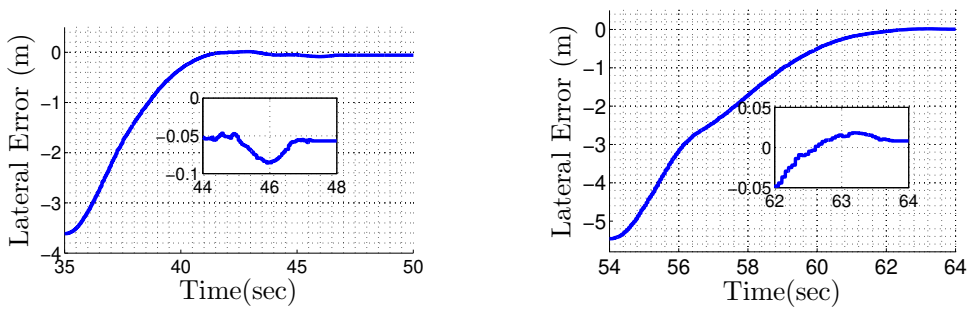

Figure 5.21: Lateral error

5.8 Conclusion

This chapter presented a YK based lateral controller for automated vehicles. The proposed control structure allows the vehicle to address and respond to different driving circumstance, meaning that the steering system is able to perform different maneuvers (i.e. lane changing, lane tracking, avoiding objects), while maintaining stability, control performance and passengers comfort.

This proposed YK control structure includes two ($T\&C$) controllers: one for tracking the desired trajectory using small look-ahead distance, and one for lane changing case presenting smoother responses and using larger look-ahead distance. The control reconfiguration is based on a decision system, measuring the lateral error and activating one of the two controllers or a part of both to enhance the control performance.
Experimental results have proven that the proposed control structure is a good way of dealing with this situations. It enhances performances of only

using a single controller for two cases. Errors are significantly reduced, and even with a deviation of 5m the vehicle reached the desired lane smoothly. The switching between controllers was gradual and stable.

The main advantage of the proposed control structure is the fact that it can be considered as a general control frame, re-configuring different controllers in a stable way in order to maximize the achievable control performance.

Other advantage is that it can be easily designed and implemented, since it requires only the tuning of the initial and final controllers.

Furthermore, other controllers can be added to the control structure handling other driving situations without impacting the stability of the closed loop.

Further works can be oriented to include more driving situations to enlarge controller capabilities and ensure high performance in any circumstance without loosing steering system stability or compromising passengers comfort, including full range speed.

Chapitre 6

Contrôle longitudinale

Below is a French summary of chapter 6.

Ce chapitre propose un système de régulateur de vitesse "Adaptive Cruise Control" (ACC) basé sur la parametrisation de YK pour satisfaire des objectifs de contrôle contradictoires dans les applications de suivi des voitures, en mettant particulièrement l'accent sur le compromis entre performance et robustesse. La structure de contrôle proposée est comparée à un contrôleur H_∞, et validée en simulation et expérimentalement en utilisant un véhicule Renault ZOE équipé d'un système de perception.

La plupart des véhicules autonomes actuels sont basés sur la fusion de plusieurs capteurs pour la détection et le suivi du véhicule leader. Contrairement aux systèmes de suivi des véhicules commerciaux qui utilisent un capteur radar pour mesurer l'inter-distance entre les véhicules. L'utilisation de capteurs multiples est obligatoire pour les tâches de conduite autonome. Cependant, chaque capteur peut présenter un bruit différent qui apparaît et disparaît dans le système.

Sans perdre de vue la généralité, considérons une seule caméra pour détecter un véhicule précédent sur la route. Il est clair que deux paramètres ont un impact sur les performances du système de perception : 1) l'algorithme spécifique développé pour détecter et suivre les objets fournissant une mesure précise ; et 2) la limitation physique du capteur lui-même. Pour une caméra, le nombre de pixels limite la résolution de l'image, donc plus le véhicule est éloigné, plus la précision de sa détection est faible. Cela implique une mesure plus imprécise qui dégradera les performances de l'ego-véhicule. Du point de vue de la réponse du véhicule, on ne peut pas s'attendre à ce qu'un seul contrôleur puisse gérer un système de suivi de voiture par caméra pour toutes les distances de véhicules détectées.

Grâce à la paramétrisation YK, le contrôleur proposé interpole de manière stable deux contrôleurs ACC ayant des objectifs contradictoires : 1) un contrôleur performant avec des capacités de poursuite rapide; et 2) un contrôleur robuste avec des capacités d'atténuation du bruit de perception. La structure multi-contrôleurs proposée utilise des outils de contrôle à la fois performants et robustes afin d'adapter le comportement de suivi de la voiture à l'état du système de perception tout en garantissant la stabilité du système ACC.

Chapter 6

Longitudinal Control

This chapter proposes a YK based Adaptive Cruise Control (ACC) system to deal with conflicting control objectives in car-following applications, with a special emphasis on the trade-off between performance and robustness. The proposed control structure is compared to H_∞ controller, and validated in simulation and experimentally using a Renault ZOE vehicle equipped with a perception system.

Most of current autonomous vehicles are based on multi-sensor fusion for leader vehicle detection and tracking. Unlike the commercial car following systems that use radar sensor to measure the inter-distance between the vehicles. The use of multiple sensors is mandatory for autonomous driving task. However, each sensor can present different noise which appears and disappears in the system.

Without loss of generality, let's consider a single camera for detecting a preceding vehicle in the road. It's clear that there are two parameters that impact the performance of the perception system: 1) the specific algorithm developed to detect and track the objects providing accurate measurement; and 2) the physical limitation of the sensor itself. For a camera, the number of pixels limit the resolution of the image so the farther away the vehicle is, the lower the accuracy in its detection. This implies a more inaccurate measurement that will degrade the ego-vehicle performance. From the vehicle response point of view, we cannot expect that a single control device can handle for example a camera-based car-following system for all detected vehicle distances.

Thanks to YK parametrization, the proposed controller interpolates in a stable manner two ACC controllers with conflicting objectives: 1) a performant controller with fast preceding tracking capabilities; and 2) a robust controller with perception noise attenuation capabilities. The proposed multi-controller structure uses tools of both performance and robust control in order to adapt car-following behavior to perception system status while guaranteeing the ACC system stability.

The chapter is organized as follows: Section 6.1 formulates the problem of two conflicting control objectives (performance/robustness) in ACC feedback control loop. A brief car following review is provided in section 6.2. Section 6.3 presents the motivations behind using YK parametrization in solving the trade-off between the robustness and performance objectives. Section 6.4 is the definition of a set of control objectives in ACC system by designing two controllers that try to maximize a criteria while neglecting the others and YK based controller interpolating them. In Section 6.5, an H_∞ controller is designed to compare its performance with the one proposed in this work. A comparative study between the multi-controller structure and H_∞ controller is provided in Section 6.6. The performance and improvement of the proposed approach tested on an experimental vehicle are shown in Section 6.7. Finally, some discussion about the proposed method and future work are presented in the last section.

6.1 Problem description

The objective of any control system is to shape the system response to a given reference with a desired performance and robustness, while minimizing the effect of noise measurement and ensuring the stability of the system [7].

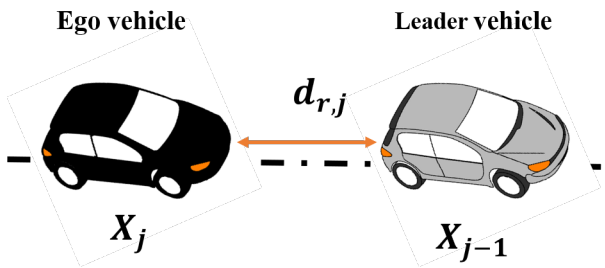

Figure 6.1: String of two vehicles

Let's consider a car following problem, where a string of N vehicles driving in the same lane one following its preceding. Figure 6.1 shows a string of two vehicles, the absolute position of the leader vehicle is X_{j-1}, the follower vehicle noted Ego vehicle is positioned at X_j. $d_{r,j}$ is the inter-distance between the two vehicles.

The ego vehicle is equipped with an ACC system. It's a car following algorithm allowing vehicles to drive behind a leader with a certain spacing policy by adapting the speed. The preceding vehicle is detected by a perception system (camera [165], radar [166] or lidar [167]) that measures the inter-distance and relative velocity with respect to the preceding vehicle. Then a control loop regulates the inter-distance.

The associated feedback loop is shown in Figure 6.2. A longitudinal vehicle model G_j is connected with an ACC controller K_i. The controller is

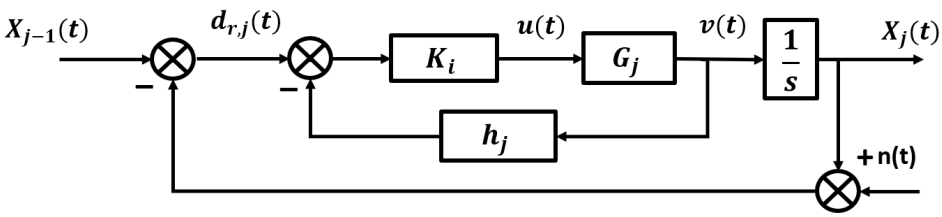

Figure 6.2: ACC control loop.

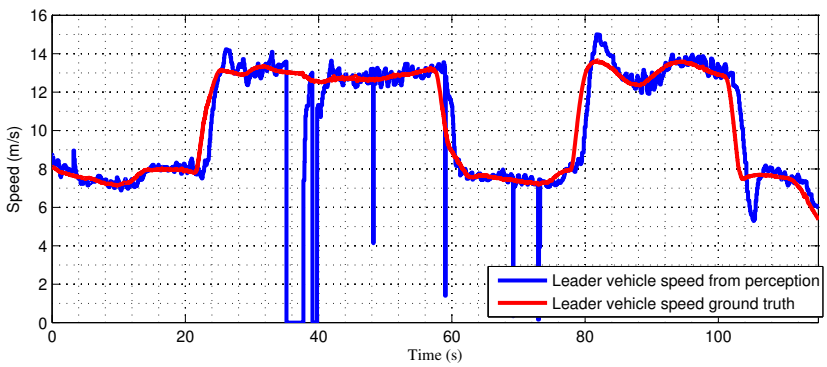

Figure 6.3: Perceived leader speed

in charge of regulating the error e_j between relative distance $d_{r,j}$ $(X_{j-1} - X_j)$ and the reference distance coming from the spacing policy. The desired inter-vehicle distance is provided by a constant time gap spacing policy [168] [169]. As shown in Eq.(6.1), the reference inter-vehicle distance d_{ref_j} is a speed-dependent constant time-gap h_j. This is reflected in a feedback regulation $H_j = h_j s + 1$ connected to the absolute position of ego-vehicle X_j.

$$d_{ref_j} = d_{std_j} + h_j v_j \tag{6.1}$$

The noise signal $n(t)$ represents mainly the leader vehicle tracking error in the perception system. This noise could be within the vehicle bandwidth, since the computation of the inter-distance is based on the fusion of data coming from cameras, Lidar and GPS. Figure 6.3 shows the leader vehicle speed while doing a car following of two robotized ZOE, the leader vehicle was driven manually, its speed was recorded using an embedded sensor (red solid line), the follower vehicle is equipped with a perception system that estimates the leader speed (blue solid line). One can notice that the perceived speed is modified by noise that can appears end disappears suddenly, the discontinuities in the perceived speed such as between seconds 30 and 40 is caused by the loss of the localization system. All frequencies higher than the vehicle bandwidth are not considered since they are automatically filtered by the vehicle model.

The design of K_i will depend on operating conditions and control objective: from perfect vehicle preceding tracking to noise reduction when the perception signal is not clean.

The perfect tracking and noise reduction are two control objectives requiring both high performance and robust control. To satisfy these control requirements, performance and robustness metrics are needed. Thus, the following relationships are defined:

- The closed loop sensitivity function S is defined as the transfer from the measurement noise $n(t)$ to the vehicle speed $v(t)$, since it's the measured output.

$$S = \frac{K_i G_j}{1 + \frac{K_i G_j H_j}{s}} \tag{6.2}$$

- The complementary sensitivity function T is defined by the transfer from the preceding vehicle position $X_{j-1}(t)$ to the ego vehicle position $X_j(t)$.

$$T = \frac{\frac{K_i G_j}{s}}{1 + \frac{K_i G_j H_j}{s}} \tag{6.3}$$

The sensitivity function S as defined in (6.2) evaluates the closed loop noise measurement attenuation capabilities, while the complementary sensitivity function T described in (6.3) defines how the system tracks reference input.

Ideally, one would like to design the controller K_i able to provide both fast tracking and noise attenuation. In other words, minimize S and make $T = 1$ in the whole frequency range. However, for a given vehicle model G_j and ACC controller K_i, $T = \frac{1}{s}S$ and satisfying both objectives is clearly not possible. A faster response needs the closed loop T bandwidth to be increased, which also makes the system more sensitive to the measurement noise $n(t)$.

Figure 6.4 shows a graphical example of two controllers designed with different objectives for the same plant G_j and spacing policy H_j. The objectives are the following: 1) a controller K_1 with a large closed loop bandwidth, therefore it exhibits a good tracking but it is very sensitive to the measurement noise; and 2) a controller K_2 where the closed loop bandwidth is reduced and consequently it provides good noise rejection with slow response. Large measurement noise was injected into the system to emulate a noise problem in the perception system (see bottom graph of Fig. 6.4). Controller K_1 exhibits a faster response but is more sensitive to measurement noise and K_2 is slower but attenuates noise in perception system.

This example illustrates the trade-off between performance and robustness, demanding more advanced control structures to achieve better performance in all circumstances.

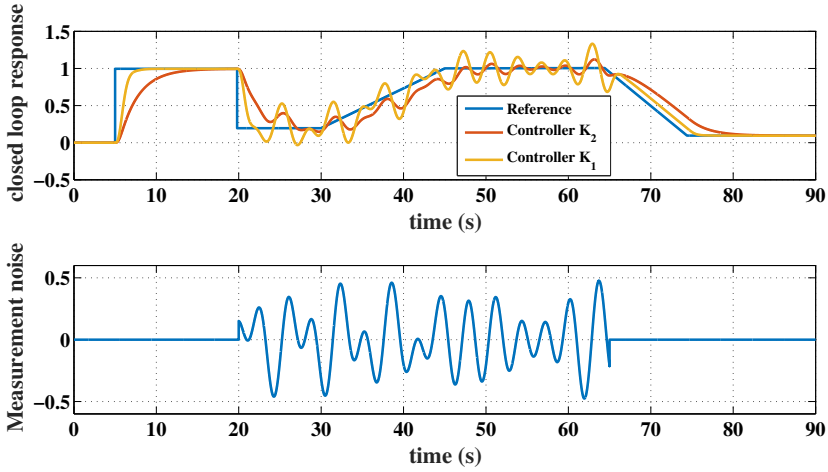

Figure 6.4: Closed loop response of controllers K_1,K_2.

The main goal of the work presented in this chapter is to design an ACC multi-objective controller structure that interpolates controllers with different control objectives, each one suitable for a specific operating condition. This will be done following the steps below:

- Design two independent ACC controllers: one with high tracking capabilities and another one rejecting measurement noise.
- Define the interpolation parameter γ able to activate the controller increasing either the tracking capabilities or noise reduction.
- Variation of γ should take into account perception system performance as an indicator about the noise level in the perceived signals.
- The multi-controller structure is based on YK parametrization, keeping the closed loop stability during controllers interpolation.

6.2 Longitudinal control review

Car-following control systems represent one of the first intelligent transportation systems applications able to relief the driver of adjusting vehicle speed based on preceding traffic, reducing fuel consumption and increasing traffic flow capacity [170].

Origin of car following applications is Cruise Control (CC) systems. The earliest cruise control system contained all mechanical parts and did not offer much functionality. It could only hold the throttle in a fixed position.

First developments introducing car following applications were carried out in the 50's by Pipes [171] and Chandler [172], they studied mathematical

models that predicted and imitated the human behavior while performing a car following. The first car-following demonstration was carried out in 1991 by the European community's PROMETHEUS program [173]. Since then, ACC and its extension by using V2V communication to Cooperative ACC (CACC) have been widely studied as car-following automated systems, providing benefits in fuel consumption [174] and traffic flow [170].

First CC systems were in use between the late 1960's and 1980's. It included only proportional feedback providing full throttle when the vehicle speed dropped 6-10 m/h below the desired cruising speed [174]. Thanks to electronic controller development, PID cruise controller were implemented in CC systems, showing significant improvements in response time, rise time, steady state error, and cruise tracking control [175]. Self tuning cruise controller is proposed in [176] where a sensitivity and a gradient filters are added to dynamically adjust the PID gains to optimally match the vehicle and driving environments. Fuzzy logic is explored in cruise control by Mazda in [177] to deal with non-flat road. Other fuzzy cruise control implementations are used to increase driver comfort, and lead to a smoother rides in all road conditions [178–182].

ACC system appears to overcome classical CC by incorporating simultaneous brake and throttle pedals control. It also incorporates a ranging sensor (usually Radar or LiDAR) to measure the inter-distance and relative velocity with respect to the preceding vehicle. Its main purpose is keeping a desired safe spacing gap towards the preceding car by the regulation of ego-vehicle's speed, it is mainly conceived for highways scenarios. ACC systems have surged as one of the firsts ADAS that proposed to employ exteroceptive sensors in the loop, profiting from the advances on embedded vehicular technology in recent years to provide an enhanced driving performance.

CACC system is an upgraded version of ACC system [183], including vehicle-to-vehicle (V2V) communications to provide more extensive preceding vehicle information (i.e. preceding vehicle acceleration) and use them in the cruise control loop. ACC system is more related to energy consumption, it allows fuel saving from 1.1% to 10.7% [174], whereas CACC system is more related to the traffic throughput since it increases the road capacities by allowing smaller spacing between vehicles and increasing safety in bad environment condition (e.g. poor vision) [184].

The most common performance objectives in car following application for both ACC and CACC systems are safety, comfort and stability. Note that two stability concepts can be distinguish: 1) Internal vehicle stability based on vehicle dynamics; 2) String stability refers to the idea of no amplification of spacing error along the string of vehicles [185] [186].
Different strategies have been proposed to define the spacing policy between vehicles. The first proposed policy is constant clearance [186, 187]. This approach consists on maintaining a constant inter-distance regardless to the vehicle speed, which increases significantly the road capacity, but does not

ensure string stability. The second approach is a Constant Time Gap (CTG) policy [188], the spacing is proportional to the vehicle speed. The latter is the most employed one and adopted by commercial ACC systems since it is the closest to the human behavior [189] and ensures string stability. In this work a classical constant time gap policy is used.

From the control point of view, numerous techniques are used to satisfy the different control design objectives [184]. Related to the ACC application, an explicit Model Predictive Control (MPC) approach is presented in [190] with collision avoidance capabilities. In [191–193] multiple approaches are proposed incorporating human factors in controller design by learning directly control parameters from human driver (i.e. spacing policy, control gain,..) in both online and offline ways. In [194], a comparative study between robust control approach and artificial intelligence based control (Fuzzy logic controller) is shown for a low speed range ACC. Authors in [195] focus on improving performance of ACC system using predictive, model-based longitudinal controls, enhancing situational awareness, and finally making use of policy learning with deep reinforcement architectures to extract the best performance, defined in a multi-objective manner, out of available control authority of the system

Concerning CACC systems, different platoon topologies are proposed depending on the direction of the communicated information:

- Unidirectional topology: vehicles information are communicated in one direction, either from predecessor to follower (PF), or from predecessor and leader to follower (PLF). The controller is designed in two parts, an ACC feedback with usually proportional-derivative (PD) controller or a proportional-integrator-derivative (PID) controller; and a feedforward filter designed to preprocess the preceding vehicle acceleration signal to obtain the CACC control input in PF topology [196–198]. In PLF topology, controller deals with two errors since the vehicle have two communications with leader and preceding vehicles.

- Bidirectional topology: the vehicle communicates with both preceding and follower vehicles which yield in a front and rear spacing errors. In [199], the two errors are handled separately, while in [200] a parameter is used to change the ratio between the two errors.

Regarding CACC control structure, [201] used a Linear Quadratic Regulator (LQR) coupled with a LQ Gaussian observer to obtain an overlapping platoon controller in case the preceding vehicle information is missing. Fuzzy logic control frame is used in [202] to imitate as closely as possible the human behavior, by defining a rule set for the spacing policy, ego-vehicle speed and relative speed. MPC technique is used in [203] to minimize the spacing and the speed error with respect to the preceding vehicle. CACC algorithm

implemented in [204] allows each vehicle in the platoon to generate its optimal reference states, and share them to the follower in order to enhance the platoon performance.
The most employed control structure in car-following field is a feedback controller that correct the spacing error, and when V2V communication is available, a feed forward controller is added to improve the vehicle response towards disturbance propagation, this control approach is used in both ACC [169] and CACC [205] systems.

Until now all these proposed control solutions rely on sensor information and vehicle environment perception. Thus, the desired performance may temporally evolve based on sensor failures or noise. According to this, any of the designed previous controllers may be affected by new signals, or noise that can appear and disappear and for which the system has not been designed, leading to poor performance or instability problems. A control structure able to cope with different (even contradictory) design objectives will allow to overcome this limitation, providing the best possible response in all circumstances. Therefore, managing the trade-off between the two conflicting objectives performance/robustness in real time can extend car-following systems capabilities.

6.3 Motivation on using Youla Kucera

The proposed solution is designing a suitable controller for each control objective and appropriately interpolating the controllers in a multi-controller structure using an online supervisor that decide what fraction of each controller to activate at each instant in order to accommodate the changes in the perception system.

The main motivations behind using YK parametrization in interpolating ACC controllers are the followings:

- It provides a control structure that can receive a control independent parameter as an interpolation signal (i.e. perception signal).
- It ensures the system stability under arbitrary interpolation according to the noise level (i.e. ensure high tracking performance in absence of noise, and robustness in the presence of noise).
- It allows the interpolation of different control structures in one controller (i.e. a proportional controller with a derivative controller).

The following section explains the performance and robustness criteria with respect to the ACC application and the steps of the YK-based ACC controller design.

6.4 Control design

An ACC controller has the objective of guaranteeing string stability that is in charge of avoiding traffic accidents and improving traffic flow in string of vehicles. String stability is defined as the attenuation of disturbances along the string of vehicles [206]. Different definitions are presented in the literature. The common part is that they all consider amplification of oscillations upstream a string of vehicles. Oscillations can be measured in different signals as described in definition in [207]:

Definition 6.4.1 *Consider a string of $m \in N$ interconnected vehicles. This system is string stable if and only if:*

$$\|Z_j(t)\| < \|Z_{j-1}(t)\|, \forall t \geqslant 0, 2 \leqslant j \leqslant m \tag{6.4}$$

where the choice of the scalar signal $Z_j(t)$ can either be the distance error, velocity, or acceleration, seems rather arbitrary.

In our work $Z_j(t) = X_j(t)$. Thus, the sufficient condition of string stability, which means that the absolute position of each vehicle must not increase as it propagates through the string is equivalent to equation (6.5).

$$\|X_j/X_{j-1}\| \leq 1 \quad for \quad j > 1 \tag{6.5}$$

String stability needs to be ensured even if operating condition changes. As already stated in section 6.1, two string stable controllers are designed : 1) a performant controller where only fast tracking of preceding vehicle speed/distance is taken into account; and 2) a robust controller to reject measurement noise in the ACC range sensor system. The mathematical formulation to guarantee the defined control objectives is provided below.

6.4.1 Performant controller criteria

Temporal response of a closed loop system can be divided in two: 1) the steady state behavior, where the controller should be able to make tracking error null; and 2) the transition behavior, which is related to the response rising time and overshoot. This temporal response is directly related to the frequency response of the system. Concretely, a large bandwidth corresponds to a faster rise time. Thus, to increase controller performance, the closed loop bandwidth should be enlarged. Mathematical formulation of performance objectives is as follows:

- Steady state error in tracking reference is null:

$$\lim_{s \to 0} T(s) = 1 \tag{6.6}$$

- Maximum tracking of the desired inter-distance vehicle distance:

$$T(s) = \frac{1}{1 + h_j s} \tag{6.7}$$

- Fast reference tracking. For a desired rise time t_r the closed loop bandwidth can be set using the following relation:

$$w_b = \frac{0.35}{t_r} \quad with \quad |T(w_b)| = -3dB \tag{6.8}$$

- Stability of the ACC closed loop:

$$Real(p_i) < 0 \quad \forall p_i \in pole(T) \tag{6.9}$$

6.4.2 Robust controller criteria

The robust controller objective is to attenuate the measurement noise within the system bandwidth. This is closely related to the S function defined in (6.2). As well as the constraint of the closed loop stability. These criteria can be mathematically expressed as:

- Noise measurement attenuation:

$$|S(s)| < \beta \quad while \quad s < jw_G \tag{6.10}$$

  where w_G is the system bandwidth, β is the desired attenuation ratio (i.e $\beta = -7dB$ for 50% attenuation).

- Stability of the ACC closed loop:

$$Real(p_i) < 0 \quad \forall p_i \in pole(S) \tag{6.11}$$

6.4.3 Nominal controllers design

The two nominal controllers are designed to fulfill the performance and robustness criteria respectively. The controllers design is based on a LTI longitudinal vehicle model of the real platform described in section 5.1 is obtained through identification techniques provided by MATLAB. A second-order transfer function is enough for modeling the vehicle behavior between commanded speed $u(t)$ and output speed $v(t)$:

$$G_{vel}(s) = \frac{e^{-0.06s}}{0.0750s^2 + 0.4383s + 1} \tag{6.12}$$

Since the vehicle receives acceleration commands, a vehicle model taking acceleration as input is deduced by adding a speed feedback as shown in figure 6.5.

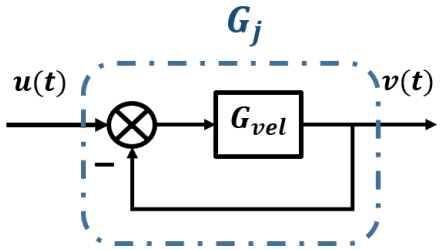

Figure 6.5: Acceleration vehicle model G_j

The resulting transfer function G_j is calculated as follows:

$$G_j = \frac{G_{vel}}{1 + G_{vel}} \tag{6.13}$$

Let's T_1 be the complementary sensitivity function of the performant controller with respect to the control system proposed in Fig. 6.2:

$$T_1 = \frac{\frac{K_1 G_j}{s}}{1 + \frac{K_1 G_j H_j}{s}} \tag{6.14}$$

Using the longitudinal vehicle model described on equations (6.12) and (6.13), the proportional controller $K_1 = P$ is designed attending the objectives formulated on equations (6.6),(6.7) and (6.8). The frequency response of $T1$ is plotted in figure 6.6 for different values of P (solid lines) within stabilizing proportional controller range.

Let's S_2 be the complementary sensitivity function of the robust closed loop:

$$S_2 = \frac{K_2 G_j}{1 + \frac{K_2 G_j H_j}{s}} \tag{6.15}$$

Based on the acceleration vehicle model in (6.13), the derivative controller $K_2 = D \times s$ is designed to satisfy the noise attenuation criteria expressed in (6.10). Figure 6.6 shows the frequency responses of the complementary sensitivity function $T2$ (dashed lines), representing the robust closed loop controlled by K_2.

The two controllers K_1 ans K_2 provide different closed loop bandwidth. For the proportional controller K_1, the system bandwidth varies from 1.28 rad/s to 1.62 rad/s. Whereas, the derivative controller K_2 leads to lower closed loop's bandwidth varying from 0.3 rad/s to 0.66 rad/s.

The chosen performant controller is $K_1 = 1.2$, it provides a good response but it is highly sensitive to noise whereas the robust controller $K_2 = 0.4$ significantly sacrifices tracking capabilities and attenuates more then 70% noise measurement within the vehicle bandwidth. The complementary sensitivity functions $T1$ and $T2$ are represented in figure 6.7 by solid

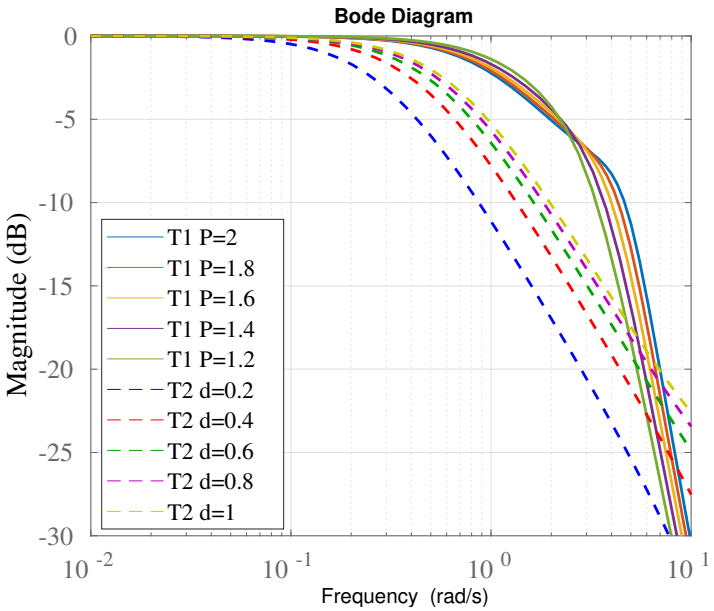

Figure 6.6: Performant and robust closed loops frequency responses for different controllers parameters P and D values.

black and red lines respectively showing the bandwidth difference. The sensitivity functions $S1$ and $S2$ are represented in figure 6.7 by dashed black and red lines respectively showing the noise attenuation level for each controller. Next section describes the proposed controller that interpolates K_1 and K_2. The proposed structure keeps the benefit of both controllers in a single controller while the stability of the final closed loop is guaranteed.

6.4.4 Parametrized controller $K(Q)$

The design of the multi-controller $K(Q) := \{K_1, K_2\}$ is done by following the steps below:

- ACC control loop modification: The basic ACC control loop presented in figure 6.2 is transformed as shown in figure 6.8. The main modification is the location of the spacing policy constant h_j in order to have a positive feedback loop allowing YK controller design according to the block diagram in figure 3.5.

- Coprime factors computation: The plant tranfer function G_j, and both controllers K_1 and K_2 transfer functions are factorized into right and left coprime factors using formulas in (3.17), (3.18). The resulting coprime factors are stable. Then, the YK parameter is deduced using (3.39).

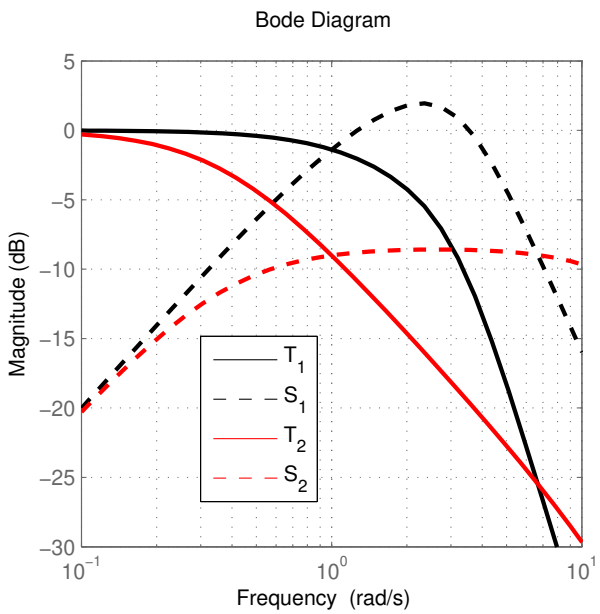

Figure 6.7: S and T responses of performant and robust controllers K_1 and K_2.

- Interpolation signal: the interpolation signal γ is provided by a designed supervisor that uses the real time measurable system signals to estimate the operating conditions following the logic below:

$$\gamma = \begin{cases} 0 & Clean \quad sensor \quad signal \\ 1 & Noisy \quad sensor \quad signal \end{cases} \tag{6.16}$$

The variation of γ relies on a decision system fed by the perception system. The later is fusing different data from different sensors to estimate the leader vehicle motion, using some fusion algorithms. The later can

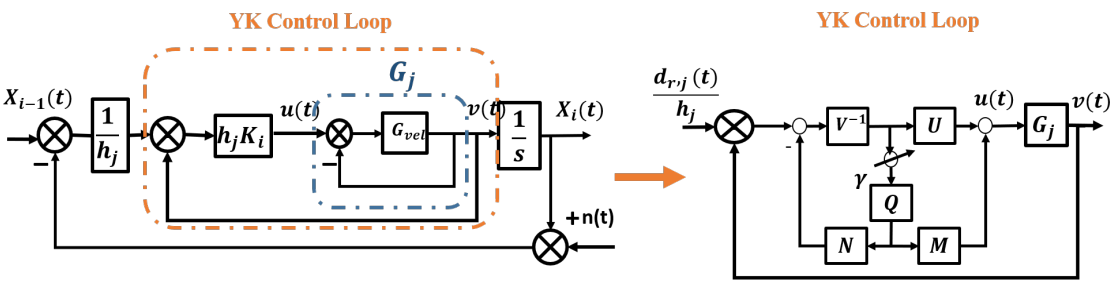

Figure 6.8: YK based ACC control loop

provide a confidence level about the quality of the measurements [208] [209]. The supervisor could be fed the performance level of the perception system. In our specific application, noise is distance related, so we just designed the γ to apply the needed level of rejection accordingly to that distance noise. It is important to remark that system stability is γ independent, meaning that γ can vary accordingly to any criteria.

The YK based ACC controller is designed to fulfill both performance and robustness objectives (see section 6.4.3) with respect to the operating conditions. For comparison purposes, H_∞ control is used as it represents one of the most widely used control technique for this problem [210–212].

6.5 H_∞ controller

The trade-off between the desired proprieties of robustness and performance is present in many control problems. The uncertainties caused either by the system environment, modeling errors, or inaccurate measurements are handled by adding robustness constraints to the controller classical goals, in particular performance and stability.

H_∞ control is a design technique that allows the simultaneous optimization of both robustness and performance criteria. While ensuring the stability of the closed loop by localizing the closed loop poles in the stable region of the complex plane. By exploiting its links to robust stability of systems [119].

Many practical applications proved the efficiency of H_∞ approach when dealing with robustness requirements. The problem of active damping of the low frequency longitudinal car oscillations is solved in [213] using H_∞ controller. A LPV feedback controller coupled with an H_∞ observer is applied to an electric ground vehicle (EGV) in which the measurement of longitudinal velocity is assumed to be uncertain. Experimental tests and comparisons showed the advantages of H_∞ technique [214]. In [215], experiments on a T-inverted pendulum showed the efficiency of the H_∞ approach to deal with the adaptation of a real-time controller's sampling period to account for the available computing resource variations.

The H_∞ control design is based on a state space computational solution that utilizes frequency-dependent weighting functions to tune controller's in order to manage the trade-off between performance and robustness objectives [216].

In order to formulate the H_∞ problem with the same control objectives as in section 6.4.3, two regulation outputs are defined:

- Z_1 represents the performance objectives (the transfer from the reference $r(t)$ to the output $y(t)$).

$$||Z_1||_\infty = ||W_T T||_\infty$$

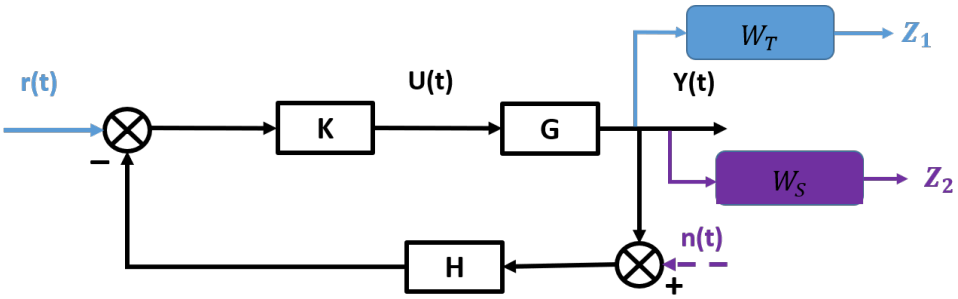

Figure 6.9: H_∞ control loop.

- Z_2 represents the robustness objectives (the transfer from the noise measurement $n(t)$ to the output $y(t)$).

$$||Z_2||_\infty = ||W_S S||_\infty$$

The solution of this H_∞ problem is to find the controller K that minimizes the infinity norm of Z_1 and Z_2.

W_T and W_S are the frequency weighting functions that are usually chosen using empirical rules. In our work, and since the H_∞ controller is designed to be compared to the proposed multi-controller, the weighting functions are set to represent the same performance and noise rejection criteria that in the YK based controller. To do so, W_T and W_S are chosen as follows:

- The complementary sensitivity function T template $1/W_T$ is chosen to make T as performant as T_1 described in section 6.4.3.

$$W_T = 1/T_1 \tag{6.17}$$

- The sensitivity function S template $1/W_S$ is chosen to make S as robust as S_2 described in section 6.4.3.

$$W_S = 1/S_2 \tag{6.18}$$

The controller is computed by minimizing the following infinite norm:

$$||W_T T||_\infty + ||W_S S||_\infty \tag{6.19}$$

To provide a fair comparison between the YK based and the H_∞ ACC systems, the controller order is fixed and include both proportional and derivative actions as proposed in K_1 and K_2 (see section 6.4). Thus, the K_{H_∞} is expressed as follows:

$$K_{H_\infty} = P_{H_\infty} + D_{H_\infty} s \tag{6.20}$$

The controller parameters P_{H_∞} and D_{H_∞} are computed using an optimization algorithm executed for a constant value of h_j using the Matlab command fsolve, which allows to solve multi-objective optimization taking into account the weighting functions W_S and W_T.

In the following section, the YK based ACC is compared to the resulted H_∞ controller in different operating conditions.

6.6 Comparison results

This section shows the behavior of the YK based the H_∞ controllers in a simulation framework. Using the vehicle model in 6.12 representing the longitudinal system of the ZOE prototype.

The comparison between the two ACC systems is conducted with respect to control criteria in sections 6.4.3. It's provided in both frequency and temporal domains.

6.6.1 Frequency domain comparison

The comparison in the frequency domain is mainly in function of sensitivity S and complementary sensitivity T functions. Notice how S is the transfer from perception noise in the relative distance to the preceding vehicle $n(t)$ to the vehicle speed $v(t)$ (see Fig.6.2). The complementary sensitivity function T is defined by the transfer from the preceding vehicle position $X_{i-1}(t)$ to the ego vehicle position $X_i(t)$, which is equal to the string stability.

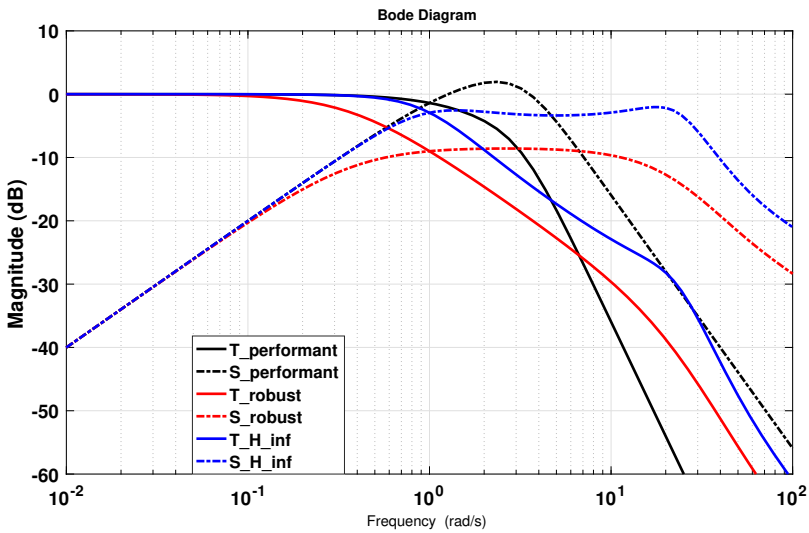

Figure 6.10: S and T responses for performant, robust and H_∞ controllers.

Figure 6.10 shows sensitivity and complementary sensitivity function of performant, robust and H_∞ controllers respectively for comparison purposes. One can see how all T responses (solid lines) are below $0dB$, so the string stability of the system is ensured; besides bandwidth of the performant (solid black line) is larger, being able to correct distance errors faster than the others. As already mentioned, this rapidity is associated to a worse noise rejection level as shown in the sensitivity function (see dotted black line). See how the robust controller is more robust to noise (dotted green line), as the peak magnitude never exceeds $-9dB$. This is associated to a slower response in its complementary sensitivity function (solid green line). Finally, H_∞ control design gives an intermediate solution, with a controller response between both performant and robust controller solutions (check solid and dotted blue lines for T and S respectively). The latter does not exploit all the system capabilities, a multi-controller design allows to perform one or the other depending on the system conditions, exploiting the system up to its limits.

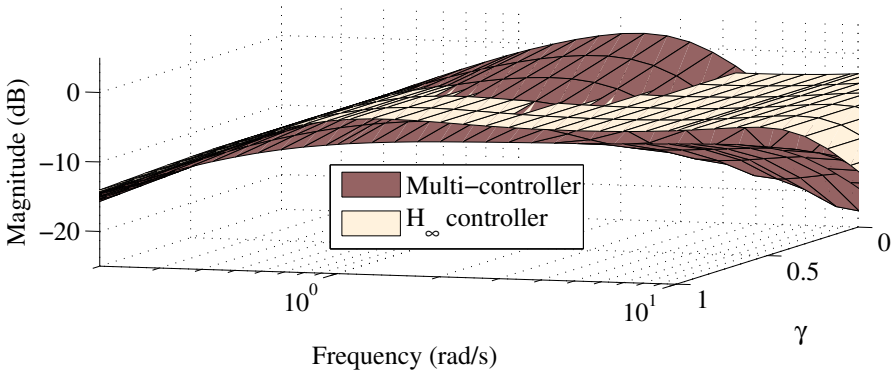

Figure 6.11: Sensitivity function S in function of γ in the YK-based multi-controller structure for car-following applications. This is compared with sensitivity function of H_∞ controller.

Figures 6.11 and 6.12 show the variation of sensitivity and complementary sensitivity transfer functions depending on the scalar factor γ of the YK-based multi control structure and H_∞ controller. By modifying the scalar factor γ representing to noise level from 0 to 1, the multi-controller is able to provide S and T responses between those corresponding to performant K_1 and robust controllers K_2. $\gamma = 0$ corresponds to operating condition where the measured inter-distance is clean and the vehicle is controlled by the performant controller, while $\gamma = 1$ repesents the situation where the perception provides a noisy signals with low confidence level and the robust controller is activated. The multi-objectives controller is able to

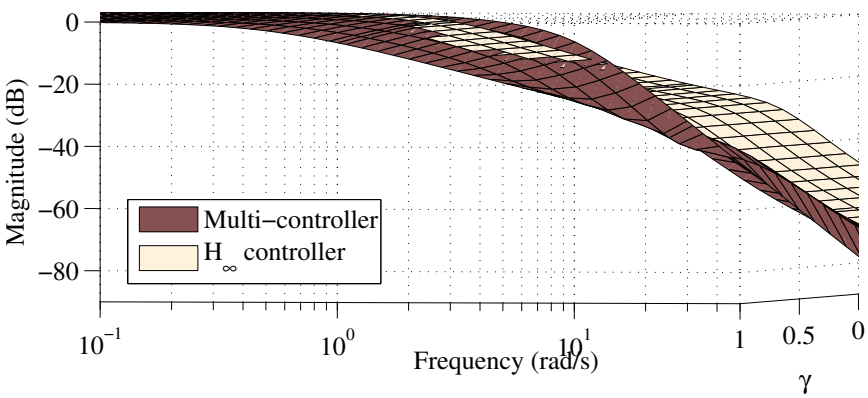

Figure 6.12: Complementary sensitivity function T in function of γ in the YK-based multi-controller structure for car-following applications. This is compared with complementary sensitivity function of H_∞ controller.

adapt the performance to the operating conditions while H_∞ provides the same behavior no mater the situation.

6.6.2 Temporal domain comparison

The YK-based and H_∞ ACC systems are used for obtaining results corresponding to a two-vehicle string in two different simulated scenarios: 1) The measurement noise is present in the system with different levels; 2) The measurement noise appears in the perception system for a period of time and disappears.

Figure 6.13 depicts a two-vehicle string car-following scenario where the trailing vehicle sensor is in charge of measuring the inter-vehicle distance presents a variable noise. Accordingly to this scenario, the proposed multi-controller structure (Ego YK) is compared to the performant (Ego K_1), robust (Ego K_2) and H_∞ (Ego H_∞) controllers.

The top graph of figure 6.13 plots leading vehicle speed and the response of the trailing one in function of the aforementioned controllers. The middle graph plots the simulated noise signal (solid blue line) added to the relative distance $d_{r,j}$ and how the scalar factor γ is changed over time (solid red line). The noise signal represents mainly the leader vehicle tracking error in the perception system, this tracking error can lead to measurement noise $n(t)$ within the vehicle bandwidth.

The tracking error in perception system is correlated to many factors such as the tracking algorithm performance [217] or visibility conditions. Additionally, the leader vehicle speed can affect the inter-distance measurement: the higher the speed, the bigger the tracking error. The scalar factor γ varies from 0 to 1 in order to adapt the YK based controller to the situa-

tion. A simple speed-dependent evolution of γ is proposed in this scenario: the higher the speed, the bigger the noise, the closer γ to unity. The bottom graph shows zoomed parts from the top graph.

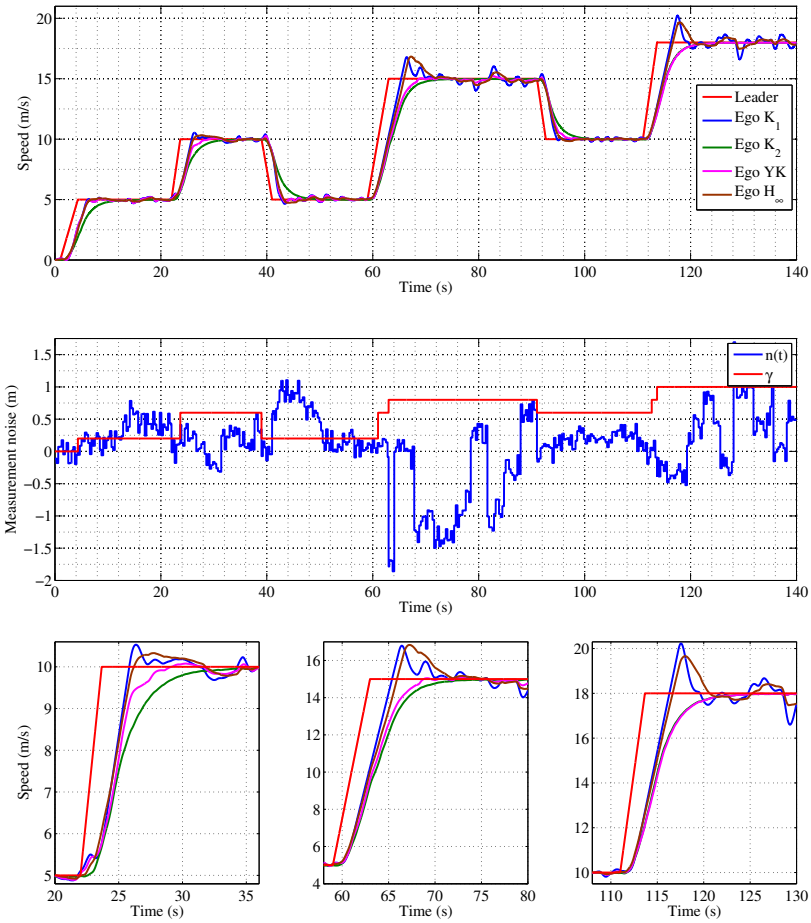

Figure 6.13: Comparison results for YK, robust, performant, and H_∞ controllers when noise is present in the perception system that measures the inter-vehicle distance in a string of two vehicles. Simulation results.

Leader vehicle (solid red line) is the first vehicle in the string following a speed profile between $0m/s$ and $18m/s$ with different acceleration/braking phases (the leader speed is clean since it's the ground truth). Ego vehicle is the second vehicle in the string equipped either with the performant controller K_1 (solid blue line), robust controller K_2 (solid green line), YK controller (solid magenta line), or H_∞ controller (solid brown line). One can see that the performant controller is the fast one but is sensitive to the noise, mostly when the speed is equal to $15m/s$ and $18m/s$ (see the second and third figures in the zoomed graph). The robust controller shows

smoother and slower response which sacrifices the tracking performances when the measurement noise is small (see the first figure in the zoomed graph). When the vehicle is equipped with YK controller, the variation of the factor γ allows the adaptation of the vehicle behavior. When the leader speed is lower or equal to $5m/s$ the factor $\gamma = 0.2$, the ego vehicle tracks the leader fast and attenuates the noise as shown in the top graph. When the leader speed is between $5m/s$ and $10m/s$ the $\gamma = 0.6$ making the noise amplitude smaller with a fast response (see first figure in the bottom graph). For high speed ($15m/s$ and $18m/s$) γ is equal to 0.8 and 1 respectively. In the case of $\gamma = 0.8$, one can see in the second figure of the bottom graph that the YK controller is faster than the robust one and it attenuates the noise. Finally, when the vehicle is controlled with the classical H_∞ controller, it shows the same behavior whether the noise is important or not and sacrifices performance over robustness.

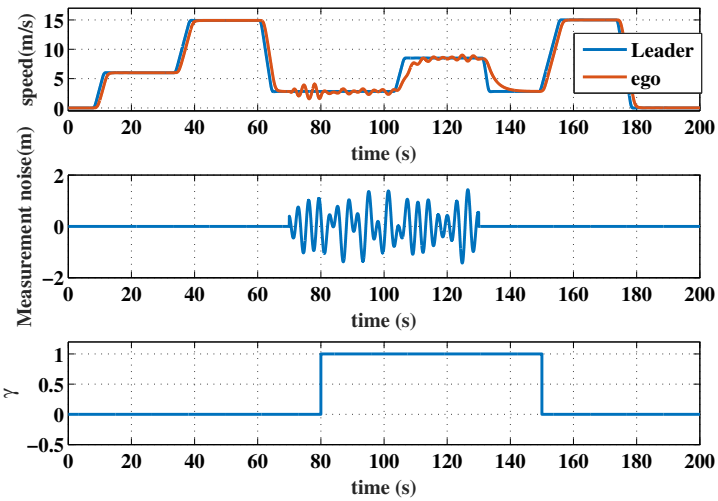

Figure 6.14: Simulation results of the YK multi-controller structure when noise is present in the perception system installed in ego-vehicle. This perception system measures the inter-vehicle distance needed in car-following applications.

Figure 6.14 depicts the performance of the multi-controller structure when the noise appears in the output of the perception system for a period of time. The top graph plots velocity responses of the two vehicles. The middle graph plots a noise signal within the vehicle bandwidth added to the relative distance $d_{r,j}$ for a period of time . The bottom graph represents how γ is changed over time. For notation, leader vehicle (solid blue line) is the first one in the string following a speed profile between $0m/s$ and $15m/s$ with different acceleration/braking phases; ego vehicle (solid red line) is the

second and last vehicle in the string equipped with the proposed multi-controller. The noise signal is added around second 75, being detected by the system a few second later by evolving γ value to the unity. Interpolating from performant to robust controller in a stable and comfortable manner. This makes the amplitude of the noise smaller, even if the controller is slower. Once the noise disappeared in second 130, the performant mode is recovered by making $\gamma = 0$ again.

From this simulation result, one can see that the YK based controller response goes either as performant or robust controller and between both, being able to be fast enough when needed and to be robust when there is an important noise in the perception system by modifying the scalar γ, always guaranteeing system stability.

6.7 Experimental results

This section shows experimental results with the proposed controller implemented in a Renault ZOE following a preceding vehicle. The experimental vehicle is completely robotized, enabling the control of throttle and brake pedals for the longitudinal motion as described in section 5.1. The control algorithm is embedded in a MicroAutoboxII (MABx) using MatLab Simulink turning at 100Hz. The experimental tests are conducted in Satory test track.

A leader vehicle is computer-generated, following a predefined speed profile, a noise signal is injected in the inter-vehicle distance. The ego vehicle is the robotized ZOE equipped with the proposed ACC system following the emulated leader.

For notation in the following figures, the emulated leader vehicle (solid blue line) is the first vehicle in the string following a speed profile that goes between $5m/s$ and $15m/s$; the ZOE prototype noted ego vehicle (solid red line) is second and last vehicle in the string equipped either with robust controller (Fig. 6.15); performant controller (Fig. 6.16) or YK multi-controller structure (Fig. 6.17). A noise signal (green solid line) of $1m$ of amplitude and a frequency within the vehicle bandwidth is injected at the relative distance computed by the emulated system from second 60 to second 105. One can see how noise is detected in the YK multi-objectives controller structure modifying γ from 0 to 1 (solid magenta line in Fig. 6.17), and thus attenuating the noise as in the robust solution. Once the noise disappears, the proposed solution is able to recover the fast tracking capability characteristic of the performant solution.

The ACC system was later tested using an artificial intelligence based perception system, the ego vehicle was equipped with a multi-sensor system for obstacle detection and leader vehicle tracking [218]. The inter vehicle distance is computed using GPS, cameras and Lidar information. The fusion

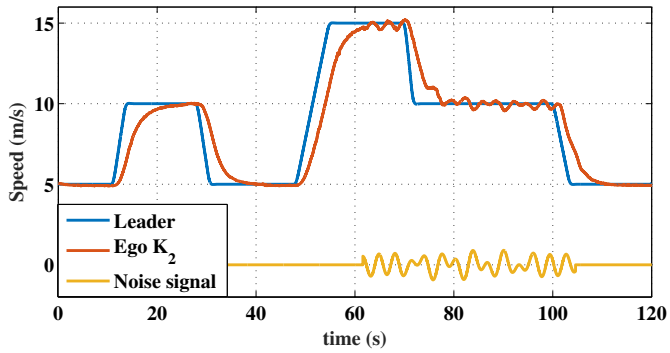

Figure 6.15: Experimental results of robust controller when noise is injected for a period of time in the inter-vehicle distance to the emulated leader. String of two vehicles.

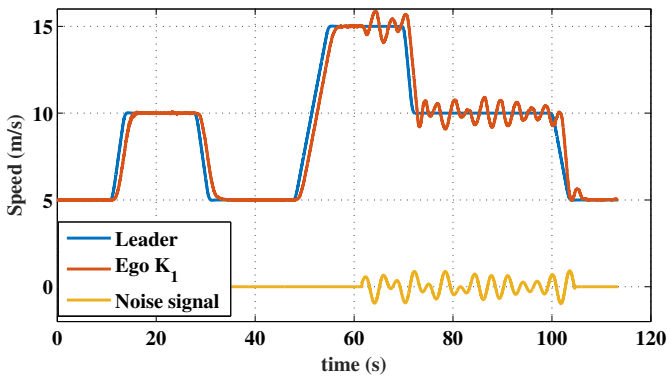

Figure 6.16: Experimental results of performant controller when noise is injected for a period of time in the inter-vehicle distance to the emulated leader. String of two vehicles.

system exhibits higher noise in the signal when inter-distances increase [217, 218].

For notation in the figures below, the leader vehicle is driven manually with a variable speed between $6m/s$ and $15m/s$, the perception system embedded on the ego vehicle perceives the leader speed (blue solid line). The ego vehicle speed (red solid line) is either controlled by the performant controller K_1 (Fig. 6.18); the robust controller K_2 (Fig. 6.19); the YK-based multi controller (Fig. 6.20) or the H_∞ controller (Fig. 6.21).

When the ego vehicle is equipped with the performant controller K_1, it tracks all the speed changes even the small oscillations (see Fig. 6.18 from second 55 to 70) which causes an unnatural behavior. Figure 6.19 shows

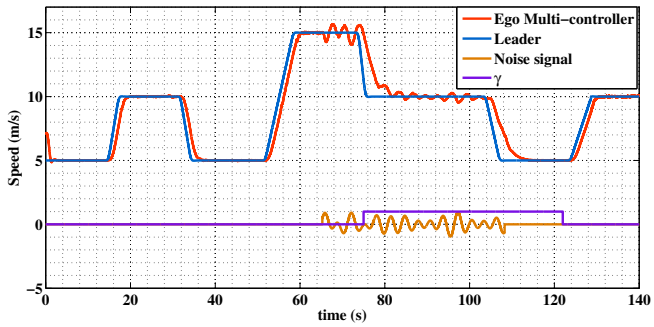

Figure 6.17: Experimental results of the YK multi-controller structure when noise is injected for a period of time in the inter-vehicle distance to the emulated leader. String of two vehicles.

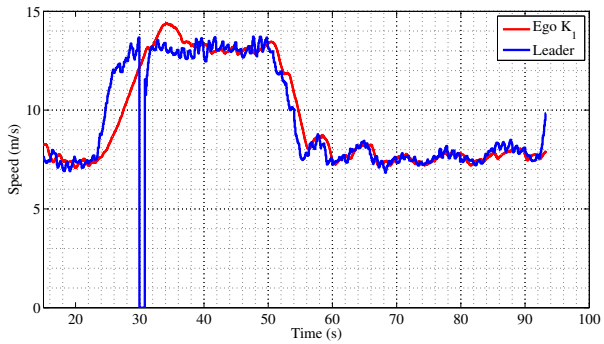

Figure 6.18: Experimental results of performant controller when the inter-vehicle distance is measured by the perception system. String of two vehicles.

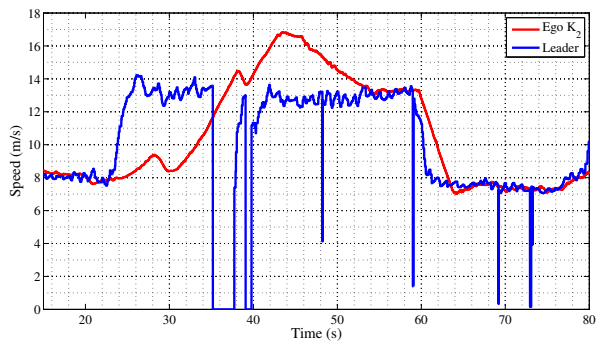

Figure 6.19: Experimental results of robust controller when noise is present in the inter-vehicle distance measured by the perception system. String of two vehicles.

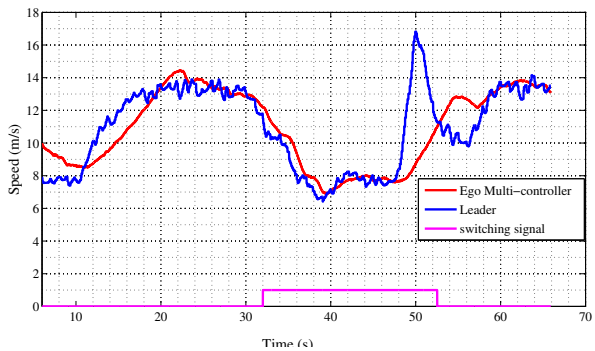

Figure 6.20: Experimental results of YK based controller when noise is present in the inter-vehicle distance measured by the perception system. String of two vehicles.

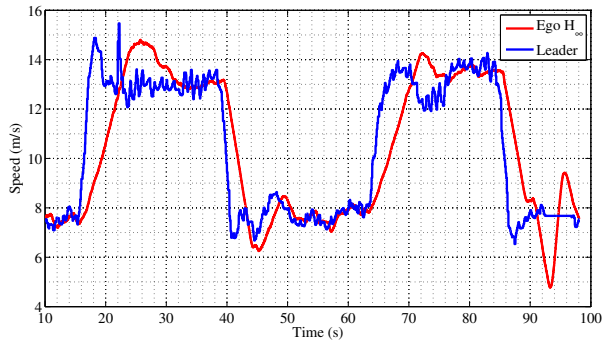

Figure 6.21: Experimental results of H_∞ controller when noise is present in the inter-vehicle distance measured by the perception system. String of two vehicles.

the results of the robust controller when the perceived speed is noisy (the discontinuities are caused by the lost of the localization signal), the vehicle response is smooth and the noise is attenuated but the tracking is slow (see the delay from second 22 to second 40), this makes the inter-distance bigger which entails even more noise in the perception system. Figure 6.20 shows how YK-based controller could be fast tracker when the noise level is low (from second 10 to second 32), and switches by moving γ to 1 (magenta solid line) to attenuate the noise when needed, being slow enough to avoid the pick in second 30. The behavior of the ego vehicle under the H_∞ controller is shown in figure 6.21, even if the perception signal doesn't present important noise in this test and no discontinuities, the controller is slow and tracks the speed oscillations with a delay.

These experimental results show that the proposed YK based ACC controller can ensure both fast tracking and noise attenuation in a control struc-

ture without trade-off. It also validates the proposed solution as a successful stable controller switching between two different controllers according to an external signal coming from the perception system.

6.8 Conclusion

This chapter presents a YK based ACC system for automated vehicles. The proposed control structure extends the ACC system capabilities by providing the best possible response in all circumstances, meaning that the controller is able to change in real time according to the noise level in the perception system, while maintaining longitudinal control stability, string stability and measurement noise rejection.

The proposed controller interpolates between two ACC controllers: 1) a proportional controller with maximum bandwidth allowing string stability, presenting high tracking capabilities; and 2) a derivative controller able to attenuate 70% of the noise signal within the vehicle bandwidth. The controllers have conflicting requirements. The interpolation signal γ decides what a fraction of each controller to activate according to the noise level in the perception system. Thanks to YK parametrization, the stability of the vehicle string is guaranteed for any arbitrary signal γ corresponding to the operating conditions (i.e. perception status or sensor failure).

The proposed controller has been compared in simulation with H_∞ based ACC controller, showing the adaptability and the evolution of the system bandwidth according to perception system. Then, it has been implemented on a robotized ZOE vehicle, exhibiting significant improvements comparing to the H_∞ controller whereas guaranteeing system stability.

The main advantage of the proposed approach is its simplicity and ability to tune the ACC controllers separately using any control technique. Also, the possibility to adapt the controller in real time to the operating conditions without losing the stability of the system, taking into account control independent parameters

Further works can be oriented to cover other car following algorithm as CACC controllers, in different topologies and dealing with multiple information sources.

Chapitre 7

Discussion

Below is a French summary of chapter 7.

Ce chapitre présente des remarques finales sur l'état des lieux présenté revue d'art, quelques lignes directrices concernant la mise en œuvre du paramétrage YK et les contrôleurs proposés avec leurs résultats de validation. ainsi que les travaux futurs pouvant découler de objectifs atteints tout au long de cette thèse.

L'un des avantages perçus du déploiement des voitures autonomes est qu'elles peuvent être utilisées comme taxi ou bus, remplaçant ou complétant le service de transport public traditionnel, offrant une combinaison de services d'auto-partage et de taxi conventionnels. Cependant, dans ce modèle de transport, la garantie de sécurité, de stabilité de contrôle du véhicule et de confort sont des exigences essentielles. Dans cette thèse, des contrôleurs multi-objectifs ont été proposés pour améliorer les performances des mouvements latéraux et longitudinaux en utilisant la paramétrisation YK.

Dans les contrôleurs latéraux et longitudinaux proposés, la commutation entre les contrôleurs était progressive et stable. Le comportement du véhicule sous les contrôleurs YK a prouvé que la reconfiguration du contrôleur de manière stable peut être une solution pour maximiser les performances de contrôle réalisables sans compromettre la robustesse et le confort à l'intérieur du véhicule. Un autre avantage est qu'il peut être facilement conçu et mis en œuvre, car il ne nécessite que le réglage des contrôleurs initial et final.

De plus, d'autres contrôleurs peuvent être ajoutés à la structure de contrôle pour gérer d'autres situations de conduite sans affecter la stabilité de la boucle fermée.

Chapter 7

Discussion

This chapter reports concluding remarks of the presented state-of-the- art review, some guidelines regarding the implementation of YK parametrization and the proposed controllers with their validation results. as well as future work that can be derived from the accomplished goals along this thesis.

7.1 Conclusion

One of the perceived advantage of deploying autonomous cars is that it can be used as taxi or bus, replacing or complementing the traditional public transport service, providing a combination of conventional car-sharing and taxi services. However, in this transport model, the guarantee of safety, vehicle control stability and comfort are essential requirements that may encourage soon deployment. In this thesis, multi-objective controllers have been proposed to enhance the performance of both lateral and longitudinal motions using YK parametrization.

Chapter 2 reviewed the state-of-the-art of the use of YK and dual YK parametrizations in different control fields. Different experimental control applications developed during the last 20 years are reported showing the efficiency of YK framework in controlling complex systems. A timeline is provided, classifying the main applications accordingly the research institution where they took place, and to the control field including: controller reconfiguration, identification, Plug&Play control, disturbance rejection, adaptive control, and fault tolerant control.

Chapter 3 and 4 presented the mathematical basis on building a YK based multi controller, as well as the closed loop stability proof using notions of system with impulse effects. The main advantage of YK based multi controller is the stability guaranty under arbitrary switching signal. A comparative study of the eight structures used in the literature concluded that one can improve the transient behavior by: 1) placing the switching signal γ

after the YK parameter Q for all the structures except for structure 4, where γ should be placed before Q to avoid overshoots; 2) when using structure 4, it is recommended to compute the YK parameter Q in order to switch from the slow to the fast controller since it takes the same time to converge that the time of the final controller. Unlike the other structures that take the same time to converge regardless to the initial and final controllers dynamics; and 3) To ensure the convergence of all structures, the maximum switching frequency should be below the fast closed loop bandwidth.

YK based lateral controller have been proposed as an efficient solution solving the trade-off between precision in trajectory tracking and comfort when the driving situation changes in lateral motion. This proposed YK control performed automatic controller reconfiguration by switching gradually between $T\&C$ controllers: one for tracking the desired trajectory, and one for lane changing. The control reconfiguration is based on a decision system, measuring the lateral error and activating one of the two controllers or a part of both. Experimental results have proven that the proposed control structure enhances vehicle performances and lateral errors are significantly reduced, while keeping passengers comfort even when performing a lane change of 5m.

The trade-off between robustness and performance when noise measurement appears in ACC systems is also solved using YK based controller. The proposed ACC controller interpolated two controllers: one with high tracking capabilities and another one rejecting measurement noise. The interpolation parameter γ able to activate the adequate controller increasing either the tracking capabilities or noise reduction. The Variation of γ varies with respect to the perception system performance considered an an indicator about the noise level in the perceived signals. The multi-controller structure is based on YK parametrization, keeping the closed loop stability during controllers interpolation. The experimental tests showed that the proposed YK based ACC controller can ensure both fast tracking and noise attenuation in a control structure without trade-off. It validates the proposed solution as a successful stable controller switching between two different controllers according to an external signal coming from the perception system.

In both lateral and longitudinal controllers, the switching between controllers was gradual and stable. The behavior of the vehicle under YK controllers proved that controller reconfiguration in stable way can be a solution to maximize the achievable control performance without compromising the robustness and the comfort inside the vehicle. Other advantage is that it can be easily designed and implemented, since it requires only the tuning of the initial and final controllers.

Furthermore, other controllers can be added to the control structure handling other driving situations without impacting the stability of the closed loop.

7.2 Future works

As a continuation of the developed work, several future works are encouraged to be pursued:

- Extend the use of YK parameter Q to reconfigure non-linear controllers. By including non-linear control techniques (i.e. sliding mode control, back-stepping)
- Integration of artificial intelligence techniques in tuning the YK parameter Q, while doing controller reconfiguration according to the desired response. For example, one can use the link between the YK parameter Q and the temporal response characteristics (i.e. rise time, overshot).
- Enhance the transient behavior while switching between controllers by optimizing the computation of coprime factors. Taking into account the response dwell-time.
- Use LPV YK control structure to design full range speed lateral controller that can ensure the same performance as the proposed one at all speeds.
- Include more driving situations to enlarge the proposed lateral controller capabilities, for example add a robust controller that will be activated where adherence limits affect the vehicle dynamics.
- Extend the ACC capabilities to ensure flexible longitudinal behavior by including variable time gap, using LPV YK controller.

Bibliography

[1] D. Rojas-Rueda, M. J. Nieuwenhuijsen, H. Khreis, and H. Frumkin, "Autonomous vehicles and public health," *Annual review of public health*, vol. 41, pp. 329–345, 2020.

[2] S. E. Shladover, "Connected and automated vehicle systems: Introduction and overview," *Journal of Intelligent Transportation Systems*, vol. 22, no. 3, pp. 190–200, 2018.

[3] R. Coppola and M. Morisio, "Connected car: technologies, issues, future trends," *ACM Computing Surveys (CSUR)*, vol. 49, no. 3, pp. 1–36, 2016.

[4] D. Youla, J. d. Bongiorno, and H. Jabr, "Modern wiener–hopf design of optimal controllers part i: The single-input-output case," *IEEE Transactions on Automatic Control*, vol. 21, no. 1, pp. 3–13, 1976.

[5] D. Youla, H. Jabr, and J. Bongiorno, "Modern wiener-hopf design of optimal controllers–part ii: The multivariable case," *IEEE Transactions on Automatic Control*, vol. 21, no. 3, pp. 319–338, 1976.

[6] V. Kučera, "Stability of discrete linear feedback systems," *IFAC Proceedings Volumes*, vol. 8, no. 1, pp. 573–578, 1975.

[7] T.-T. Tay, I. Mareels, and J. B. Moore, *High performance control*. Springer Science & Business Media, 1997.

[8] H. Niemann, "Dual youla parameterisation," *IEE Proceedings-Control Theory and Applications*, vol. 150, no. 5, pp. 493–497, 2003.

[9] J. Bendtsen and K. Trangbaek, "Multiple model adaptive control using dual youla-kucera factorisation," *IFAC Proceedings Volumes*, vol. 45, no. 13, pp. 63–68, 2012.

[10] G. C. Newton, L. A. Gould, and J. F. Kaiser, "Analytical design of linear feedback controls," 1957.

[11] C. Desoer, R.-W. Liu, J. Murray, and R. Saeks, "Feedback system design: The fractional representation approach to analysis and synthesis," *IEEE Transactions on Automatic Control*, vol. 25, no. 3, pp. 399–412, 1980.

[12] M. Vidyasagar, "Control systems synthesis: A factorization approach, volume 8 of north holland system and control series," 1985.

[13] J. Pommaret and A. Quadrat, "Generalized bezout identity," *Applicable Algebra in Engineering, Communication and Computing*, vol. 9, no. 2, pp. 91–116, 1998.

[14] D. Liberzon, *Switching in systems and control*. Springer Science & Business Media, 2003.

[15] A. Packard, "Gain scheduling via linear fractional transformations," *Systems & control letters*, vol. 22, no. 2, pp. 79–92, 1994.

[16] W. J. Rugh and J. S. Shamma, "Research on gain scheduling," *Automatica*, vol. 36, no. 10, pp. 1401–1425, 2000.

[17] L. Zaccarian and A. R. Teel, "The l2 (l2) bumpless transfer problem for linear plants: Its definition and solution," *Automatica*, vol. 41, no. 7, pp. 1273–1280, 2005.

[18] J. Stoustrup and H. Niemann, "Starting up unstable multivariable controllers safely," in *Proceedings of the 36th IEEE Conference on Decision and Control*, vol. 2, pp. 1437–1438, IEEE, 1997.

[19] J. P. Hespanha and A. S. Morse, "Switching between stabilizing controllers," *Automatica*, vol. 38, no. 11, pp. 1905–1917, 2002.

[20] J. Moore, L. Xia, and K. Glover, "On improving control-loop robustness of model-matching controllers," *Systems & control letters*, vol. 7, no. 2, pp. 83–87, 1986.

[21] B. P. Rasmussen and Y. J. Chang, "Stable controller interpolation and controller switching for lpv systems," *Journal of dynamic systems, measurement, and control*, vol. 132, no. 1, p. 011007, 2010.

[22] W. Xie and T. Eisaka, "Design of lpv control systems based on youla parameterisation," *IEE Proceedings-Control Theory and Applications*, vol. 151, no. 4, pp. 465–472, 2004.

[23] J. Hespanha and A. Morse, "Towards the high performance control of uncertain processes via supervision," in *Proceedings of the 30th Conference on Information Sciences and Systems*, vol. 405, p. 410, Citeseer, 1996.

[24] O. Cifdaloz, A. A. Rodriguez, and J. M. Anderies, "Control of distributed parameter systems subject to convex constraints: Applications to irrigation systems and hypersonic vehicles," in *Decision and Control, 2008. CDC 2008. 47th IEEE Conference on*, pp. 865–870, IEEE, 2008.

[25] K. Trangbaek, J. Stoustrup, and J. Bendtsen, "Stable controller reconfiguration through terminal connections," *IFAC Proceedings Volumes*, vol. 41, no. 2, pp. 331–335, 2008.

[26] K. Trangbaek and J. Bendtsen, "Stable controller reconfiguration through terminal connections. a practical example," in *Control and Automation, 2009. ICCA 2009. IEEE International Conference on*, pp. 2037–2042, IEEE, 2009.

[27] S. V. Johansen, C. S. Kallesøe, J. D. Bendtsen, and P. Andersen, "Stepwise commissioning of a steam boiler with stability guarantees," in *Control Conference (ECC), 2016 European*, pp. 49–54, IEEE, 2016.

[28] F. Navas, V. Milanés, and F. Nashashibi, "Using plug&play control for stable acc-cacc system transitions," in *Intelligent Vehicles Symposium (IV), 2016 IEEE*, pp. 704–709, IEEE, 2016.

[29] F. Navas and V. Milanés, "Mixing v2v-and non-v2v-equipped vehicles in car following," *Transportation research part C: emerging technologies*, vol. 108, pp. 167–181, 2019.

[30] I. Mahtout, F. Navas, D. Gonzalez, V. Milanés, and F. Nashashibi, "Youla-kucera based lateral controller for autonomous vehicle," in *ITSC 2018-21st IEEE International Conference on Intelligent Transportation Systems*, 2018.

[31] F. Blanchini, D. Casagrande, S. Miani, and U. Viaro, "Stable lpv realization of parametric transfer functions and its application to gain-scheduling control design," *IEEE Transactions on Automatic Control*, vol. 55, no. 10, pp. 2271–2281, 2010.

[32] F. D. Bianchi and R. S. S. Peña, "Interpolation for gain-scheduled control with guarantees," *Automatica*, vol. 47, no. 1, pp. 239–243, 2011.

[33] J. C. Carmona and V. M. Alvarado, "Active noise control of a duct using robust control theory," *IEEE Transactions on control systems technology*, vol. 8, no. 6, pp. 930–938, 2000.

[34] J. Langer and I. D. Landau, "Combined pole placement/sensitivity function shaping method using convex optimization criteria," *Automatica*, vol. 35, no. 6, pp. 1111–1120, 1999.

[35] S. Liebich, C. Anemüller, P. Vary, P. Jax, D. Rüschen, and S. Leonhardt, "Active noise cancellation in headphones by digital robust feedback control," in *2016 24th European Signal Processing Conference (EUSIPCO)*, pp. 1843–1847, IEEE, 2016.

[36] T. Yucelen, A. S. Sadahalli, and F. Pourboghrat, "Active noise control in a duct using output feedback robust control techniques," in *Proceedings of the 2010 American Control Conference*, pp. 3506–3511, IEEE, 2010.

[37] B. Francis and A. Tannenbaum, "Feedback control theory," *McMillan, New York*, vol. 1992, 1992.

[38] I. D. Landau, "On the use of youla-kucera parametrization in adaptive active noise and vibration control-a review," *International Journal of Control*, no. just-accepted, pp. 1–25, 2018.

[39] J. J. Martinez and M. Alma, "Improving playability of blu-ray disc drives by using adaptive suppression of repetitive disturbances," *Automatica*, vol. 48, no. 4, pp. 638–644, 2012.

[40] M. Doumiati, J. Martinez, O. Sename, L. Dugard, and D. Lechner, "Road profile estimation using an adaptive youla–kučera parametric observer: Comparison to real profilers," *Control Engineering Practice*, vol. 61, pp. 270–278, 2017.

[41] T.-B. Airimiţoaie and I. D. Landau, "Indirect adaptive attenuation of multiple narrow-band disturbances applied to active vibration control," *IEEE Transactions on control systems technology*, vol. 22, no. 2, pp. 761–769, 2013.

[42] I. D. Landau, A. C. Silva, T.-B. Airimitoaie, G. Buche, and M. Noe, "Benchmark on adaptive regulation—rejection of unknown/time-varying multiple narrow band disturbances," *European Journal of control*, vol. 19, no. 4, pp. 237–252, 2013.

[43] I. D. Landau, T.-B. Airimitoaie, R. Meléndez, and L. Dugard, "Why one should use youla-kucera parametrization in adaptive feedforward noise attenuation?," 2019.

[44] S. J. Elliott and P. A. Nelson, "Active noise control," *IEEE signal processing magazine*, vol. 10, no. 4, pp. 12–35, 1993.

[45] J. Zeng and R. De Callafon, "Recursive filter estimation for feedforward noise cancellation with acoustic coupling," *Journal of sound and vibration*, vol. 291, no. 3-5, pp. 1061–1079, 2006.

[46] X. Chen, T. Jiang, and M. Tomizuka, "Pseudo youla–kucera parameterization with control of the waterbed effect for local loop shaping," *Automatica*, vol. 62, pp. 177–183, 2015.

[47] X. Chen and M. Tomizuka, "New repetitive control with improved steady-state performance and accelerated transient," *IEEE Transactions on Control Systems Technology*, vol. 22, no. 2, pp. 664–675, 2013.

[48] Z. Wu, M. Zhang, Z. Chen, and P. Wang, "Youla parameterized adaptive vibration suppression with adaptive notch filter for unknown multiple narrow band disturbances," *Journal of Vibration and Control*, p. 1077546318794539, 2018.

[49] M. Tomizuka, "Dealing with periodic disturbances in controls of mechanical systems," *Annual Reviews in Control*, vol. 32, no. 2, pp. 193–199, 2008.

[50] I. D. Landau, A. Constantinescu, and D. Rey, "Adaptive narrow band disturbance rejection applied to an active suspension—an internal model principle approach," *Automatica*, vol. 41, no. 4, pp. 563–574, 2005.

[51] S. Valentinotti, B. Srinivasan, U. Holmberg, D. Bonvin, C. Cannizzaro, M. Rhiel, and U. Von Stockar, "Optimal operation of fed-batch fermentations via adaptive control of overflow metabolite," *Control engineering practice*, vol. 11, no. 6, pp. 665–674, 2003.

[52] A. Luca, P. Rodriguez-Ayerbe, and D. Dumur, "Control of disturbed lpv systems in a lmi setting," *IFAC Proceedings Volumes*, vol. 44, no. 1, pp. 4149–4154, 2011.

[53] F. B. Amara, P. T. Kabamba, and A. G. Ulsoy, "Adaptive sinusoidal disturbance rejection in linear discrete-time systems—part ii: Experiments," *Journal of dynamic systems, measurement, and control*, vol. 121, no. 4, pp. 655–659, 1999.

[54] T. Tang, B. Qi, and T. Yang, "Youla–kucera parameterization-based optimally closed-loop control for tip–tilt compensation," *IEEE Sensors Journal*, vol. 18, no. 15, pp. 6154–6160, 2018.

[55] U. Forssell and L. Ljung, "Closed-loop identification revisited," *Automatica*, vol. 35, no. 7, pp. 1215–1241, 1999.

[56] I. D. Landau and A. Karimi, "Recursive algorithms for identification in closed loop: A unified approach and evaluation," *Automatica*, vol. 33, no. 8, pp. 1499–1523, 1997.

[57] S. Karaboyas and N. Kalouptsidis, "Efficient adaptive algorithms for arx identification," *IEEE Transactions on signal processing*, vol. 39, no. 3, pp. 571–582, 1991.

[58] J. W. van Wingerden, "The asymptotic variance of the pbsidopt algorithm," *IFAC Proceedings*, vol. 45, no. 16, pp. 1167–1172, 2012.

[59] H. Hjalmarsson, M. Gevers, and F. D. Bruyne, "For model-based control design, closed-loop identification gives better performance," *Automatica*, vol. 32, no. 12, pp. 1659–1673, 1996.

[60] M. Sznaier and M. C. Mazzaro, "An lmi approach to control-oriented identification and model (in) validation of lpv systems," *IEEE Transactions on Automatic Control*, vol. 48, no. 9, pp. 1619–1624, 2003.

[61] J. V. Salcedo and M. Martinez, "Lpv identification of a turbocharged diesel engine," *Applied Numerical Mathematics*, vol. 58, no. 10, pp. 1553–1571, 2008.

[62] P. L. D. Santos, J. A. Ramos, and J. M. de Carvalho, "Identification of linear parameter varying systems using an iterative deterministic-stochastic subspace approach," in *In European Control Conference European*, pp. 4867–4873, 2007.

[63] F. Hansen, G. Franklin, and R. Kosut, "Closed-loop identification via the fractional representation: Experiment design.," in *American Control Conference*, pp. 1422–1427, 1989.

[64] R. Schrama, "An open-loop solution to the approximate closed-loop identification problem," *IFAC Proceedings Volumes*, vol. 24, no. 3, pp. 761–766, 1991.

[65] M. Gevers, L. Ljung, and P. Van den Hof, "Asymptotic variance expressions for closed-loop identification," *Automatica*, vol. 37, no. 5, pp. 781–786, 2001.

[66] S. G. Douma, P. M. Van den Hof, and O. H. Bosgra, "Controller tuning freedom under plant identification uncertainty: double youla beats gap in robust stability," *Automatica*, vol. 39, no. 2, pp. 325–333, 2003.

[67] F. De Bruyne, B. Anderson, and N. Linard, "The hansen scheme revisited," in *Decision and Control, 1998. Proceedings of the 37th IEEE Conference on*, vol. 1, pp. 706–711, IEEE, 1998.

[68] A. Sekunda, H. Niemann, N. K. Poulsen, and I. Santos, "Closed loop identification using a modified hansen scheme," in *Journal of Physics: Conference Series*, vol. 659, p. 012009, IOP Publishing, 2015.

[69] J. Bendtsen and K. Trangbaek, "Closed-loop identification for control of linear parameter varying systems," *Asian Journal of Control*, vol. 16, no. 1, pp. 40–49, 2014.

[70] K. Trangbaek and J. Bendtsen, "Lpv identification of a heat distribution system," in *IEEE International Conference In Control Applications*, pp. 2178–2183, 2010.

[71] J. Bendtsen, K. Trangbaek, and J. Stoustrup, "Plug-and-play control—modifying control systems online," *IEEE Transactions on Control Systems Technology*, vol. 21, no. 1, pp. 79–93, 2011.

[72] N. Linard and B. D. Anderson, "Identification of nonlinear plants under linear control using youla-kucera parametrizations," in *Decision and Control, 1996., Proceedings of the 35th IEEE Conference on*, vol. 1, pp. 1094–1098, IEEE, 1996.

[73] N. Linard and B. Anderson, "Identification of nonlinear plants using left coprime fractional based representations," in *Control Conference (ECC), 1997 European*, pp. 772–777, IEEE, 1997.

[74] A. K. Sekunda, H. H. Niemann, N. K. Poulsen, and I. F. Santos, "Closed loop identification of a piezoelectrically controlled radial gas bearing: Theory and experiment," *Proceedings of the Institution of Mechanical Engineers, Part I: Journal of Systems and Control Engineering*, vol. 232, no. 7, pp. 926–936, 2018.

[75] K. Trangbaek, "Controller reconfiguration through terminal connections based on closed-loop system identification1," *IFAC Proceedings Volumes*, vol. 42, no. 6, pp. 25–30, 2009.

[76] F. Navas, V. Milanés, and F. Nashashibi, "Youla-kucera based online closed-loop identification for longitudinal vehicle dynamics," in *2017 21st International Conference on System Theory, Control and Computing (ICSTCC)*, pp. 88–93, IEEE, 2017.

[77] J. Moore and T. Tay, "Loop reconvery via hinf/h2 sensitivity recovery," *International Journal Control*, vol. 49, no. 4, pp. 1249–1271, 1989.

[78] Z. Wang, I. Mareels, and J. Moore, "Adaptive disturbance rejection," in *Decision and Control, 1991., Proceedings of the 30th IEEE Conference on*, pp. 2836–2841, IEEE, 1991.

[79] V. Yadav, P. G. Voulgaris, and M. V. Salapaka, "Stabilization of nested systems with uncertain subsystem communication channels," in *42nd IEEE International Conference on Decision and Control (IEEE Cat. No. 03CH37475)*, vol. 3, pp. 2853–2858, IEEE, 2003.

[80] T. T. Tay *et al.*, "Enhancing robust controllers with adaptive techniques," 1989.

[81] Z. Wang, *Performance Issues in Adaptive Control.* PhD thesis, University of Newcastle, 1991.

[82] Y. Teo and T. Tay, "Design of al/sup 1/-optimal regulator: the limits of performance approach," *IEEE transactions on automatic control*, vol. 40, no. 12, pp. 2114–2119, 1995.

[83] T. Tay and J. B. Moore, "Enhancement of fixed controllers via adaptive-q disturbance estimate feedback," *Automatica*, vol. 27, no. 1, pp. 39–53, 1991.

[84] J. Bendtsen, K. Trangbaek, and J. Stoustrup, "Plug-and-play control modifying control systems online," *IEEE Transactions on Control Systems Technology*, vol. 21, no. 1, pp. 79–93, 2013.

[85] Y. Zhang and J. Jiang, "Bibliographical review on reconfigurable fault-tolerant control systems," *Annual reviews in control*, vol. 32, no. 2, pp. 229–252, 2008.

[86] H. Niemann and J. Stoustrup, "Reliable control using the primary and dual youla parameterizations," in *Decision and Control, 2002, Proceedings of the 41st IEEE Conference on*, vol. 4, pp. 4353–4358, IEEE, 2002.

[87] K. Zhou and Z. Ren, "A new controller architecture for high performance, robust, and fault-tolerant control," *IEEE Transactions on automatic control*, vol. 46, no. 10, pp. 1613–1618, 2001.

[88] S. X. Ding, G. Yang, P. Zhang, E. L. Ding, T. Jeinsch, N. Weinhold, and M. Schultalbers, "Feedback control structures, embedded residual signals, and feedback control schemes with an integrated residual access," *IEEE Transactions on Control Systems Technology*, vol. 18, no. 2, pp. 352–367, 2009.

[89] H. Niemann and J. Stoustrup, "Passive fault tolerant control of a double inverted pendulum a case study," *Control engineering practice*, vol. 13, no. 8, pp. 1047–1059, 2005.

[90] H. Niemann and J. Stoustrup, "An architecture for fault tolerant controllers," *International Journal of Control*, vol. 78, no. 14, pp. 1091–1110, 2005.

[91] H. Niemann, "A setup for active fault diagnosis," *IEEE Transactions on Automatic Control*, vol. 51, no. 9, pp. 1572–1578, 2006.

[92] H. Niemann, "A model-based approach to fault-tolerant control," *International Journal of Applied Mathematics and Computer Science*, vol. 22, no. 1, pp. 67–86, 2012.

[93] J. Stoustrup, "An observer parameterization approach to active fault diagnosis with applications to a drag racing vehicle," *IFAC Proceedings Volumes*, vol. 42, no. 8, pp. 591–596, 2009.

[94] C. Hua, S. X. Ding, and Y. A. Shardt, "A new method for fault tolerant control through q-learning," *IFAC-PapersOnLine*, vol. 51, no. 24, pp. 38–45, 2018.

[95] L. Li, H. Luo, S. X. Ding, Y. Yang, and K. Peng, "Performance-based fault detection and fault-tolerant control for automatic control systems," *Automatica*, vol. 99, pp. 308–316, 2019.

[96] J. Stoustrup, "Plug & play control: Control technology towards new challenges," *European Journal of Control*, vol. 15, no. 3-4, pp. 311–330, 2009.

[97] A. G. Michelsen and K. Trangbaek, "Local controller synthesis for plug and play processes by decomposition," in *2009 IEEE International Conference on Control and Automation*, pp. 2223–2228, IEEE, 2009.

[98] B. Anderson, T. Brinsmead, D. Liberzon, and A. Stephen Morse, "Multiple model adaptive control with safe switching," *International journal of adaptive control and signal processing*, vol. 15, no. 5, pp. 445–470, 2001.

[99] K. Trangbaek, "Safe lpv controller switching," in *Decision and Control and European Control Conference (CDC-ECC), 2011 50th IEEE Conference on*, pp. 3428–3433, IEEE, 2011.

[100] H. Niemann, J. Stoustrup, and R. B. Abrahamsen, "Switching between multivariable controllers," *Optimal control applications and methods*, vol. 25, no. 2, pp. 51–66, 2004.

[101] H. Niemann and N. K. Poulsen, "Controller architectures for switching," in *American Control Conference, 2009. ACC'09.*, pp. 1098–1103, IEEE, 2009.

[102] S. R. Friedrich and M. Buss, "Parameterizing robust manipulator controllers under approximate inverse dynamics: A double-youla approach," *International Journal of Robust and Nonlinear Control*, vol. 29, no. 15, pp. 5137–5163, 2019.

[103] W. Xie, "Design of switched linear control systems based on youla parameterization with average dwell time," *International Journal of Systems Science*, vol. 50, no. 1, pp. 203–215, 2019.

[104] F. Navas, V. Milanés, C. Flores, and F. Nashashibi, "Multi-model adaptive control for cacc applications," *IEEE Transactions on Intelligent Transportation Systems*, vol. 99, pp. 1 – 11, 2020.

[105] H. Niemann and N. K. Poulsen, "Fault tolerant control for uncertain systems with parametric faults," *IFAC Proceedings Volumes*, vol. 39, no. 13, pp. 480–485, 2006.

[106] H. Han, Y. Yang, L. Li, and S. X. Ding, "Control performance based fault detection for nonlinear systems," in *Decision and Control (CDC), 2017 IEEE 56th Annual Conference on*, pp. 6358–6363, IEEE, 2017.

[107] H. Han, Y. Yang, L. Li, and S. X. Ding, "Performance-based fault detection and fault-tolerant control for nonlinear systems with ts fuzzy implementation," *IEEE transactions on cybernetics*, 2019.

[108] W. Xie, "H∞ performance realisation and switching controller design for linear time-invariant plant," *IET Control Theory & Applications*, vol. 10, no. 4, pp. 424–430, 2016.

[109] S. R. Friedrich and M. Buss, "A simple architecture for arbitrary interpolation of state feedback," *IEEE Control Systems Letters*, vol. 3, no. 2, pp. 469–474, 2019.

[110] I. D. Landau and R. Meléndez, "Active noise control: Adaptive vs. robust approach," in *Control and Automation (MED), 2017 25th Mediterranean Conference on*, pp. 799–804, IEEE, 2017.

[111] C. E. Kinney and R. A. de Callafon, "Robust estimation for automatic controller tuning with application to active noise control," in *Model-Based Control:*, pp. 107–124, Springer, 2009.

[112] B. Vau and I. D. Landau, "Youla-kucera adaptive feedback disturbance rejection in the presence of plant uncertainties," 2019.

[113] R. A. Meléndez, I. D. Landau, L. Dugard, and G. Buche, "Data driven design of tonal noise feedback cancellers," *IFAC-PapersOnLine*, vol. 50, no. 1, pp. 916–921, 2017.

[114] S. Yin, H. Luo, and S. X. Ding, "Real-time implementation of fault-tolerant control systems with performance optimization," *IEEE Transactions on Industrial Electronics*, vol. 61, no. 5, pp. 2402–2411, 2013.

[115] H. Niemann, "Parameterisation of extended systems," *IEE Proceedings-Control Theory and Applications*, vol. 153, no. 2, pp. 221–227, 2006.

[116] F. Navas Matos, *Analyse de stabilité pour la reconfiguration de contrôleurs dans des véhicules autonomes.* PhD thesis, Paris Sciences et Lettres, 2018.

[117] M. Spong and M. Vidyasagar, "Robust linear compensator design for nonlinear robotic control," *IEEE Journal on Robotics and Automation*, vol. 3, no. 4, pp. 345–351, 1987.

[118] M. Morari and E. Zafiriou, *Robust process control.* Morari, 1989.

[119] O. Sename, P. Gaspar, and J. Bokor, *Robust control and linear parameter varying approaches: application to vehicle dynamics*, vol. 437. Springer, 2013.

[120] D. Zhang and B. Wei, "A review on model reference adaptive control of robotic manipulators," *Annual Reviews in Control*, vol. 43, pp. 188–198, 2017.

[121] I. Mareels and J. W. Polderman, "Adaptive systems," in *Adaptive Systems*, pp. 1–26, Springer, 1996.

[122] G. C. Goodwin and K. S. Sin, *Adaptive filtering prediction and control.* Courier Corporation, 2014.

[123] S. Fekri, M. Athans, and A. Pascoal, "Issues, progress and new results in robust adaptive control," *International Journal of Adaptive Control and Signal Processing*, vol. 20, no. 10, pp. 519–579, 2006.

[124] B. Hencey and A. G. Alleyne, "A robust controller interpolation design technique," *IEEE Transactions on Control Systems Technology*, vol. 18, no. 1, pp. 1–10, 2009.

[125] R. Zhang, A. G. Alleyne, and D. E. Carter, "Generalized multivariable gain scheduling with robust stability analysis," 2005.

[126] A. Pierre and G. Pascal, "A convex characterization of gain-scheduled h∞ controllers," *IEEE Trans Autom Control*, vol. 40, no. 5, pp. 853–864, 1995.

[127] H. Niemann and J. Stoustrup, "An architecture for implementation of multivariable controllers," in *American Control Conference, 1999. Proceedings of the 1999*, vol. 6, pp. 4029–4033, IEEE, 1999.

[128] H. Niemann, "Parameterisation of extended systems," *IEE Proceedings-Control Theory and Applications*, vol. 153, no. 2, pp. 221–227, 2006.

[129] C. Nett, C. Jacobson, and M. Balas, "A connection between state-space and doubly coprime fractional representations," *IEEE Transactions on Automatic Control*, vol. 29, no. 9, pp. 831–832, 1984.

[130] A. J. Telford and J. B. Moore, "Doubly coprime factorizations, reduced-order observers, and dynamic state estimate feedback," *International Journal of Control*, vol. 50, no. 6, pp. 2583–2597, 1989.

[131] P. Hippe, "Modified doubly coprime fractional representations related to the reduced-order observer," *IEEE transactions on automatic control*, vol. 34, no. 5, pp. 573–576, 1989.

[132] J. Y. Ishihara and R. M. Sales, "Doubly coprime factorizations related to any stabilizing controllers in state space," *Automatica*, vol. 35, no. 9, pp. 1573–1577, 1999.

[133] M. S. Verma, "Coprime fractional representations and stability of nonlinear feedback systems," *International Journal of control*, vol. 48, no. 3, pp. 897–918, 1988.

[134] C. A. Desoer and M. G. Kabuli, "Right factorization of a class of time-varying nonlinear systems," *IEEE Transactions on automatic Control*, vol. 33, no. 8, pp. 755–757, 1988.

[135] G. Chen and R. J. de Figueiredo, "Construction of the left coprime fractional representation for a class of nonlinear control systems," *Systems & Control Letters*, vol. 14, no. 4, pp. 353–361, 1990.

[136] A. Paice and A. Van der Schaft, "Stable kernel representations as nonlinear left coprime factorizations," in *Proceedings of 1994 33rd IEEE Conference on Decision and Control*, vol. 3, pp. 2786–2791, IEEE, 1994.

[137] D. D. Bainov and P. S. Simeonov, "Systems with impulse effect: stability, theory and applications," 1989.

[138] J. B. Moore, K. Glover, and A. Telford, "All stabilizing controllers as frequency-shaped state estimate feedback," *IEEE Transactions on Automatic Control*, vol. 35, no. 2, pp. 203–208, 1990.

[139] H. H. Niemann, P. Søgaard-Andersen, and J. Stoustrup, "Loop transfer recovery for general observer architectures," *International Journal of Control*, vol. 53, no. 5, pp. 1177–1203, 1991.

[140] F. Navas, I. Mahtout, V. Milanés, and F. Nashashibi, "Youla-kucera control structures for switching," in *CCTA 2018-2nd IEEE Conference on Control Technology and Applications*, 2018.

[141] T. Jochem and D. Pomerleau, "Life in the fast lane: The evolution of an adaptive vehicle control system," *AI magazine*, vol. 17, no. 2, pp. 11–11, 1996.

[142] A. Broggi, M. Bertozzi, A. Fascioli, C. G. L. Bianco, and A. Piazzi, "The argo autonomous vehicle's vision and control systems," *International Journal of Intelligent Control and Systems*, vol. 3, no. 4, pp. 409–441, 1999.

[143] S. Thrun, M. Montemerlo, H. Dahlkamp, D. Stavens, A. Aron, J. Diebel, P. Fong, J. Gale, M. Halpenny, G. Hoffmann, *et al.*, "Stanley: The robot that won the darpa grand challenge," *Journal of field Robotics*, vol. 23, no. 9, pp. 661–692, 2006.

[144] A. Broggi, P. Cerri, M. Felisa, M. C. Laghi, L. Mazzei, and P. P. Porta, "The vislab intercontinental autonomous challenge: an extensive test for a platoon of intelligent vehicles," *International Journal of Vehicle Autonomous Systems*, vol. 10, no. 3, pp. 147–164, 2012.

[145] K. Jo, M. Lee, D. Kim, J. Kim, C. Jang, E. Kim, S. Kim, D. Lee, C. Kim, S. Kim, *et al.*, "Overall reviews of autonomous vehicle a1—system architecture and algorithms," in *8th IFAC IAV*, 2013.

[146] J. Ziegler, P. Bender, M. Schreiber, H. Lategahn, T. Strauss, C. Stiller, T. Dang, U. Franke, N. Appenrodt, C. G. Keller, *et al.*, "Making bertha drive—an autonomous journey on a historic route," *IEEE Intelligent transportation systems magazine*, vol. 6, no. 2, pp. 8–20, 2014.

[147] R. Marino, S. Scalzi, and M. Netto, "Nested pid steering control for lane keeping in autonomous vehicles," *Control Engineering Practice*, vol. 19, no. 12, pp. 1459–1467, 2011.

[148] S. Hima, B. Lusseti, B. Vanholme, S. Glaser, and S. Mammar, "Trajectory tracking for highly automated passenger vehicles," *IFAC Proceedings Volumes*, vol. 44, no. 1, pp. 12958–12963, 2011.

[149] G. Tagne, R. Talj, and A. Charara, "Higher-order sliding mode control for lateral dynamics of autonomous vehicles, with experimental validation," in *2013 IEEE Intelligent Vehicles Symposium (IV)*, pp. 678–683, IEEE, 2013.

[150] E. Maalouf, M. Saad, and H. Saliah, "A higher level path tracking controller for a four-wheel differentially steered mobile robot," *Robotics and Autonomous Systems*, vol. 54, no. 1, pp. 23–33, 2006.

[151] E. Onieva, J. E. Naranjo, V. Milanés, J. Alonso, R. García, and J. Pérez, "Automatic lateral control for unmanned vehicles via genetic

algorithms," *Applied Soft Computing*, vol. 11, no. 1, pp. 1303–1309, 2011.

[152] P. Falcone, F. Borrelli, J. Asgari, H. E. Tseng, and D. Hrovat, "Predictive active steering control for autonomous vehicle systems," *IEEE Transactions on control systems technology*, vol. 15, no. 3, pp. 566–580, 2007.

[153] R. Attia, R. Orjuela, and M. Basset, "Coupled longitudinal and lateral control strategy improving lateral stability for autonomous vehicle," in *2012 American Control Conference (ACC)*, pp. 6509–6514, IEEE, 2012.

[154] H.-S. Tan and J. Huang, "Design of a high-performance automatic steering controller for bus revenue service based on how drivers steer," *IEEE Transactions on Robotics*, vol. 30, no. 5, pp. 1137–1147, 2014.

[155] B.-C. Luan, I.-H. Lee, H.-S. Tan, K. Li, D. Yuan, and F.-C. Chou, "Design and field testing of a lane following control system with a camera based on t&c driver model," tech. rep., SAE Technical Paper, 2016.

[156] V. Milanes, F. Navas, D. Gonzalez, and I. Mahtout, "On the passenger acceptance of driverless shuttles," *IEEE Intelligent Transportation Systems Magazine*, 2020.

[157] D. González, F. Navas, I. Mahtout, and V. Milanés, "A first approach for a passenger-centered behavior on driverless vehicles," in *2020 28th Mediterranean Conference on Control and Automation (MED)*, pp. 182–187, IEEE, 2020.

[158] F. Borrelli, P. Falcone, T. Keviczky, J. Asgari, and D. Hrovat, "Mpc-based approach to active steering for autonomous vehicle systems," *International Journal of Vehicle Autonomous Systems*, vol. 3, no. 2, pp. 265–291, 2005.

[159] R. Rajamani, *Vehicle dynamics and control*. Springer Science & Business Media, 2011.

[160] C. M. Kang, S.-H. Lee, and C. C. Chung, "Comparative evaluation of dynamic and kinematic vehicle models," in *53rd IEEE Conference on Decision and Control*, pp. 648–653, IEEE, 2014.

[161] Y. Kozaki, G. Hirose, S. Sekiya, and Y. Miyaura, "Electric power steering (eps)," *Motion and Control*, vol. 6, pp. 9–15, 1999.

[162] A. Badawy, J. Zuraski, F. Bolourchi, and A. Chandy, "Modeling and analysis of an electric power steering system," tech. rep., SAE Technical Paper, 1999.

[163] H. Matsuoka, "Development and future outlook of steering systems," *JTEKT Engineering Journal*, no. 1013E, p. 8, 2016.

[164] K. Yamamoto, O. Sename, D. Koenig, and P. Moulaire, "Design and experimentation of an lpv extended state feedback control on electric power steering systems," *Control Engineering Practice*, vol. 90, pp. 123–132, 2019.

[165] G. P. Stein, O. Mano, and A. Shashua, "Vision-based acc with a single camera: bounds on range and range rate accuracy," in *IEEE IV2003 Intelligent Vehicles Symposium. Proceedings (Cat. No. 03TH8683)*, pp. 120–125, IEEE, 2003.

[166] J. Wenger, "Automotive radar-status and perspectives," in *IEEE Compound Semiconductor Integrated Circuit Symposium, 2005. CSIC'05.*, pp. 4–pp, IEEE, 2005.

[167] G. R. Widmann, M. K. Daniels, L. Hamilton, L. Humm, B. Riley, J. K. Schiffmann, D. E. Schnelker, and W. H. Wishon, "Comparison of lidar-based and radar-based adaptive cruise control systems," *SAE transactions*, pp. 126–139, 2000.

[168] D. Swaroop and K. Rajagopal, "A review of constant time headway policy for automatic vehicle following," in *Intelligent Transportation Systems, 2001. Proceedings. 2001 IEEE*, pp. 65–69, IEEE, 2001.

[169] S. Moon, I. Moon, and K. Yi, "Design, tuning, and evaluation of a full-range adaptive cruise control system with collision avoidance," *Control Engineering Practice*, vol. 17, no. 4, pp. 442–455, 2009.

[170] D. Schrank, B. Eisele, and T. Lomax, "Tti's 2012 urban mobility report," *Texas A&M Transportation Institute. The Texas A&M University System*, vol. 4, 2012.

[171] L. A. Pipes, "An operational analysis of traffic dynamics," *Journal of applied physics*, vol. 24, no. 3, pp. 274–281, 1953.

[172] R. E. Chandler, R. Herman, and E. W. Montroll, "Traffic dynamics: studies in car following," *Operations research*, vol. 6, no. 2, pp. 165–184, 1958.

[173] M. Brackstone and M. McDonald, "A comparison of eu and us progress in the development of longitudinal advanced vehicle control and safety systems (avcss)," *Transport Reviews*, vol. 20, no. 2, pp. 173–190, 2000.

[174] A. Shaout and M. Jarrah, "Cruise control technology review," *Computers & electrical engineering*, vol. 23, no. 4, pp. 259–271, 1997.

[175] J. R. Winkelman and M. K. Liubakka, "Self-tuning speed control for a vehicle," Aug. 10 1993. US Patent 5,235,512.

[176] T. Kato, Y. Mizuno, T. Natsume, and M. Tsujii, "Automotive cruise control using self-tuning regulator," tech. rep., SAE Technical Paper, 1991.

[177] Y. Anan, S. Ando, and T. Murai, "Automatic fuzzy speed control system for vehicle," Sept. 22 1992. US Patent 5,148,721.

[178] Y. Anan, S. Ando, T. Murai, Y. Kubo, and T. YAMANE, "Cruise control systems with fuzzy control technology," 1991.

[179] H. Takahashi, "Control system for automotive vehicle for controlling vehicle driving behavior with feature of harmonization of vehicular driving condition dependent control and driver's driving tendency adapted control," Nov. 10 1992. US Patent 5,162,997.

[180] M. Kayano and K. Itah, "Improvement of automatic cruising for truck using fuzzy control," *JSAE*, vol. 44, 1990.

[181] T. Murai, "Automatic speed control system," Oct. 13 1992. US Patent 5,154,250.

[182] A. Kawano, Y. Sano, H. Umeda, T. Nishimura, Y. Miyata, and K. Inagaki, "Cruise control device for motor vehicles," July 14 1992. US Patent 5,129,475.

[183] S.-B. Choi and J. K. Hedrick, "Vehicle longitudinal control using an adaptive observer for automated highway systems," in *Proceedings of 1995 American Control Conference-ACC'95*, vol. 5, pp. 3106–3110, IEEE, 1995.

[184] K. C. Dey, L. Yan, X. Wang, Y. Wang, H. Shen, M. Chowdhury, L. Yu, C. Qiu, and V. Soundararaj, "A review of communication, driver characteristics, and controls aspects of cooperative adaptive cruise control (cacc)," *IEEE Transactions on Intelligent Transportation Systems*, vol. 17, no. 2, pp. 491–509, 2015.

[185] D. Swaroop, "String stability of interconnected systems: An application to platooning in automated highway systems," 1997.

[186] D. Swaroop and J. K. Hedrick, "String stability of interconnected systems," *IEEE transactions on automatic control*, vol. 41, no. 3, pp. 349–357, 1996.

[187] P. A. Ioannou and C.-C. Chien, "Autonomous intelligent cruise control," *IEEE Transactions on Vehicular technology*, vol. 42, no. 4, pp. 657–672, 1993.

[188] D. Swaroop and J. K. Hedrick, "Constant spacing strategies for platooning in automated highway systems," 1999.

[189] S. E. Shladover, C. Nowakowski, X.-Y. Lu, and R. Ferlis, "Cooperative adaptive cruise control: Definitions and operating concepts," *Transportation Research Record*, vol. 2489, no. 1, pp. 145–152, 2015.

[190] G. Naus, J. Ploeg, M. Van de Molengraft, W. Heemels, and M. Steinbuch, "Design and implementation of parameterized adaptive cruise control: An explicit model predictive control approach," *Control Engineering Practice*, vol. 18, no. 8, pp. 882–892, 2010.

[191] K. Yi and I.-K. Moon, "A driver-adaptive stop-and-go cruise control strategy," in *IEEE International Conference on Networking, Sensing and Control, 2004*, vol. 1, pp. 601–606, IEEE, 2004.

[192] J. E. Naranjo, C. González, R. García, and T. De Pedro, "Cooperative throttle and brake fuzzy control for acc + stop&go maneuvers," *IEEE Transactions on Vehicular Technology*, vol. 56, no. 4, pp. 1623–1630, 2007.

[193] J. Wang, L. Zhang, D. Zhang, and K. Li, "An adaptive longitudinal driving assistance system based on driver characteristics," *IEEE Transactions on Intelligent Transportation Systems*, vol. 14, no. 1, pp. 1–12, 2012.

[194] V. Milanés, J. Villagrá, J. Godoy, and C. González, "Comparing fuzzy and intelligent pi controllers in stop-and-go manoeuvres," *IEEE Transactions on Control Systems Technology*, vol. 20, no. 3, pp. 770–778, 2011.

[195] N. K. Ure, M. U. Yavas, A. Alizadeh, and C. Kurtulus, "Enhancing situational awareness and performance of adaptive cruise control through model predictive control and deep reinforcement learning," in *2019 IEEE Intelligent Vehicles Symposium (IV)*, pp. 626–631, IEEE, 2019.

[196] G. Naus, R. Vugts, J. Ploeg, M. Van de Molengraft, and M. Steinbuch, "Towards on-the-road implementation of cooperative adaptive cruise control," *Proc. 16th World Congr. Exhib. Intell. Transp. Syst. Serv*, 2009.

[197] G. J. Naus, R. P. Vugts, J. Ploeg, M. J. van de Molengraft, and M. Steinbuch, "String-stable cacc design and experimental validation: A frequency-domain approach.," *IEEE Transactions on vehicular technology*, vol. 59, no. 9, pp. 4268–4279, 2010.

[198] S. Öncü, J. Ploeg, N. Van de Wouw, and H. Nijmeijer, "Cooperative adaptive cruise control: Network-aware analysis of string stability," *IEEE Transactions on Intelligent Transportation Systems*, vol. 15, no. 4, pp. 1527–1537, 2014.

[199] H. Hao and P. Barooah, "On achieving size-independent stability margin of vehicular lattice formations with distributed control," *IEEE Transactions on Automatic Control*, vol. 57, no. 10, pp. 2688–2694, 2012.

[200] I. Herman, D. Martinec, Z. Hurák, and M. Šebek, "Nonzero bound on fiedler eigenvalue causes exponential growth of h-infinity norm of vehicular platoon," *IEEE Transactions on Automatic Control*, vol. 60, no. 8, pp. 2248–2253, 2014.

[201] S. S. Stankovic, M. J. Stanojevic, and D. D. Siljak, "Decentralized overlapping control of a platoon of vehicles," *IEEE Transactions on Control Systems Technology*, vol. 8, no. 5, pp. 816–832, 2000.

[202] J. Pérez, V. Milanés, J. Godoy, J. Villagra, and E. Onieva, "Cooperative controllers for highways based on human experience," *Expert Systems with Applications*, vol. 40, no. 4, pp. 1024–1033, 2013.

[203] T. Stanger and L. del Re, "A model predictive cooperative adaptive cruise control approach," in *IEEE American Control Conference (ACC)*, pp. 1374–1379, June 2013.

[204] W. B. Dunbar and D. S. Caveney, "Distributed receding horizon control of vehicle platoons: Stability and string stability," *IEEE Transactions on Automatic Control*, vol. 57, no. 3, pp. 620–633, 2011.

[205] J. Ploeg, "Analysis and design of controllers for cooperative and automated driving," *Eindhoven University of Technology*, 2014.

[206] J. Ploeg, B. T. Scheepers, E. Van Nunen, N. Van de Wouw, and H. Nijmeijer, "Design and experimental evaluation of cooperative adaptive cruise control," in *2011 14th International IEEE Conference on Intelligent Transportation Systems (ITSC)*, pp. 260–265, IEEE, 2011.

[207] J. Ploeg, A. Serrarens, and G. Heijenk, "Connect & drive: design and evaluation of cooperative adaptive cruise control for congestion reduction," *Journal of Modern Transportation*, vol. 19, pp. 207–213, September 2011.

[208] E. Capellier, F. Davoine, V. Frémont, J. Ibañez-Guzman, and Y. Li, "Evidential grid mapping, from asynchronous lidar scans and rgb images, for autonomous driving," in *2018 21st International Conference*

on Intelligent Transportation Systems (ITSC), pp. 2595–2602, IEEE, 2018.

[209] J. Hu, B. Zheng, C. Wang, C. Zhao, X. Hou, Q. Pan, and Z. Xu, "A survey on multi-sensor fusion based obstacle detection for intelligent ground vehicles in off-road environments.," *Frontiers Inf. Technol. Electron. Eng.*, vol. 21, no. 5, pp. 675–692, 2020.

[210] J. C. Doyle, K. Glover, P. P. Khargonekar, and B. A. Francis, "State-space solutions to standard h/sub 2/and h/sub infinity/control problems," *IEEE Transactions on Automatic control*, vol. 34, no. 8, pp. 831–847, 1989.

[211] T. Başar and P. Bernhard, *H-infinity optimal control and related minimax design problems: a dynamic game approach.* Springer Science & Business Media, 2008.

[212] A. Isidori and A. Astolfi, "Disturbance attenuation and h/sub infinity/-control via measurement feedback in nonlinear systems," *IEEE transactions on automatic control*, vol. 37, no. 9, pp. 1283–1293, 1992.

[213] D. Lefebvre, P. Chevrel, and C. Perrier, "H-infinity control and μ-analysis for active control of vehicle longitudinal oscillations," *IFAC Proceedings Volumes*, vol. 34, no. 1, pp. 11–16, 2001.

[214] H. Zhang, G. Zhang, and J. Wang, "h_∞ observer design for lpv systems with uncertain measurements on scheduling variables: Application to an electric ground vehicle," *IEEE/ASME Transactions on Mechatronics*, vol. 21, no. 3, pp. 1659–1670, 2016.

[215] D. Robert, O. Sename, and D. Simon, "An h_∞ lpv design for sampling varying controllers: Experimentation with a t-inverted pendulum," *IEEE Transactions on Control Systems Technology*, vol. 18, no. 3, pp. 741–749, 2009.

[216] I. Yaesh and U. Shaked, "Two-degree-of-freedom h/sub infinity/-optimization of multivariable feedback systems," *IEEE Transactions on Automatic Control*, vol. 36, no. 11, pp. 1272–1276, 1991.

[217] J. Beltrán, I. Cortés, A. Barrera, J. Urdiales, C. Guindel, F. García, and A. de la Escalera, "A method for synthetic lidar generation to create annotated datasets for autonomous vehicles perception," in *2019 IEEE Intelligent Transportation Systems Conference (ITSC)*, pp. 1091–1096, IEEE, 2019.

[218] F. García, A. Prioletti, P. Cerri, and A. Broggi, "Phd filter for vehicle tracking based on a monocular camera," *Expert Systems with Applications*, vol. 91, pp. 472–479, 2018.

RÉSUMÉ

Les véhicules automatisés reçoivent de plus en plus d'attention en raison de leur potentiel d'améliorer la vie des conducteurs, d'assurer la sécurité routière, d'accroître la capacité routière ou de réduire les émissions de carbone. Une conduite autonome adéquate exige la stabilité du véhicule, la précision du mouvement et un comportement naturel garantissant le confort des passagers à l'intérieur du véhicule. Cependant, les situations de conduite changent en fonction de l'aménagement de la route et des interactions potentielles avec d'autres agents de la circulation. En outre, les capacités du véhicule peuvent être dégradées en raison des limites des capteurs embarqués ou de la complexité de l'algorithme traitant les données de perception. Cette thèse propose une architecture de contrôle multi-objectifs qui peut adapter le comportement du véhicule pour surmonter les changements dans les conditions de fonctionnement et assurer la performance du véhicule et maintenir la stabilité du mouvement avec un comportement naturel de véhicule.
Dans cette thèse, nous proposons de nouvelles structures de contrôle basées sur la reconfiguration des contrôleurs, améliorant l'état de l'art des techniques de contrôle latéral et longitudinal en résolvant les problèmes suivants : 1) Le compromis entre la précision dans le suivi de la trajectoire et le confort lorsque la situation de conduite change dans le mouvement latéral; 2) Le compromis entre la robustesse et la performance lorsque le bruit apparaît dans la mesure de l'nter-distance dans les systèmes Adaptive Cruise Control (ACC). La stabilité du contrôleur proposé est garantie grâce à la parametrisation de Youla-Kucera.
La validation des structures de contrôle proposées est assurée par la simulation et l'expérimentation en temps réel avec un véhicule Renault ZOE. L'adaptabilité des contrôleurs aux tâches de conduite autonome est démontrée.

MOTS CLÉS

Véhicules autonomes; Reconfiguration des contrôleurs; Parametrisation de Youla-Kucera; Contrôle multi-objectifs .

ABSTRACT

Automated vehicles are getting more and more attention because of their potential to improve drivers' lives, ensuring road safety, increasing highway capacity, or reducing carbon emissions. Proper autonomous driving requires vehicle stability, precise motion, and natural behavior guaranteeing comfort for passengers inside the vehicle. However, driving situations change depending on the road layout and potential interactions with other traffic agents. Furthermore, vehicle capabilities can be degraded because of the on-board sensors' limitations, or the complexity of the algorithm processing the perception data. This thesis proposes a multi-objective control architectures that can adapt the vehicle behavior to overcome the changes in the operating conditions and assure vehicle performance and stability.
The automated control system should be able to address any circumstances ranging from a sudden change in the driving situation (i.e. lane change, obstacle avoidance) to an inaccurate measurement. This thesis uses Youla-Kucera (YK) parametrization to design control structures able to recognize the driving situation changes, adapting the controller response to satisfy the required performance level and keeping the motion stability with a natural vehicle behavior.
In this thesis we propose novel control structures based on controller reconfiguration, improving both lateral and longitudinal control state-of-the-art by solving the following problems: 1) The trade-off between precision in trajectory tracking and comfort when the driving situation changes in lateral motion; 2) The trade-off between robustness and performance when noise measurement appears in Adaptive Cruise Control (ACC) systems. The stability of the proposed controller is guaranteed thanks to YK parametrization.
The validation of the proposed control structures is provided in both simulation and real-time experimentation using a Renault ZOE vehicle. The adaptability of the controllers to autonomous driving tasks is proved in different operating conditions.

KEYWORDS

Autonomous vehicles; Controller reconfiguration; Youla-Kucera parametrization; Multi-objective control.